AN ABSTRACT OF THE THESIS OF

Kevin M. Groom for the degree of Master of Science in Civil
Engineering presented on January 21, 1992.

Title: Nonlinear Finite-Element Modeling of Intercomponent
Connections in Light-Frame Wood Structures

Abstract approved: _____
Robert J. Leichti

Nailed connections have nonlinear load-displacement
relations. Modeling these connections in an assembled
structure would require a great amount of computational time
because of the large number of degrees of freedom.
Replacing these connections with energetically-equivalent
nonlinear springs reduces the number of degrees of freedom,
and leads to computational efficiency in full structure
models. This study examined four connections that were used
in a light-frame structure that was built and tested under
simulated wind loads. The connections examined were an
exterior wall-to-floor connection, an interior wall-to-roof
truss connection, an exterior wall-to-exterior wall
connection, and an interior wall-to-exterior wall
connection.

The details of the four connections were modeled by using the finite-element method as either a two-dimensional plane stress model, or a three-dimensional model. Characteristics from three of the models were compared to experimental results from tests of connections, and the comparison showed good agreement between the connections and the models. The characteristic load-translation and moment-rotation responses of the detailed models were then summarized as computationally efficient springs.

NONLINEAR FINITE-ELEMENT MODELING OF
INTERCOMPONENT CONNECTIONS IN
LIGHT-FRAME WOOD STRUCTURES

by

Kevin M. Groom

A THESIS

submitted to

Oregon State University

in partial fulfillment of
the requirements for the
degree of

Master of Science

Completed January 21, 1992

Commencement June 1992

APPROVED:

Assistant Professor of Civil Engineering in charge of major.

Chair/of Department of Civil Engineering.

Dean of Graduate School

Date thesis is presented_____ January 21, 1992

Typed by_____ Kevin M. Groom

ACKNOWLEDGEMENT

I would like to thank several people for their help and support supplied to me throughout my education.

First of all I would like to thank my office mate and friend, Bo Kasal. His knowledge and technical advice saved me many headaches.

I also want to thank my parents for financial support while I was an undergraduate, and financial help as a graduate student. Without their help I never would have been able to complete my education.

Finally, I would like to thank Cath for all she has done. She has been my main source of encouragement and support throughout my college career.

TABLE OF CONTENTS

LIST OF FIGURES

LIST OF TABLES

LIST OF APPENDIX FIGURES

NONLINEAR FINITE-ELEMENT MODELING OF INTERCOMPONENT CONNECTIONS IN LIGHT-FRAME WOOD STRUCTURES

1. INTRODUCTION

Through the centuries, wood has played a major role in family dwellings and other light-frame buildings. As the price of lumber and construction costs increase, the design of economical and efficient wood structures demands a complete understanding of the structural system. Over-design adds cost in both material and labor, while under-designing can result in loss of serviceability or structural failure, which if catastrophic could lead to loss of life.

One of the least understood features of design and analysis of light-frame wood buildings is that of load sharing among substructures under horizontal and vertical loading. Current design method assumes the load is distributed according to tributary area. However, the true load distribution is now thought to be a function of subsystems stiffness and the intercomponent connections.

Typical intercomponent connections of light-frame structures are the central focus of this research. The need for this research originated as part of a larger cooperative effort between teams at Oregon State University (OSU) and Washington State University (WSU) to help engineers

understand and design for load sharing capabilities among
substructures.

Justification

Today's housing construction is based on a design of
individual components such a wall, floor, truss, and
connection. The interaction of these components with one
another is ignored or given very little attention in design
specifications. Although this is the case, engineers have
recognized the interaction between components through full
scale testing of light-frame structures (Phillips 1990,
Tuomi and McMutcheon 1974).

Neglecting the interaction between the structural
intercomponents is the main reason buildings are either over
designed, leading to added material and labor costs, or
under designed, which can lead to reduced structural safety.
The majority of failures occur when some components in the
building are over designed, while others are unsafe. For
example, field surveys done in hurricane and earthquake
areas show that after foundation failures, caused by a
combination of wind and water, the most severe damage was a
result of the connections failing between the walls and roof
(Liska and Bohannan 1973). Other connections such as wall
to floor and wall to wall had a tendency to fail as well.
Laboratory testing of a full-scale house under simulated

snow and wind loads produced similar results (Tuomi and McMutcheon 1974).

Recent research has produced a number of accurate procedures to analyze components found in wood buildings (Falk and Itani 1989, Loferski and Gamalath 1989, Polensek and Schimel 1986). A procedure is needed to analyze a full three-dimensional building in such a manner that today's practicing engineers and builders can use it. Improved knowledge in the use of three-dimensional modelling and load sharing among different components in wood buildings will lead to efficiency in design.

Objectives

The overall objective of the cooperative research project (Polensek 1988) was to develop and verify a method for predicting displacements and reactions of complete light-frame wood buildings. The approach was to develop a quasi-superelement for each substructure using commercial software. Thus, the complex nonlinear behavior of the structure is represented by a computationally efficient model using available technology.

The main objective of this portion of the project was to present a method of reducing a detailed two or three-dimensional model of an intercomponent connection to an energetically equivalent set of rotational and load-displacement springs, a quasi-superelement. These models can subsequently be used in a full-structure model. The specific objectives were:

1) To develop nonlinear finite element models of the intercomponent connections used in a full-scale structure tested at WSU.

2) To verify the models through the use of testing or previous research.

3) To reduce the finite-element models of the intercomponent connections to a set of energetically-equivalent nonlinear springs for use in a global finite-element model of the structure

tested at WSU.

The light-frame wood structure that was constructed and subjected to simulated wind loads at WSU is shown in Figure 1-1.
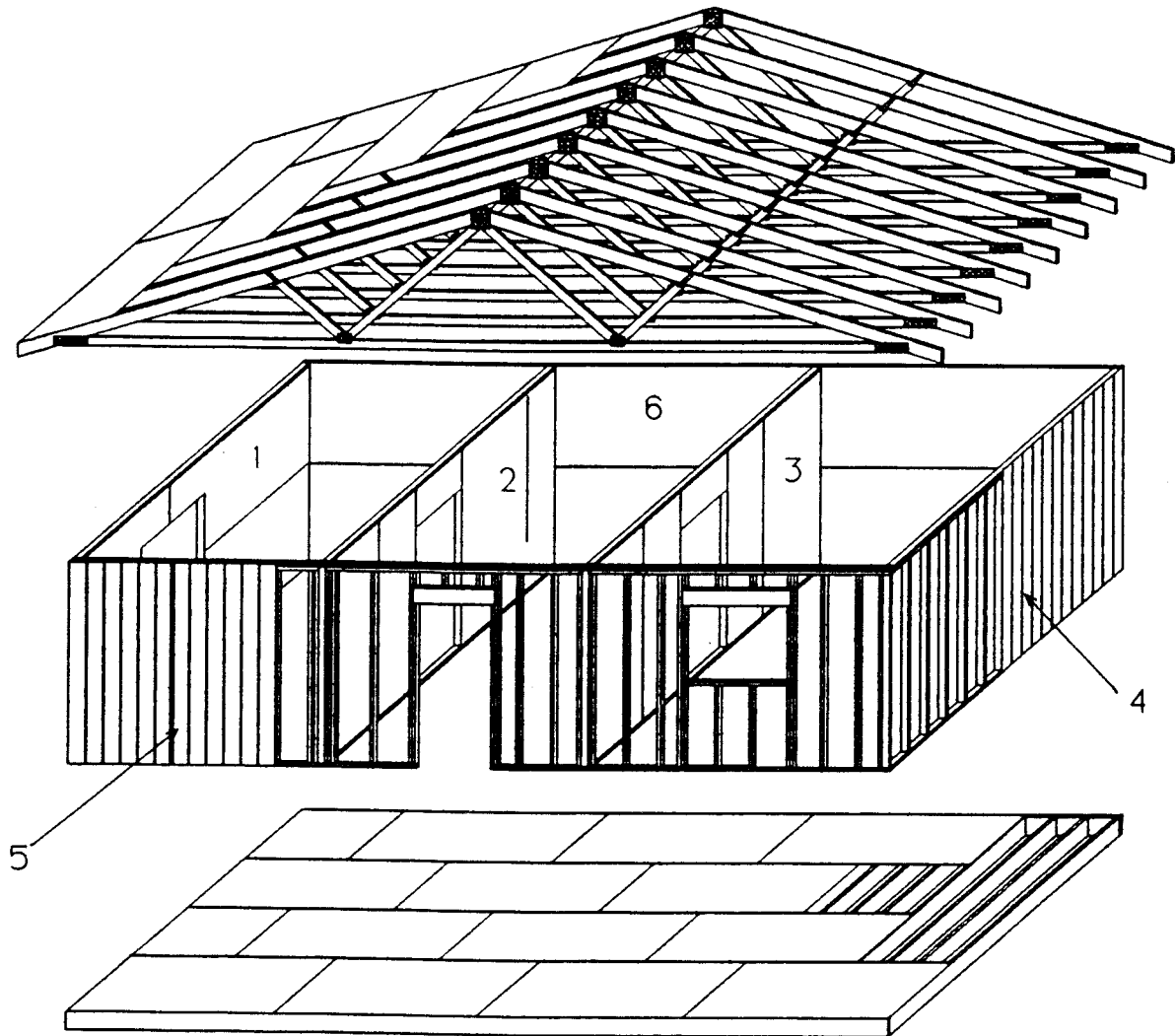
Figure 1-1. Three-dimensional view of experimental
structure.

2. REVIEW OF LITERATURE

Nail Shear

There are numerous research reports involving nails loaded in shear. Standard nail shear testing procedures are outlined in standard test method D1761 (American Society for Testing and Materials [ASTM], 1990). These tests offer lateral resistance to two members fastened by a single nail with a load applied through cross head movement. Load and differential movement are monitored, and a load-slip curve could be generated.

Polensek and Bastendorff (1987) determined load-slip curves for 17 different nail shear conditions by varying material type, nail size and grain orientation. The testing procedures in ASTM 1761 were followed with the exceptions that the load rate was accelerated to accommodate the large number of samples, and the load was applied in a manner such that no eccentricity was introduced.

Pellicane (1991) performed load-slip tests on 6d and 8d common wire nails fastening 11 different types of sheathing side members to both Douglas-fir and Engelmann spruce. He fit his data into an empirically based equation developed by McLain (1976) of the form:

$$Load = A*\log_{10}(1 + B*Slip) \qquad\qquad 1-1$$

where A and B are curve-fitting parameters.

Research done by Mack (1966) showed that the nail connection stiffness is influenced by many factors including, but not limited to, species, nail diameter, nail type, moisture content, density and direction of grain.

Phillips (1990) tested seven types of nailed connections. The results of these tests will be used in the final analysis of the project, since these were the same materials used in the structure. These tests were performed parallel to the grain of the sheathing and the main member. Although Phillips stated that the grain direction of the plywood had little effect on the load-slip relation, the grain direction of the base material significantly affected the load-slip relation (Mack 1966, Phillips 1990).

Hilton, Polensek and Atherton (1976) concluded that nail spacing along the grain in the range of ½ to 6 in. does not effect the load slip relation. They showed that these conclusions can be extended to a wider nail spacing.

Loferski and Polensek (1982) developed empirical equations which represented the load-slip behavior of laterally loaded nailed joints found in wood stud walls as a tri-linear curve composed of three joint stiffnesses K_i, where i = 1, 2, or 3. The joint stiffnesses were composed of nine regression constants as well as Wilkinson's slip

modulus (Wilkinson 1972 and 1974), specific gravities of the stud and plywood, and the percent of early wood present in the stud. The equations were based on tests done on ⅜-in. Douglas-fir plywood fastened to Southern pine studs with a 6d, galvanized, wire, box nail. The equations were then applied to a ⅜-in. Douglas-fir plywood sheathing fastened to a Douglas-fir stud with a 6d nail, and the results showed good agreement between the predicted values and the experimental tests.

A finite-element model based on the theory of beams on elastic foundations was developed by Foschi (1974). He modeled and tested a glulam rivet driven through a pre-drilled steel plate into a Douglas-fir sample. He concluded that the model is only acceptable to approximate the initial stiffness of the load-slip relation, especially when the nail head is rigidly fixed. Hunt and Bryant (1990) used the work done by Foschi and produced a finite-element method that constructed a load-slip curve with some accuracy. This technique can be used to obtain relationships that can not be found in past literature.

A finite-element method was used by Komatsu (1989) to predict the nonlinear load-slip curve of a timber joint with steel side plates. Four types of wood, including Douglas-fir, and five types of nails were used in load-slip tests to compare to the finite-element method. Komatsu concluded that the finite-element method could accurately be used to

predict the load-slip behavior of a timber joint with a steel side plate unless the slip deformation exceeded roughly the order of the nail diameter. Komatsu also pointed out that as the density of the timber became higher and/or the nail size increased beyond those examined, the finite-element solution was less accurate.

Nail Withdrawal

Nail withdrawal values are needed for a complete finite-element model of an intercomponent connection. However, with the exception of a single load-withdrawal diagram in the Wood Handbook (Forest Products Laboratory 1987), the load-displacement relationship of common nails in withdrawal from the face of a member has not been studied. Although, research by Ehlbeck (1979) produced nail-withdrawal curves for threaded nails which showed how the load-withdrawal relationship varied with the angle of the thread.

Many sources provide empirical formulas and tables to find the ultimate load of a nail in withdrawal (Ehlbeck 1979, NFPA 1988, ICBO 1988, FPL 1987, Faherty 1982). However none of these give the relationship of the withdrawal as a function of load.

ASTM D1761 (1985) provides guidelines for nail withdrawal tests. These tests do not require that the

displacement be monitored along with the load, therefore, only the ultimate load is found.

A load-withdrawal curve for a 16d nail fastening a Douglas-fir stud to the end of another Douglas-fir stud was produced in earlier research (Polensek and Bastendorff 1987). The load-withdrawal relation is linear up to a distinct yield point, where the load then drops off.

Connection Testing/Modelling

Polensek (1978) states that in reference to deflections, stresses, and slips computed by theoretical analysis on stud and joint properties of wood stud walls, the effects of errors in the material properties of the wall coverings have a minor effect on the final results. Therefore, standard design values for plywood and gypsum can be used. Polensek stated that doubling the stiffness of the stud-plywood joints increased the load capacity of wood stud walls by 13% and decreased the maximum deflection by 8%. Doubling the stiffness of the stud-gypsum joint increased the ultimate load by 5% and decreased the maximum deflection by 4%.

Jenkins, Polensek, and Bastendorff (1979) conducted slip tests on plywood-stud and gypsum-stud interfaces. The tests were performed with 4-mil polyethylene plastic strips with 2 oil-lubricated interfaces between the sheathing and

studs. Tests were also performed with no friction reducing materials between the sheathing and studs. They concluded that under short-term loads the presence of interlayer friction has no effect on the load slip relation.

Loferski and Gamalath (1989) designed a simple model to predict the rotational stiffness of nail joints. The model incorporated nail withdrawal, nail head embedment, and crushing at the wood-to-wood interface between the main and side members. The rotational stiffness was found by a mechanical analog that used springs, which corresponded to the joint actions described above. The model was verified with good agreement using linear properties for the wood and nails. The model, however, was applicable to a two member joint, and did not take into account any resistance contributed by nail shear.

A finite-element program, COMPCON, was introduced by Polensek and Schimel (1986). COMPCON was based on orthotropic plane-strain elements and gap elements. The plane-strain elements were used to model lumber and sheathing materials. The gap elements consisted of a set of two mutually perpendicular springs with a piece-wise linear load-deflection relation that allowed for the nonlinear properties of nails in shear and withdrawal. Although COMPCON is very accurate when compared to experimental results, it is limited to two dimensional models, and is not

very versatile when compared to today's commercially available software.

3. NAIL TESTING

Finite-element models of intercomponent connections require various load-displacement relations for the different loading conditions of each nail. The loading condition for each nail is a function of materials being joined, such as plywood-to-wood or gypsum board-to-wood, and the direction of the load, shear or withdrawal. Phillips (1990) and Polensek and Bastendorff (1987) provided the necessary load-displacement information for plywood-to-wood and gypsum board-to-wood in shear. However, nail shear with metal side plates and withdrawal load-displacement data were not available in the literature. Therefore, some shear and withdrawal testing were necessary.

Shear Tests

One of the intercomponent connections being evaluated had a steel-to-wood interface fastened with both 8d and $1\frac{1}{4}$-in. joist hanger nails (JHN). Although Polensek and Bastendorff (1987) provided a load-displacement relation for the 8d nail, steel-to-wood interface, no data was available for the JHN. While data were available for the 8d nail, shear tests were conducted on both the JHNs and the 8d

nails. Two sets of shear tests with metal side plates were performed for each nail, one set for a load-displacement relation parallel to the grain and the other for a relation perpendicular to the grain. Fifteen replications were performed for each joint configuration.

Materials

The stud material used in these tests was Douglas-fir 2×4s, with a No. 2 grade. They were purchased from a local lumber supplier. The wood was air dried until an average moisture content (MC) of 12.5% (oven-dry basis) was reached. The average specific gravity of the wood was 0.46. The modulus of elasticity (E) was determined from a static bending test using the apparatus given in Figure 3-1. Weights (P) were hung at midspan on a 6-ft span and deflections (δ) measured with a dial gauge having 0.001-in. resolution. The E was determined from:

$$E = \frac{PL^3}{48\delta I}$$

3-1

The average E of the 15 pieces was 1.80×10^6 psi. When fabricating nail shear test specimens, knots and other defects were not allowed.
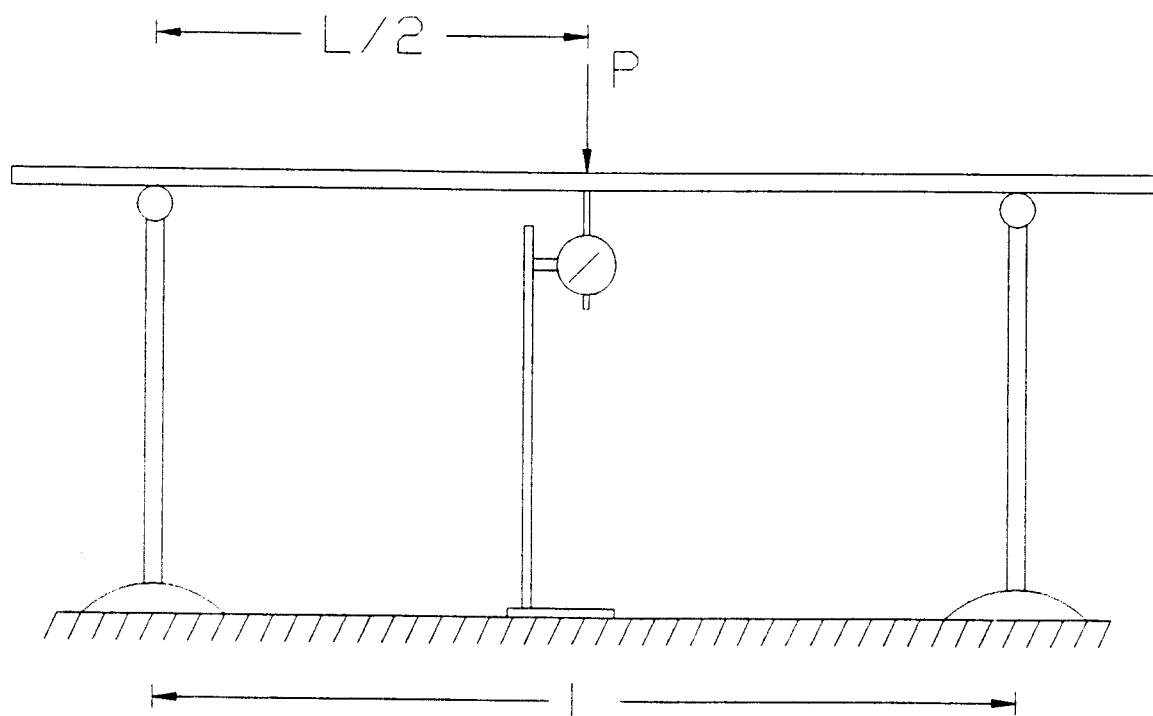
Figure 3-1. Static bending test to determine the elasticity (E) of studs used in shear tests.

The steel side plates were fabricated from 18-gauge galvanized steel, the material of the framing anchor. Holes with a 0.17-in. diameter were drilled in the plate to match the hole pattern of the framing anchor and for attachment to the testing apparatus.

The nails used in the tests were bright common wire 8d nails and 1¼-in. JHN purchased from a local supplier.

Testing Methods

The testing arrangement for the JHN tested parallel to the grain is shown in Figure 3-2. A nail pattern was chosen to match the nail pattern used in the full-scale structural test performed by Phillips (1990). A linear variable differential transformer (LVDT) was mounted on either side of the stud and monitored the slip of the steel plate relative to the wood. The stud was fixed to the base by passing two ⅜-in. bolts through steel angles, and bolting the angles to the base. This testing arrangement was chosen over the ASTM arrangement because it comes closer to resembling the actual conditions, and the base could be used again for later testing of other intercomponent connections.

A shear load was applied at a constant rate of 0.1 in./min. in a screw driven testing machine. The load was monitored with a 5,000-lb load cell. Readings of the two LVDTs and the load cell were recorded at a rate of 1
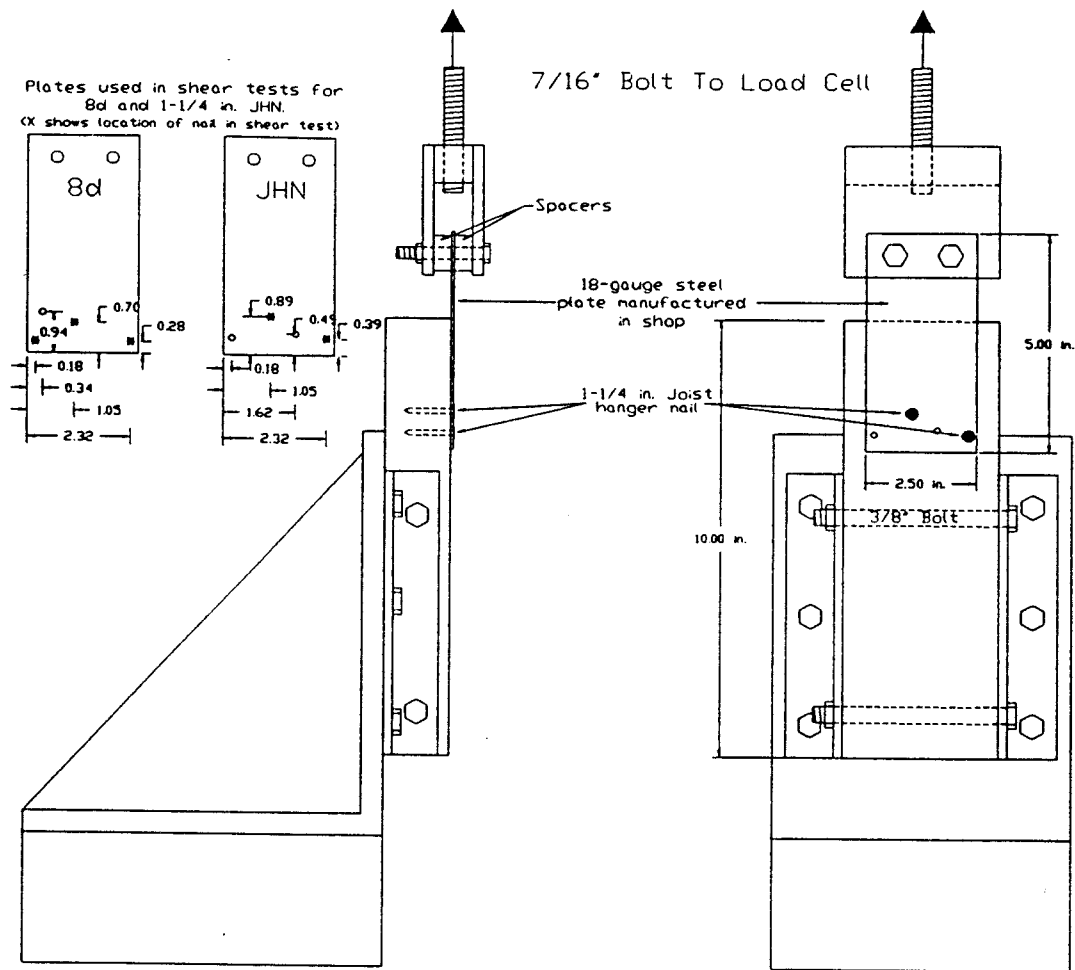
Figure 3-2. Apparatus used to test 1½-in. joist hanger nails (JHN) and 8d nails in shear.

reading/sec. with a personal computer and data acquisition software, until failure occurred. Failure was defined as a sudden drop in the resulting load.

The length of the 8d nails was greater than 1½-in., therefore two studs were fastened together with a pair of ½ × 2½-in. lag screws. The nailing pattern of the 8d nails was also different than that of the JHNs, and required the use of three 8d nails. Then loading followed the procedures outlined above. The two LVDTs were averaged to give a single value for slip. The load-slip results were plotted and yielded a family of curves.

Results

A typical load-displacement curve for an 8d nail with a metal side plate loaded in shear is shown in Figure 3-3. It should be noted that the curve in Figure 3-3 represents the resistance of two nails. To obtain the results for a single nail the load would simply be divided by two. The curves generated from the 8d shear tests represent the resistance of three nails, and therefore the load should be divided by three to obtain the resistance of a single nail. The results of all four shear tests are shown in Figures A1-A4 of Appendix A.

The results for each nail load in shear parallel and perpendicular-to-grain directions of the main member were
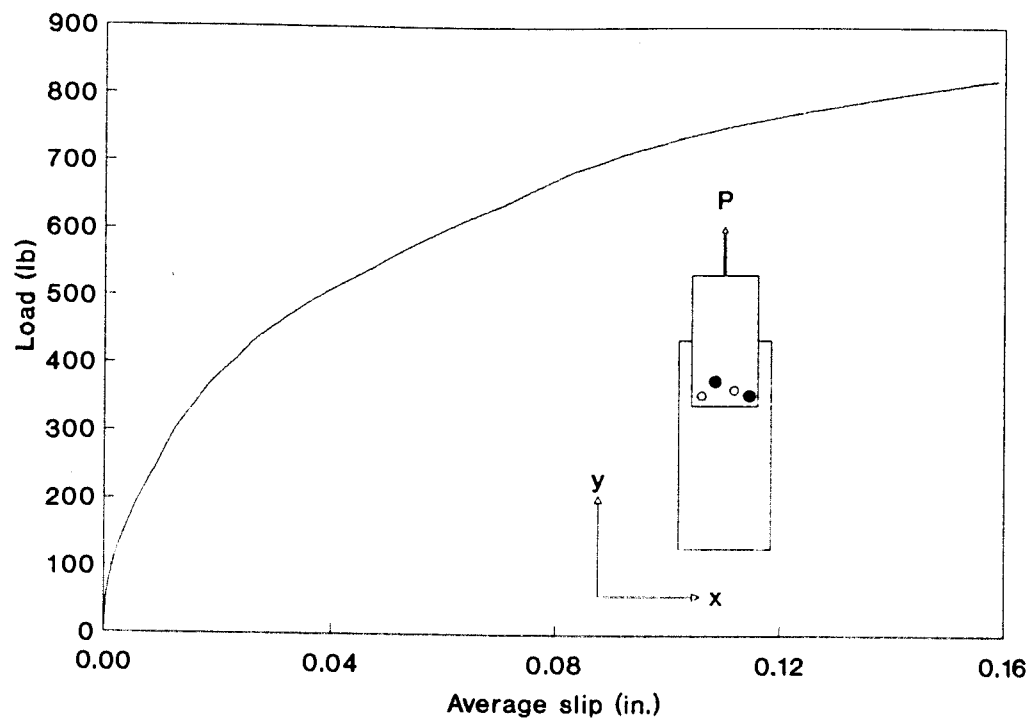
Figure 3-3. Typical load-slip curve of two 1¼-in. JHN
passing through 18-gauge galvanized steel into a Douglas-fir
stud.

subjected to regression analysis over the data range from the test start until the maximum load. The regression results are summarized in Table 3-1 where slip is used to predict load.

Table 3-1. Summarized Results of Load-Slip For a Single Nail Loaded in Shear with Steel Side Plates.

Nail	Grain Orientation	Regression Equation[a]	r^2
8d	Parallel	Load = 1764 * $\text{Slip}^{.5992}$	.83
8d	Perpendicular	Load = 2259 * $\text{Slip}^{.5982}$	.88
JHN	Parallel	Load = 1202 * $\text{Slip}^{.5303}$	.94
JHN	Perpendicular	Load = 1347 * $\text{Slip}^{.5653}$	.89

[a] Load is expressed in lb, and slip in in.

Withdrawal and Pull-through Tests

For the finite-element models to completely represent the mechanical behavior of the various connections, nail withdrawal and nail head pull-through load-displacement curves were needed. Separation of members in the connection is caused by one of the following actions: either the nail in the base material is withdrawn, as would be the case for two studs nailed together, or the action would combine withdrawal of the nail from the base material, with the pulling through of the nail head from the side member. The second action may be the case for plywood or gypsum nailed to a stud.

To account for every combination used in the finite-element models eight withdrawal tests and three pull-through tests had to be performed.

Materials

The wood for the withdrawal tests was different than that of the shear tests. Douglas-fir 2×4s with a No. 2 grade were used for the withdrawal tests. The average MC and specific gravity based on oven-dry weights was 9.4% and 0.47 respectively. The average E of the wood was 1.77×10^6 psi. The plywood used for the pull-through tests was ½-in. exterior sheathing. The gypsum sheathing was also ½-in. thick.

Five types of nails (1¼-in. JHN, 6d, 8d, 10d and 16d) were used for the withdrawal tests, and three types (drywall nails, 6d and 8d) were used for the pull-through tests.

Testing Methods

Where feasible the ASTM methods of testing nails in withdrawal were followed (ASTM 1985). The testing arrangements for the withdrawal and pull-through tests are shown in Figures 3-4 and 3-5.

To testing machine

P

LVTD removed
to show nail

Nail Head Grip

Nail

Wood/
Member

Load Cell
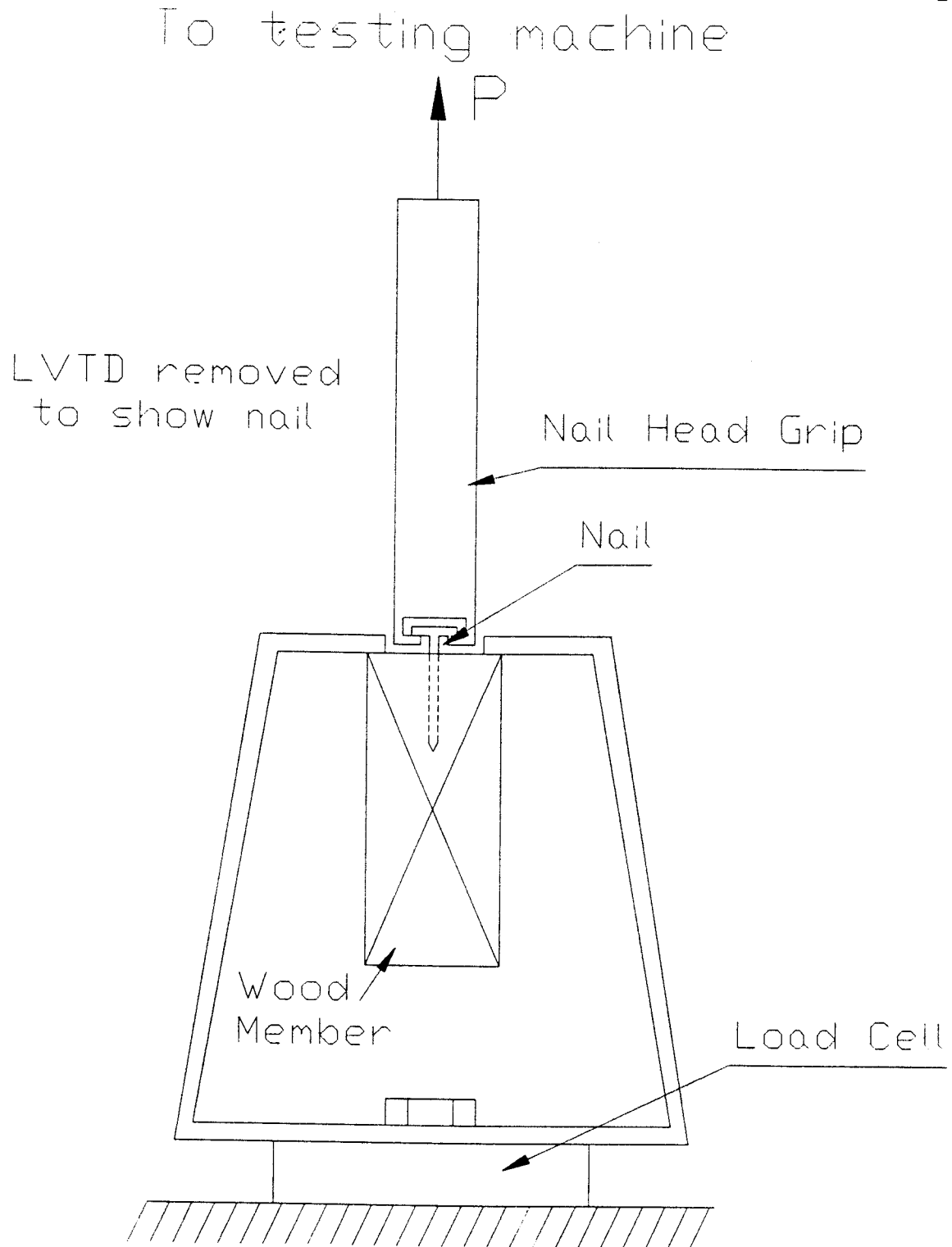
Figure 3-4. Testing apparatus for nail withdrawal tests.
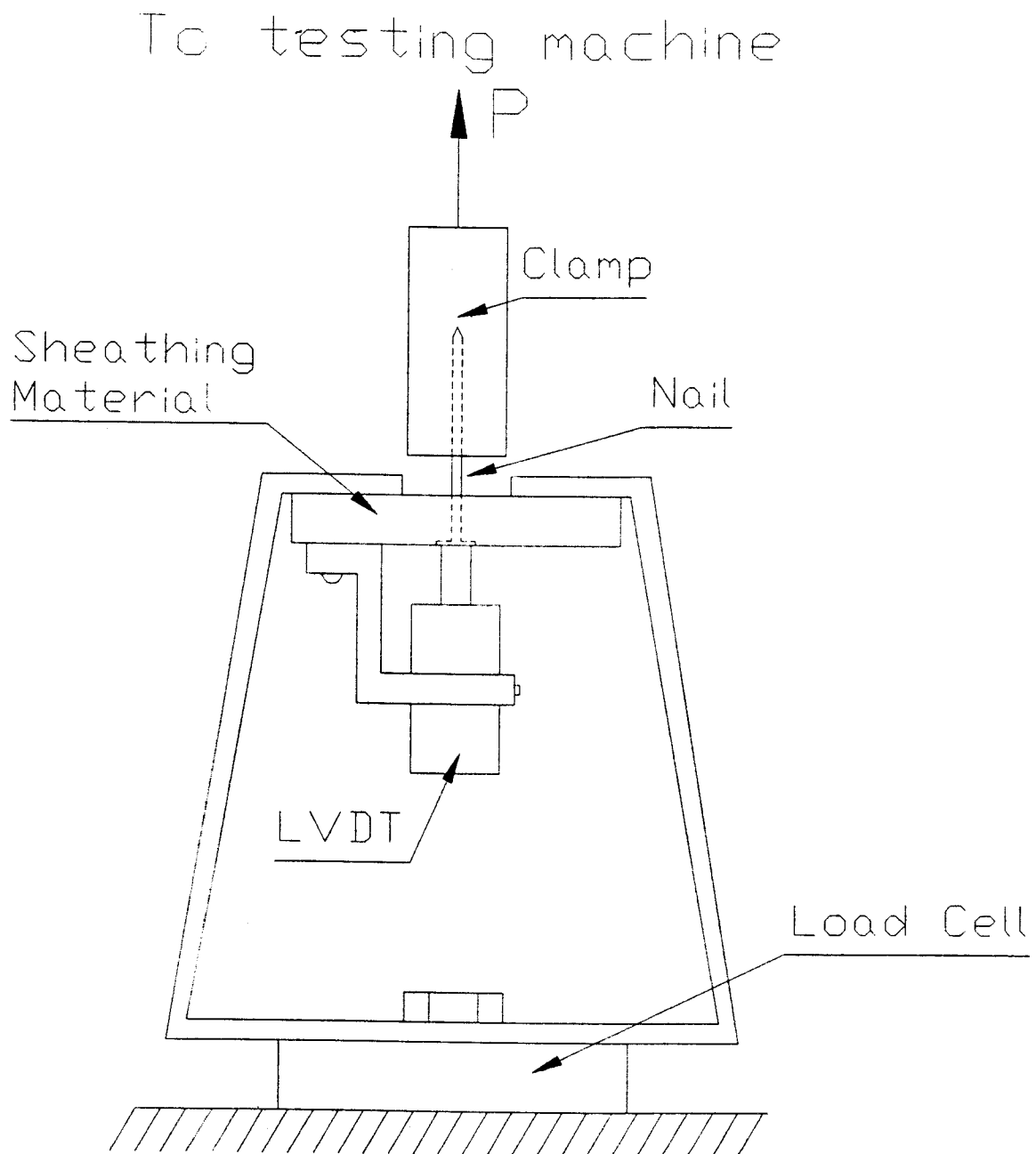
Figure 3-5. Testing apparatus for nail-head pull-through
tests.

Withdrawal

For the withdrawal tests, two LVDTs were mounted on the shaft that connected the nail-head grip to the cross head of the testing machine. The testing machine was operated at a constant rate of 0.01 in./min. Loads and displacements were recorded with a computer-controlled data acquisition system, which took readings at a rate of one reading/sec. The displacements of the two LVDTs were averaged and reported as a single number. Fifteen replicates were tested for each joint type.

Since the method of driving a nail is known to influence the characteristics of the joint (Phillips 1990, Polensek 1988), the nails were hand driven to match the conditions of the real structure. The nails were driven into the side grain without deference to radial or tangential orientation. A portion of the nail shank was left exposed from the wood to account for the metal, sheathing and/or stud through which it would have passed.

The Wood Handbook (FPL 1987) shows a typical nail withdrawal curve for a nail driven into Douglas-fir. This curve has a kink in the initial portion of the curve which would lead one to think that the joint stiffens at a certain load. After performing several withdrawal tests, two load-withdrawal patterns developed. One pattern followed the curve shown in the Wood Handbook, and the other pattern was linear up to a proportional limit. Close examination of

specimens being tested revealed that the kink, which formed in some of the tests, was a result of specimen settlement in the test apparatus. The wood was not fixed in the apparatus and may not have made complete contact with the steel testing fixture. The specimen settlement was caused by an imperfect fit of the wood member in the fixture, or because the nail was not quite perpendicular to the wood member. After the specimen settled under some load, the withdrawal curve was accurate. Since the curves that had no settlement problems were linear to a proportional limit, the curves with the kinks were adjusted. The initial portion of the curve, which represented the stiffness of the settlement and nail withdrawal combined, was disregarded, and the remaining portion of the curve was shifted to the left so that the actual nail withdrawal stiffness started from the origin. This is shown in Figure 3-6.

The plotted load-displacement data, shown in Appendix A, indicated that the nails had linear load-displacement relations up to a proportional limit where the relationship became nonlinear as the load approached the maximum value, as shown in Figure 3-6, after which the curve would either level off, or begin to degrade slightly. Since the finite-element models required that all the slopes of the nonlinear constitutive relations were non-negative, the final portions of the curves were assumed to be flat. The relationship between the applied load and the resulting withdrawal was
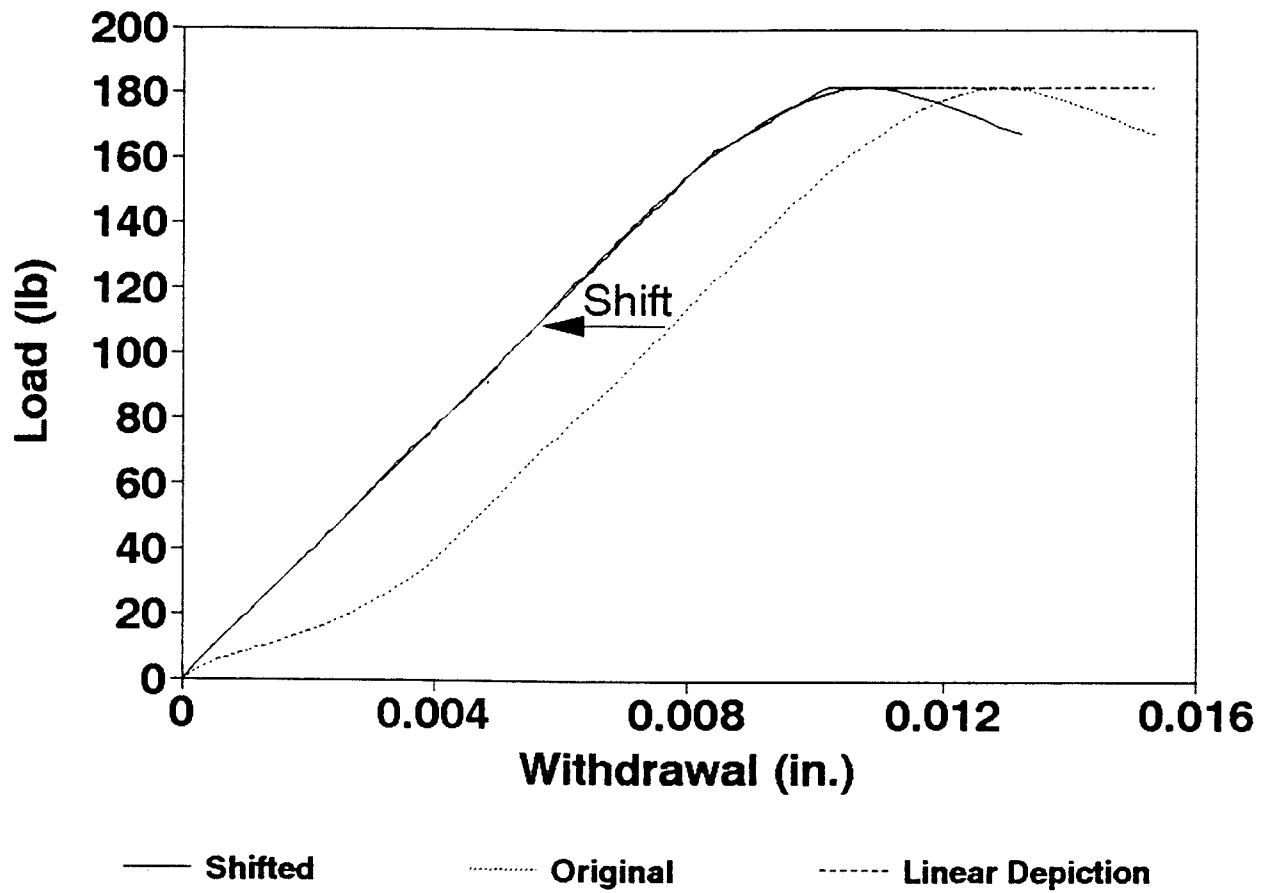
Figure 3-6. Typical nail-withdrawal curve.

represented by the initial stiffness, proportional limit,

maximum withdrawal load, and the withdrawal at the maximum

load. This information is given in Table 3-2.

Table 3-2. Load-Displacement Results from Withdrawal Tests, n=15.

Nail[a] Shaft Exposed	Initial Stiffness (lb/in.)	Proportional Limit (lb)	Maximum Load (lb)	Withdrawal at Maximum Load (in.)
JHN				
.2	45950(14950)[b]	185(39)	251(47)	.0080(.0038)
6d				
$\frac{1}{2}$	45540(8885)	240(62)	299(94)	.0079(.0022)
8d				
.2	37930(14590)	164(29)	241(49)	.0098(.0019)
$\frac{1}{2}$	23820(9267)	153(31)	181(30)	.0100(.0038)
10d				
$1\frac{1}{2}$	35160(16810)	154(39)	194(28)	.0096(.0037)
2	25390(12710)	88(20)	117(23)	.0070(.0018)
16d[c]				
$1\frac{1}{2}$	35600(8037)	218(43)	218(43)	.0066(.0022)
2	38630(23940)	202(55)	202(55)	.0064(.0025)

[a] Shaft exposed in inches.

[b] Parentheses indicate standard deviation.

[c] Sudden failure occurred in each test, therefore Proportional Limit and Maximum Load are the same.

Pull-through

When a joint is loaded such that a tensile load exists

causing a separation between the sheathing and base

material, the nailhead may be drawn through the sheathing.

Embedment of the nail head occurs if the bearing stress

created by the tensile load and bearing area of the nailhead

exceeds the compression strength of the sheathing. The nail

head may embed itself into the sheathing material, and

eventually pull-through if the nail does not first withdraw completely from the base material. The pull-through mechanism is an important characteristic of light-frame behavior.

For the pull-through test the nail was hand driven until the head was flush with the sheathing material. The specimen was then placed in the testing fixture, and the nail shaft was held fixed in a clamp fastened to the testing machine. One LVDT was mounted on the bottom side of the plywood. The core of the LVDT rested on the head of the nail so as to follow the movement as the test progressed. The testing apparatus is shown in Figure 3-5. The testing parameters and data acquisition set-up were the same as the withdrawal tests. Fifteen replicates for each nail type (6d, 8d and drywall nail) were performed.

Two types of curves were obtained from the pull-through tests. The gypsum sheathing produced curves that are best represented with bi-linear curves until failure, and the plywood sheathing is best represented with tri-linear curves. Typical curves are shown in Figures 3-7 and 3-8.

For the purpose of the finite-element model, the pull-through of the drywall nail through the gypsum can be described using the same points on the load-displacement relationship as for the withdrawal curve, and the data are listed in Table 3-3.
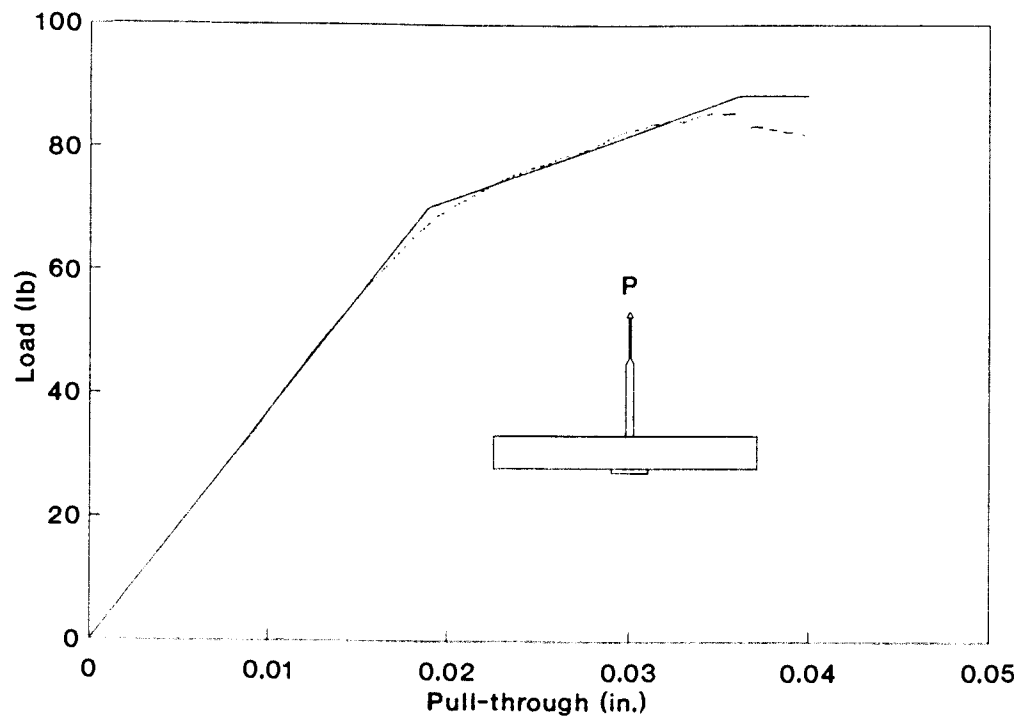
Figure 3-7. Typical nail-head pull-through curve of a
drywall nail passing through ½-in. gypsum board.
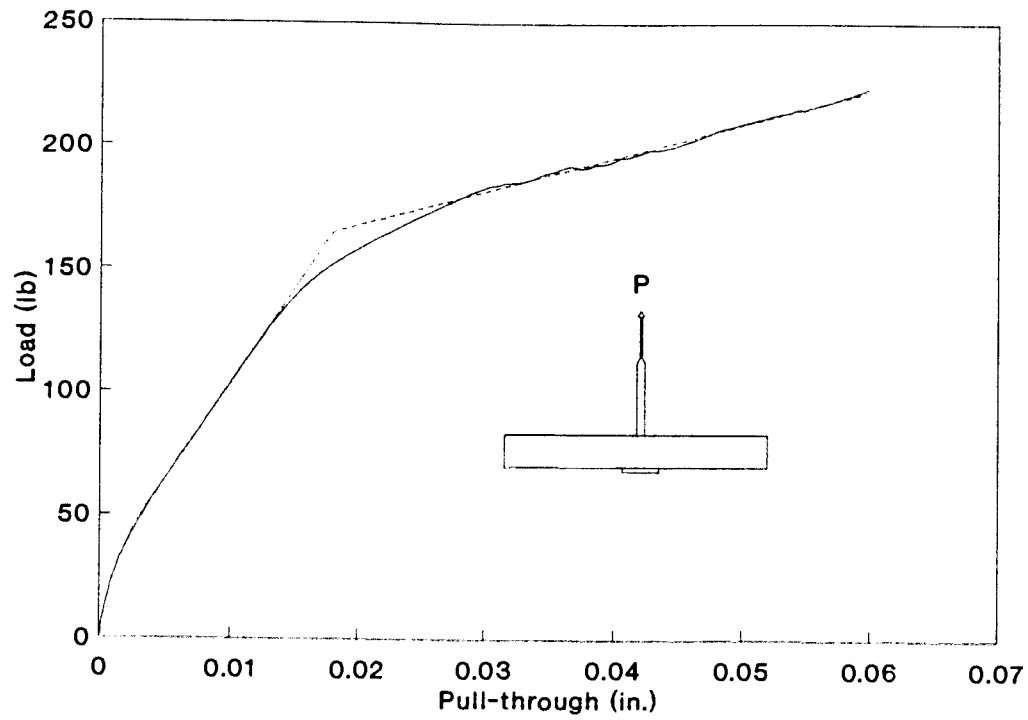
Figure 3-8. Typical nail-head pull-through curve of an 8d
nail passing through ½-in. exterior plywood sheathing.

The pull-through of the 6d and 8d nails were carried out until a displacement of 0.06-in. was reached. These curves required five variables to describe their tri-linear representation. The results are listed in Table 3-4.

Table 3-3. Load-Displacement Results of Pull-through Tests of a Drywall Nail Through ½-in. Gypsum Board Sheathing, n=15.

Nail	Initial Stiffness (lb/in.)	Proportional Limit (lb)	Maximum Load (lb)	Pull-through at Maximum Load (in.)
Drywall	4120(1030)[a]	61(12)	84(12)	.0157(.0044)

[a] Parentheses indicate standard deviation.

Table 3-4. Load-Displacement Results of Pull-through Tests of 6d and 8d Nails Through ½-in. Exterior Sheathing, n=15.

Nail	Initial Stiffness (lb/in.)	Proportional Limit (lb)	Second Stiffness (lb/in.)	Second[a] Load (lb)	Third Stiffness (lb/in.)
6d	18720(3586)[b]	77(35)	7684(1525)	176(38)	1418(504)
8d	16940(3609)	56(15)	6912(1320)	175(56)	1434(433)

[a] Second load indicates the load at which the third stiffness starts.
[b] Parentheses indicate standard deviation.

4. WALL-TO-FOUNDATION CONNECTION

The finite-element model of the complete structure requires the characteristics of the wall-to-foundation intercomponent connection. However, the connection includes many degrees of freedom, some of which are nonlinear. Thus, a reduced form with fewer degrees of freedom but the same behavioral characteristics is needed.

The connection, shown in Figure 4-1, was used to connect the transverse exterior walls to the floor system in the full-scale test by Phillips (1990). The wood used for the construction was Douglas-fir. A 2×6 (nominal) was used for the sill plate, and the floor joist and rim joist were 2×10's. The interior sheathing was ½-in. gypsum, and the exterior sheathing was ½-in. T1-11 exterior plywood siding. The sill plate was bolted to a concrete floor with 1-in. bolts spaced 2 ft on center to provide a rigid connection. Since the exterior sheathing did not extend to cover the sill plate, Simpson 66T T-straps were installed every 4 ft to provide added stiffness. The T-straps were 14 gauge, galvanized steel, and fastened with four-16d nails in the sill plate and three-16d nails in the rim joist.
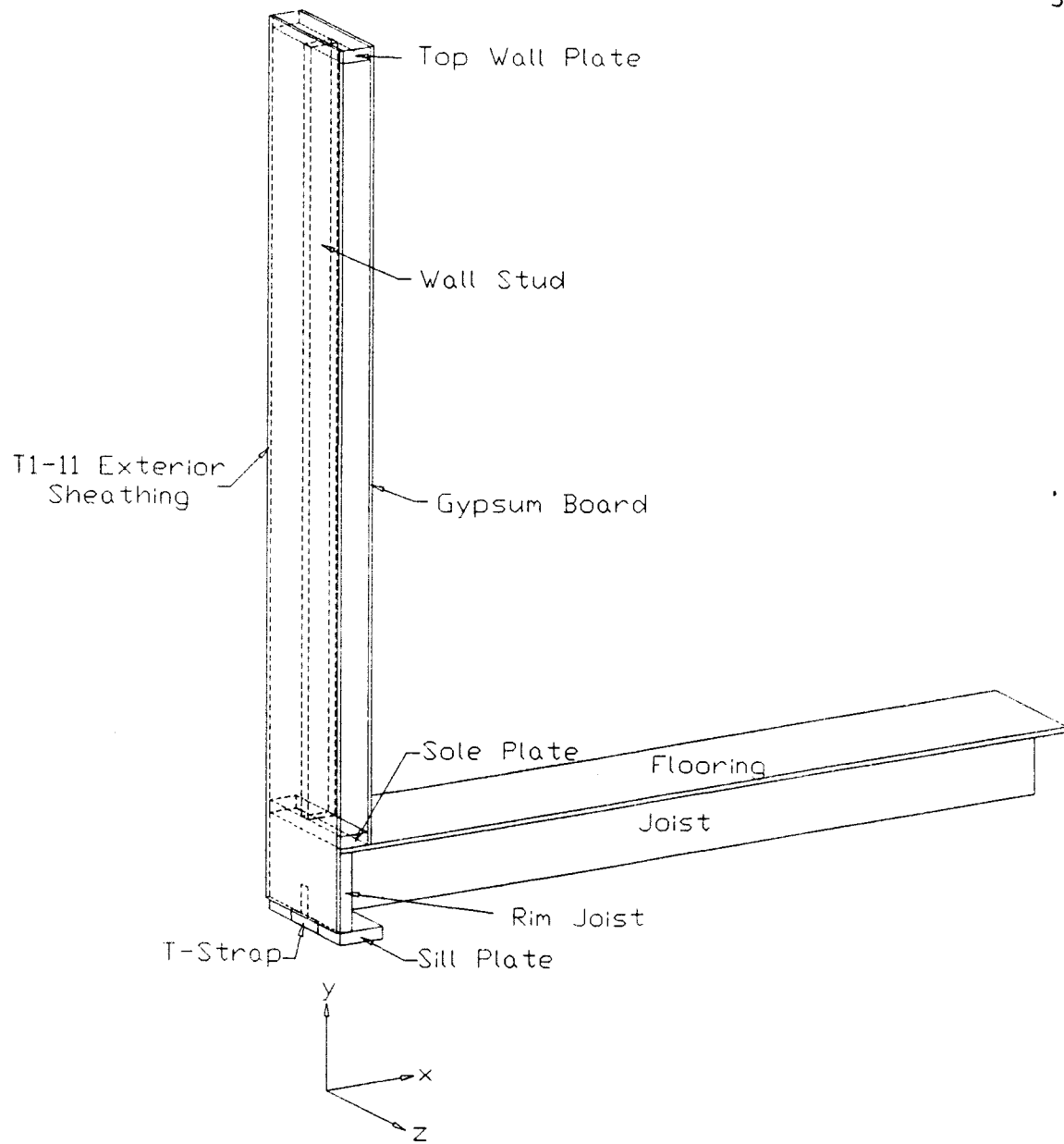
Figure 4-1. Exterior wall-to-foundation connection used in the full-scale structure test.

<u>Wall-to-Floor Connection Experimental Procedure</u>

The experimental data are from the work by Polensek and Schimel (1986). A summary of their relevant experimental procedures and results are outlined here.

Polensek and Schimel tested the rotational restraint of a 16-in. wide section of a wall-to-foundation connection. The testing followed three phases. Phase I was the nondestructive testing of the 91-in. Douglas-fir studs to determine their E. Phase II, the assembled panels were nondestructively tested in flexure to define the composite panel stiffness. The panels consisted of Douglas-fir studs with ⅜-in. exterior plywood and ½-in. gypsum sheathing nailed to either side. The test panel was simply supported and loaded by a line load at midspan. Phase III tests used phase II panels nailed to a sill and header to provide rotational restraint (Figure 4-2). Rigid boundaries were established by fixing the top and bottom of each assembled panel to two steel back plates; one was free to move horizontally, and one was fixed. Five different panels from phase III were loaded until a midspan deflection of 2-in. was reached or until rupture occurred.

Each panel in the phase II and III tests had a different nail pattern. Of the five patterns tested, panel 5 had the nail pattern most like that used in the actual wall system shown in Figure 4-1, and therefore, panel 5 was
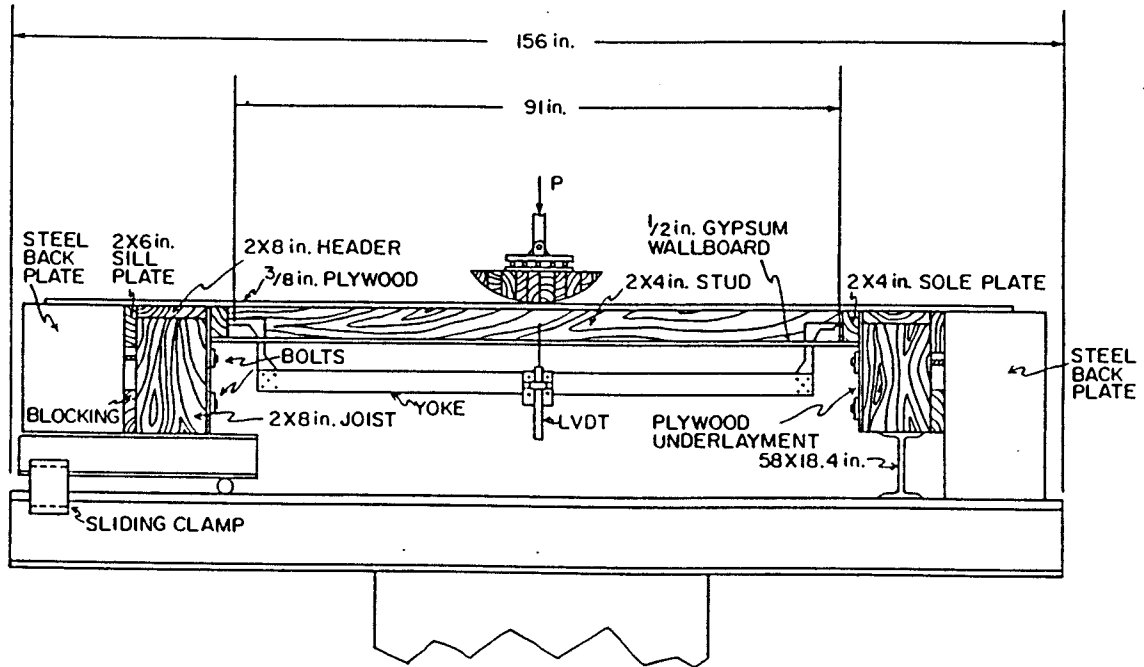
Figure 4-2. Construction of completed phase III panel (Polensek and Schimel 1986).

selected as the verification case. The results of the midspan deflection as a function of the load are shown as a solid line in Figure 4-3.

Analytical Procedure

Two different finite-element models were developed assuming plane stress conditions. The first finite-element model was developed to verify the analysis procedure. Experimental information for panel 5 from Polensek and Schimel (1986) were used. The second model represented the wall-to-foundation connection as used in the full structure. This model is very similar to the verification model, but slightly different material properties and geometries are used. For each of the detailed two-dimensional finite-element models for the wall-to-foundation intercomponent connection, all of the essential details and degrees of freedom were included.

In nonlinear analysis, the global stiffness matrix is reformed after each iteration, which increases the time needed to solve nonlinear problems. The iterative solution phase followed the Newton-Raphson technique. The load-displacement and moment-rotation results of the second detailed finite-element model were subsequently used at the connection characteristics in the full-structure finite-element model.
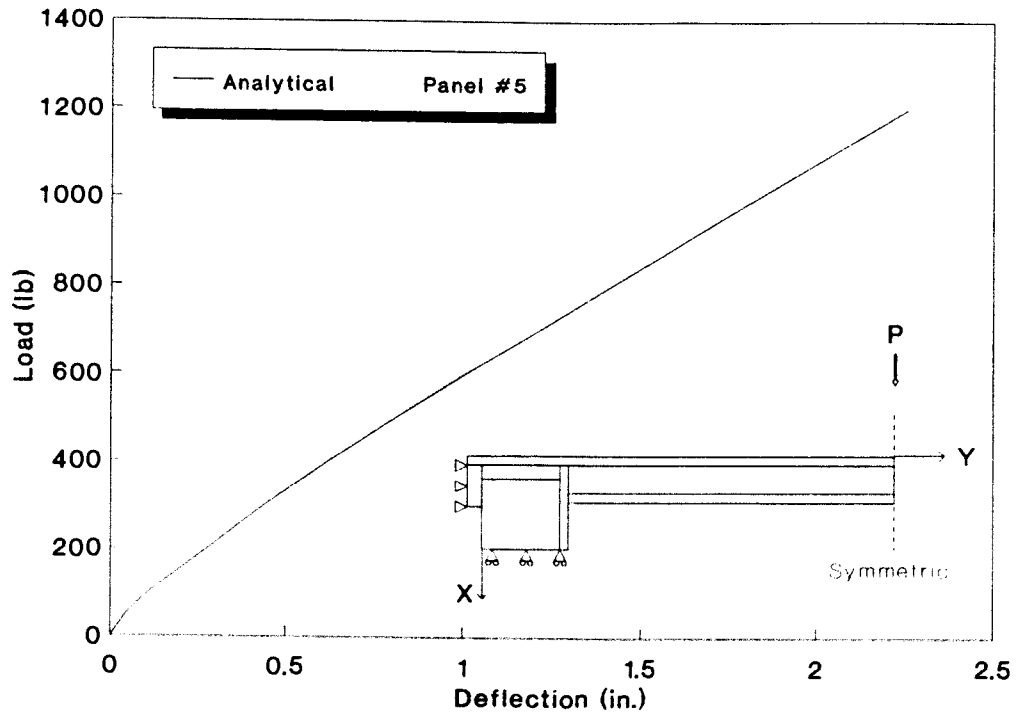
Figure 4-3. Midspan load-deflection relation of the wall assembly due to a concentrated load at midspan.

The Wood

The wood was modeled with four- and eight-node plane stress isoparametric solids. The four-node element is shown in Figure 4-4. Each node had two degrees of freedom, translation in the nodal x and y-directions. Material properties consisted of two moduli of elasticity (E_x and E_y), Poisson's ratio (μ_{xy}) and the shear modulus (G_{xy}). The thickness of each material was also needed to complete the element definition. For the verification model all material properties were taken from bending and coupon tests performed by Polensek and Schimel (1986).

For the model of the wall-to-foundation connection used in the full-scale test, the material properties of the framing members are based on the longitudinal E, E_L, obtained from Phillips (1990). Bodig and Jayne (1982) provided Poisson's ratios for softwoods, $\mu_{LR} = 0.37$, $\mu_{LT} = 0.42$, $\mu_{RL} = 0.041$, $\mu_{TL} = 0.033$, $\mu_{RT} = 0.47$ and $\mu_{TR} = 0.35$, where L, R and T represent longitudinal, radial and tangential directions respectively. Using symmetry of the compliance matrix, the E in the radial, E_R, and tangential, E_T, directions can be calculated from:

$$E_R = E_L * \frac{\mu_{RL}}{\mu_{LR}}$$

<div align="right">4-1</div>
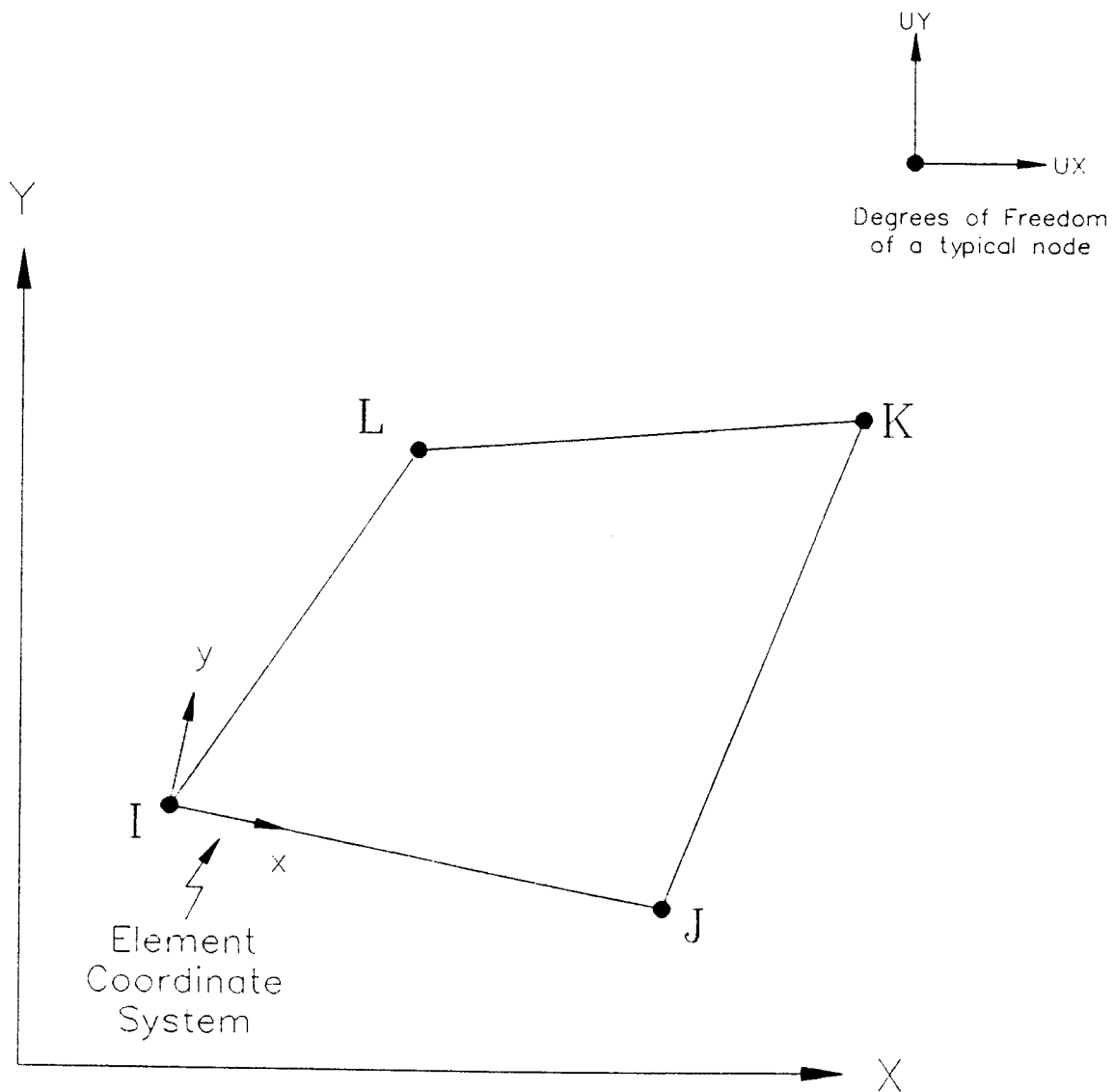
Figure 4-4. Four-node plane stress isoparametric solid used to model wood and sheathing.

$$E_T = E_L * \frac{\mu_{TL}}{\mu_{LT}} \qquad\qquad 4-2$$

The shear moduli, G_{ij} were calculated internally by:

$$G_{LR} = \frac{E_L E_R}{(1 + 2\mu_{LR}) E_L + E_R} \qquad\qquad 4-3$$

$$G_{LT} = \frac{E_L E_T}{(1 + 2\mu_{LT}) E_L + E_T} \qquad\qquad 4-4$$

$$G_{RT} = \frac{E_R E_T}{(1 + 2\mu_{RT}) E_R + E_T} \qquad\qquad 4-5$$

The material properties of the flooring and sheathing used in the full-scale test were not determined, therefore the material properties of the verification model were used. This was justified because Polensek (1978), showed that errors in properties of wall coverings has little effect on final results.

The T-Straps

The T-straps that connected the rim joist to the sill plate was modeled with a two-dimensional elastic beam. The individual elements were defined by two nodes. Each node had three degrees of freedom, translations in the x and y-directions and rotation about the z-axis. The cross sectional area, depth, and bending moment of inertia, I_{zz}, were included with the material properties E_x, μ_{xy}, and G_{xy}.

The Nails

The nails were modeled with a two-node, nonlinear, load-deflection element as shown in Figure 4-5. The element can be thought of as a spring that either elongates under tension or shortens under compression. These elements had only one degree of freedom at each node, a translation along the nodal coordinate axis, the direction of which is defined by the user. The load-deflection relation was defined by a piece-wise linear curve. Each nail required two load-deflection elements to define it: one for shear either parallel or perpendicular to the grain depending on the orientation of the wood, and one for withdrawal or pullthrough mode. The nail element was defined by using a node from two adjacent materials. For example, a node from the gypsum and a node from the stud were used to form a nail
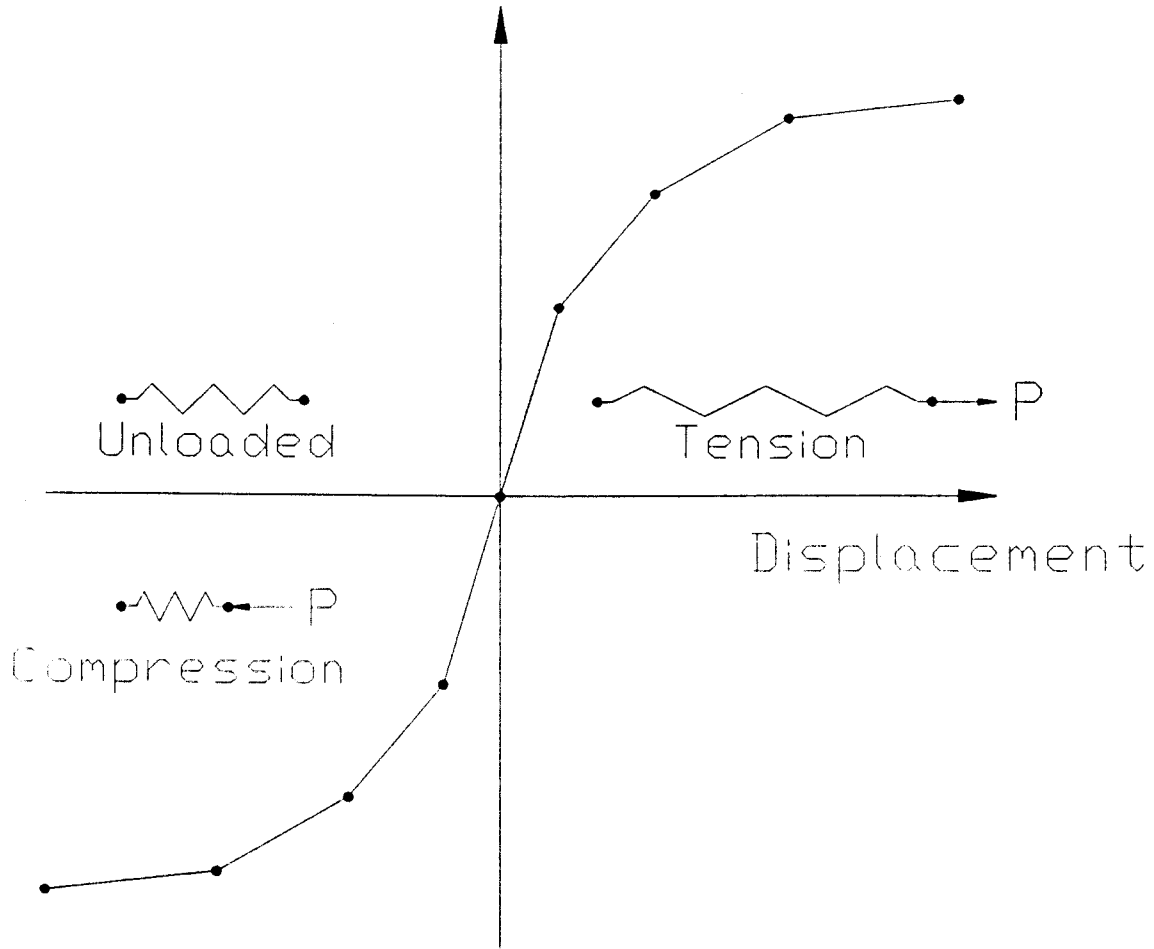
Figure 4-5. Two-node, nonlinear, load-displacement element used to model nails and gaps.

element connecting the two materials. Both nail elements share the same set of nodes.

The load-slip and load-withdrawal curves were defined by three or four pairs of coordinates from the piece-wise linear curves obtained from nail testing described in Chapter 2. The coordinates used in the verification model for shear and withdrawal at each joint are shown in Table 4-1.

The Gaps

A load-deflection element with a high compressive resistance (1×10^7 lb/in.) and little or no tensile resistance (1×10^{-3} lb/in.) was used to model the gaps; this ensured that the materials did not overlap when loaded in compression, but could separate in tension.

The Assembled Models and Results

Verification Model

The verification model consisted of 205 nodes, each with a capability of having 2 degrees of freedom, depending on boundary conditions. The nodes were assembled into a total of 274 elements with a total of 192 degrees of freedom. Of those, 125 were plane stress elements representing the wood and sheathing materials, 74 were

Table 4-1. Load-Displacement Curves for Shear and Withdrawal used in the Verification Model[a].

Joint	Shear		Withdrawal	
	Slip	Load	Withdrawal	Load
Stud-Plywood	0	0	0	0
	.0009	90.1	.0278	253
	.0224	178	2	254
	.1003	241		
Stud-Gypsum	0	0	0	0
	.002	30.8	.027	30
	.03	70.0	2	31
	.120	94.9		
Stud-Sole Plate	0	0	0	0
Joist-Rim Joist	.1092	240	.0229	277
	.3707	392	2	278
	.6077	639		
Joist-Subfloor	0	0	0	0
	.0009	90.1	.0278	253
	.0224	178	2	254
	.1003	241		
Joist-Sill Plate	0	0	0	0
	.0038	65	.0055	154
	.0131	130	.0096	194
	.0337	190	2	195
	.0868	260		
Sole Plate-	0	0	0	0
Subfloor-Rim	.0026	78	.0278	253
Joist	.0290	165	2	254
	.1011	214		

[a] Polensek and Schimel 1986.

nonlinear load-deflection elements representing the 37 nails in the model, with the remaining 75 being gap elements. The finite-element mesh is shown in Figure 4-6. The nailing schedule used in the verification model is shown in Table 4-
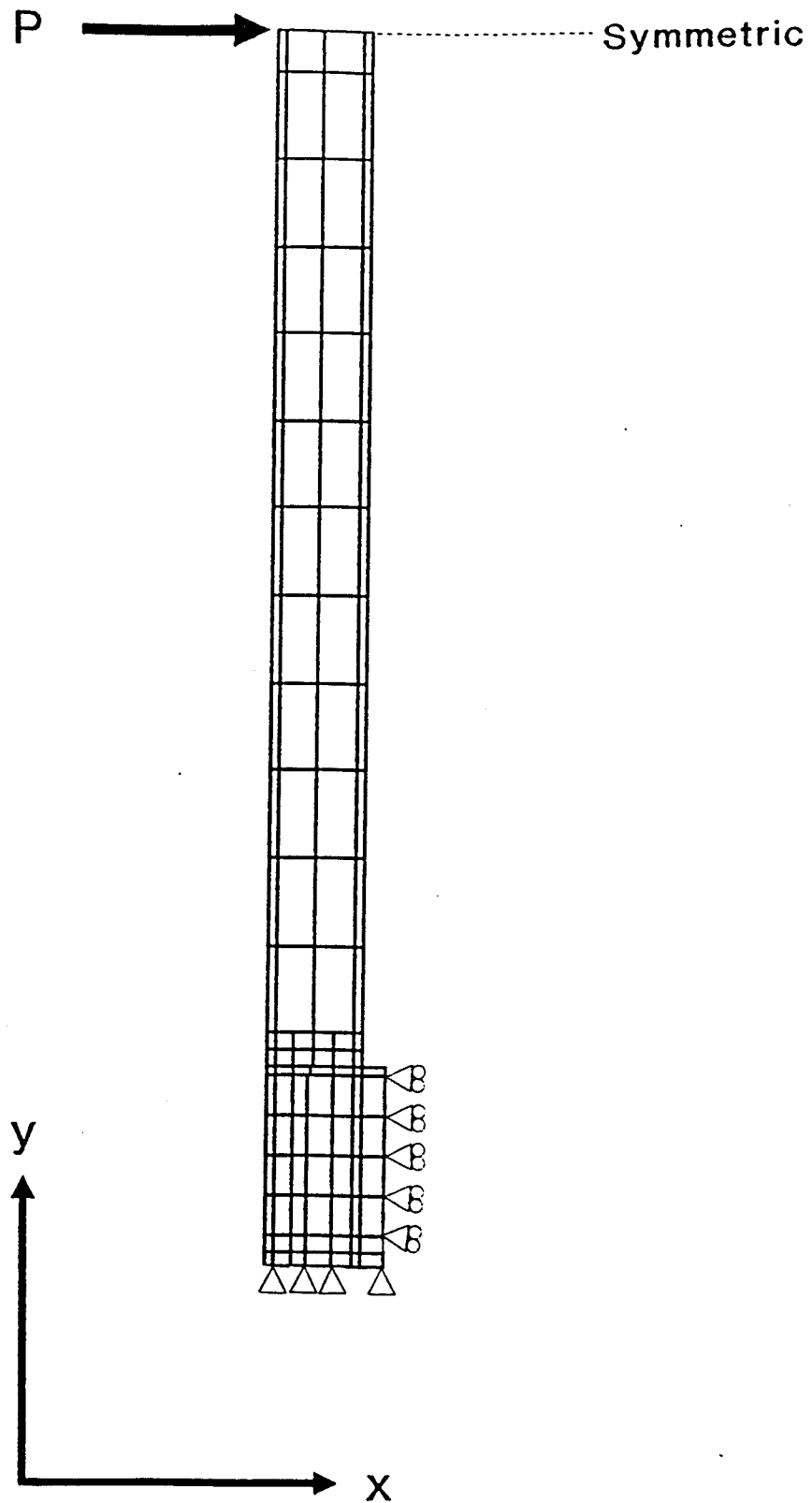
Figure 4-6. Finite-element mesh used for the verification connection model.

2. The top of the mesh represents the symmetry line of the

Table 4-2. Nailing Schedule used for Verification Model[a].

Joint	Nail type	Configuration	number/spacing
Stud-Plywood	6d	face nail	12 in.
Stud-Gypsum Board	4d drywall	face nail	8 in.
Stud-Sole Plate	16d	end nail	two
Joist-Flooring	8d	face nail	6 in.
Joist-Rim Joist	16d	end nail	two
Joist-Sill Plate	10d	toe nail	two
Sole Plate- Subfloor-Rim Joist	16d	face nail	16 in.

[a] Polensek and Schimel 1986.

test by Polensek and Schimel. The boundary conditions

(shown on Figure 4-2) at the line of symmetry were fixed in

the y-direction to model the symmetric condition. The joist

and sill plate were allowed to slide in the test, but were

restrained against rotation, therefore the joist and sill in

the finite-element model were only fixed in the x-direction.

The loading was accomplished by applying a point load

in the positive x-direction to the uppermost left node.

Twenty-two load steps were imposed to ensure a smooth load-

deflection curve was obtained. The analysis was run on a

microcomputer which had a 25 MHz 80386 processor with a math

coprocessor and took about 1 hr to run.

The resulting load-deflection curve is shown in Figure

4-3 as the solid line. The test panel required a load of

1140 lb to produce a deflection of 2 in. The finite-element

model required 1100 lb to produce the same results, which is only a 3.5% error.

This model showed that the process of using the two-dimensional plane stress elements in conjunction with the nonlinear load-deflection elements produced adequate results when predicting rotational stiffnesses of intercomponent connections.

Full-structure connection model

The connection used in the full-scale structure tested is very similar to that of the verification model. Therefore, the same procedure was used with some degree of confidence. The finite-element mesh was modified slightly to accommodate the different member sizes and boundary conditions; however it was felt that the method used was still valid and did not require separate verification tests.

The finite-element mesh used for the full-structure connection model is shown in Figure 4-7. The model consisted of 399 elements, which when assembled yielded a model with 329 nodes. There were 183 plane-stress elements of which the majority were the four-node type. The eight-node elements were used as transition elements to go from a coarse mesh to a finer mesh, for example, where the wall stud met the sole plate. There were 110 nail elements representing 55 nails, and the remaining 106 elements were gap elements. The nailing schedule and load-displacement curves used in the model of the full-scale house connection
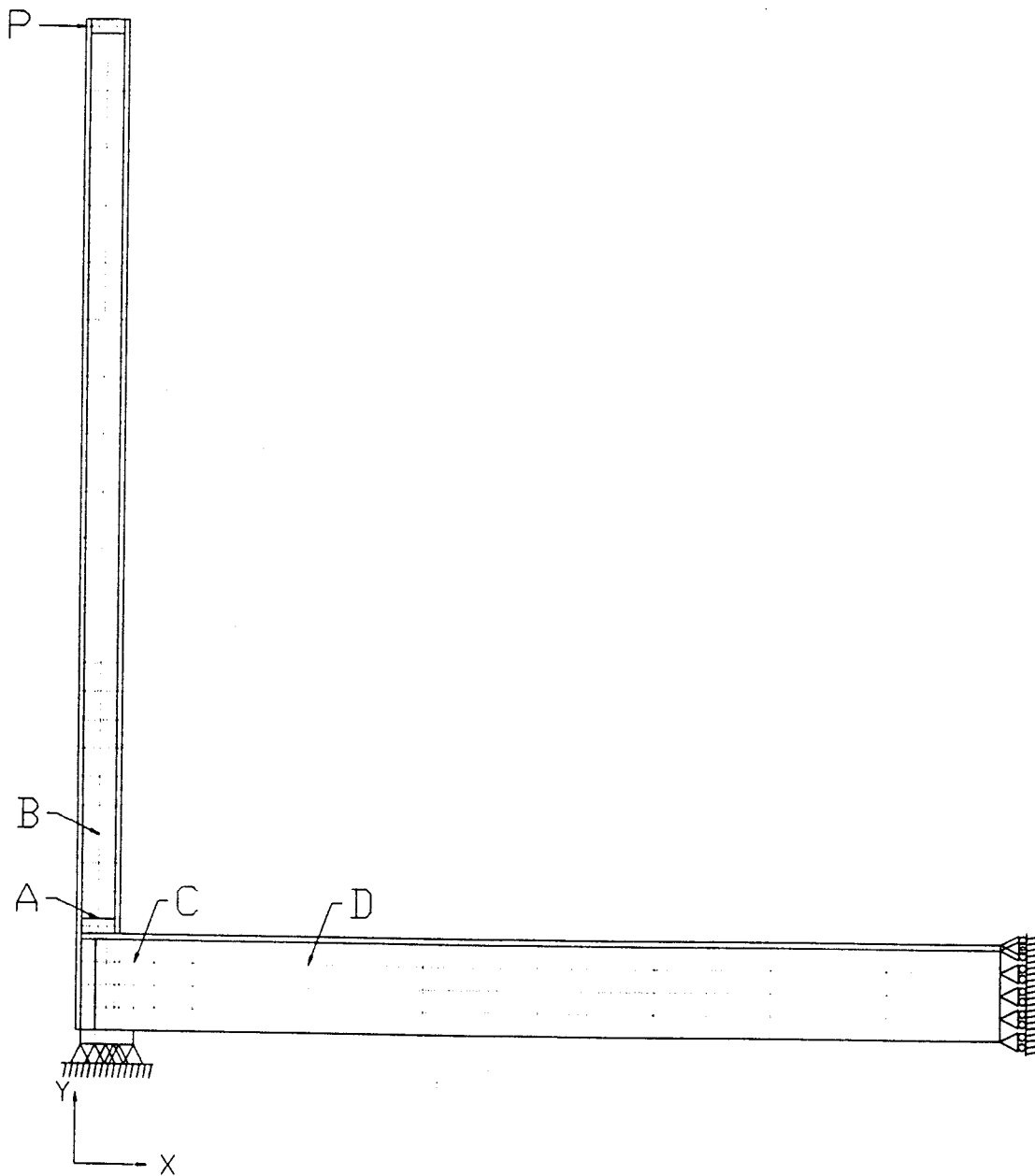
Figure 4-7. Finite-element mesh used for the full-scale structure connection model.

are shown in Tables 4-3 and 4-4.

Table 4-3. Nailing Schedule used for the Full-Structure Connection Model[a].

Joint	Nail type	Configuration	number/spacing
Stud-Plywood	6d	face nail	12 in.
Stud-Gypsum	No. 11	face nail	7 in.
Stud-Sole Plate	16d	end nail	two
Joist-Flooring	8d	face nail	10 in.
Joist-Rim Joist	16d	end nail	three
Joist-Sill Plate	10d	toe nail	two
T Strap-Rim Joist	16d	face nail	three
T Strap-Sole Plate	16d	face nail	four
Sole Plate- Flooring-Rim Joist	16d	face nail	8 in.

[a] Phillips 1990.

When comparing this model to the verification model, the two obvious changes are the extension of the floor, and the wall. It was felt that the floor would have a contribution to the overall displacements of the connection. Therefore, the floor was extended to one half of the total span. Any contributions offered after that were felt to be negligible. Since this connection was not symmetric, the wall was extended to its full height. The top wall plate was added to make the model complete.

The bottom row of nodes on the sill plate were fixed in both the x and y-directions. The nodes at the cut end of the floor were held in the x-direction only and were allowed to slide freely in the y-direction.

Table 4-4. Load-Displacement Curves for Shear and Withdrawal used in the Full-Structure Connection Model.

Joint	Shear		Withdrawal	
	Slip	Load	Withdrawal	Load
Stud-Plywood	[a]		0	0[b]
			.0063	80
			.0210	170
			.0249	180
			.0570	240
Stud-Gypsum	[c]		0	0[b]
			.018	60
			.031	80
			1	81
Stud-Sole Plate	0	0	0	0[d]
Joist-Rim Joist	.0011	130	.01	188
	.0030	260	1	189
	.0056	390		
Joist-Subfloor	0	0	0	0[b]
	.02	65	.006	54
	.06	125	.029	172
	.16	224	.035	181
	.20	256		
Joist-Sill Plate[e]	0	0	0	0
	.0038	65	.0055	154
	.0131	130	.0096	194
	.0337	190	2	195
	.0868	260		
Sole Plate-	0	0	0	0
Subfloor-Rim	.0170	80	.0064	202
Joist	.0476	160	1	203
	.0872	240		
	.1338	320		
	.1855	400		

Unless otherwise noted, the data is from Phillips 1990.
[a] Jenkins et al. 1979. Load = (875*Slip + 140)[1-exp(-250*Slip)]
[b] Combined withdrawal and pullthrough.
[c] Jenkins et al. 1979. Load = (160*Slip + 61)[1-exp(-250*Slip)]$^{2.5}$
[d] Polensek and Bastendorff 1987.
[e] Polensek and Schimel 1986.

Moment-rotation relation. The moment-rotation relation
for the exterior wall closing on the foundation was obtained
by applying 21 load steps to the top of the wall in the
positive x-direction. The top plate of the wall was held
against rotation by coupling the nodes in the y-direction.
This allowed the top plate to move in any direction, but it
would remain horizontal. This, in conjunction with the two
16d nails fastening the stud to the top plate, provided the
necessary boundary conditions.

The moment was obtained by multiplying the applied load
(P) by the distance to the flooring, 95.125-in. The
rotation was obtained by dividing the differences in x-
translation of nodes A and B by their distance from each
other to calculate the rotation of the stud. From this the
rotation of the foundation was subtracted by following a
similar procedure for nodes C and D. This gave the relative
rotation for the wall to the foundation.

The displaced structure is shown in Figure 4-8. The
connection details at the bottom and top of the wall are
shown in Figures 4-8b and c, and in these it can be seen
that much of the rotation is attributable to the joint slip
between the exterior sheathing and the rim joist. This
allowed the wall to pivot about the sole plate.

The moment-rotation relation for the exterior wall-to-
foundation connection opening (counter clockwise rotation of
the wall) was obtained in a similar fashion, but the 21 load

Figure 4-8. Displaced structure for the closing of the connection of the full-scale structure. a) full model, displacement scale = 1. b) wall-to-foundation connection, displacement scale = 2. c) wall-to-top plate connection, displacement scale = 2.

steps were applied to the opposite side of the wall in the negative x-direction. All boundary conditions were the same. The same nodes were used to calculate the rotations of the wall and foundation

The displaced structure of the connection opening is shown in Figure 4-9. The close up of the connection shows that nail slip did not play a major role. Most of the rotation was a result of nail withdrawal between the sole plate and floor, and between the exterior sheathing and the wall stud under bending.

The final moment-rotation diagram is shown in Figure 4-10. As can be expected, the closing resistance was stiffer than the opening resistance. This is because the loads for opening rotations are resisted by nail withdrawal. Little contribution from nail shear occurs when the connection is opening.

Load-uplift relation. The load-uplift relation was obtained by applying 21 load steps in the positive y-direction to the top of the wall stud. Since the connection was stiffer when trying to close, the connection had a tendency to open when loaded to find the uplift resistance. To combat this the top of the wall was held in the x-direction; this eliminated any rigid body rotations that would have occurred with an uplift load. However, the wall was allowed to slide freely in the y-direction.
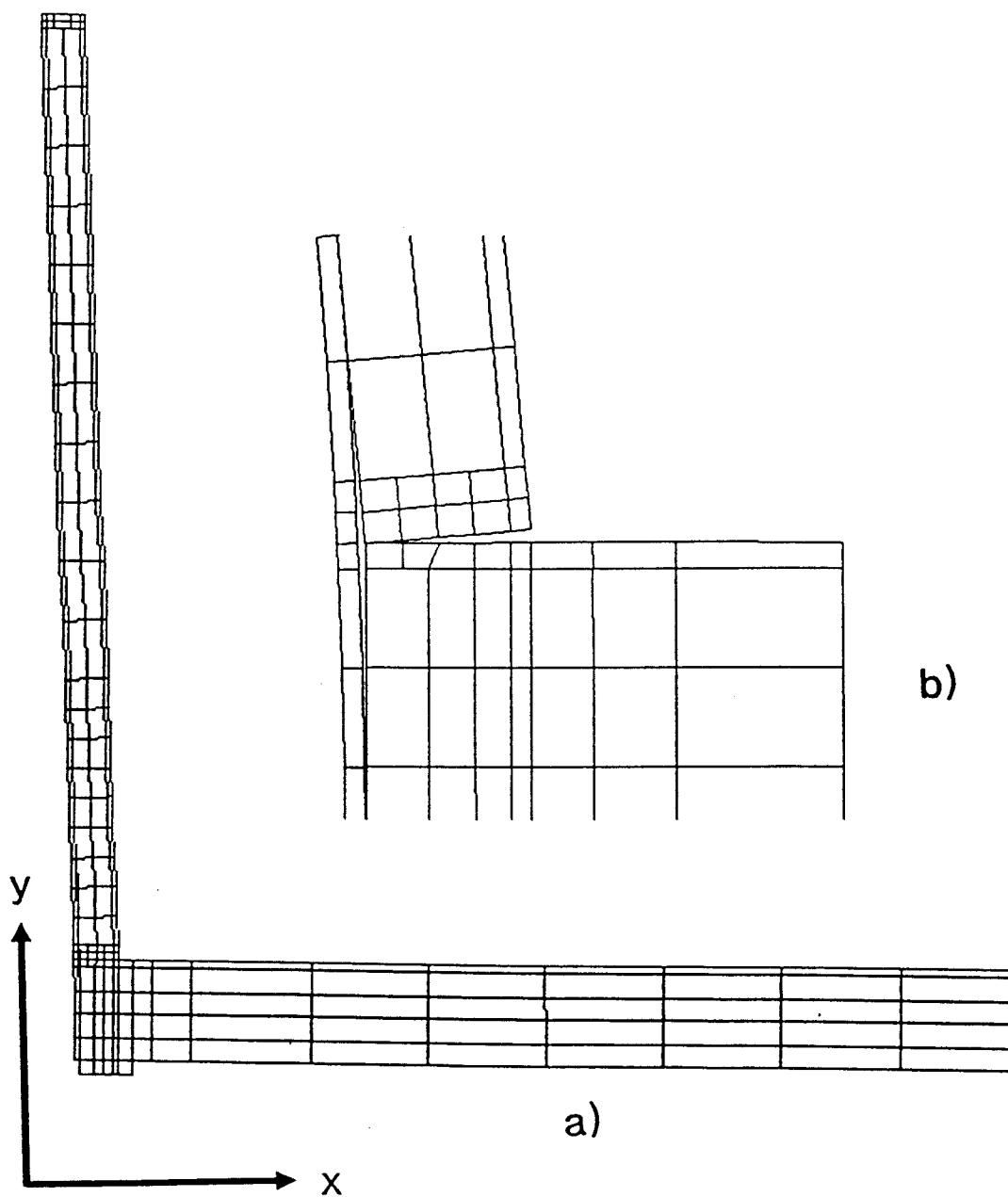
Figure 4-9. Displaced structure for the opening of the connection of the full-scale structure. a) full model, displacement scale = 1. b) detail, displacement scale = 2.
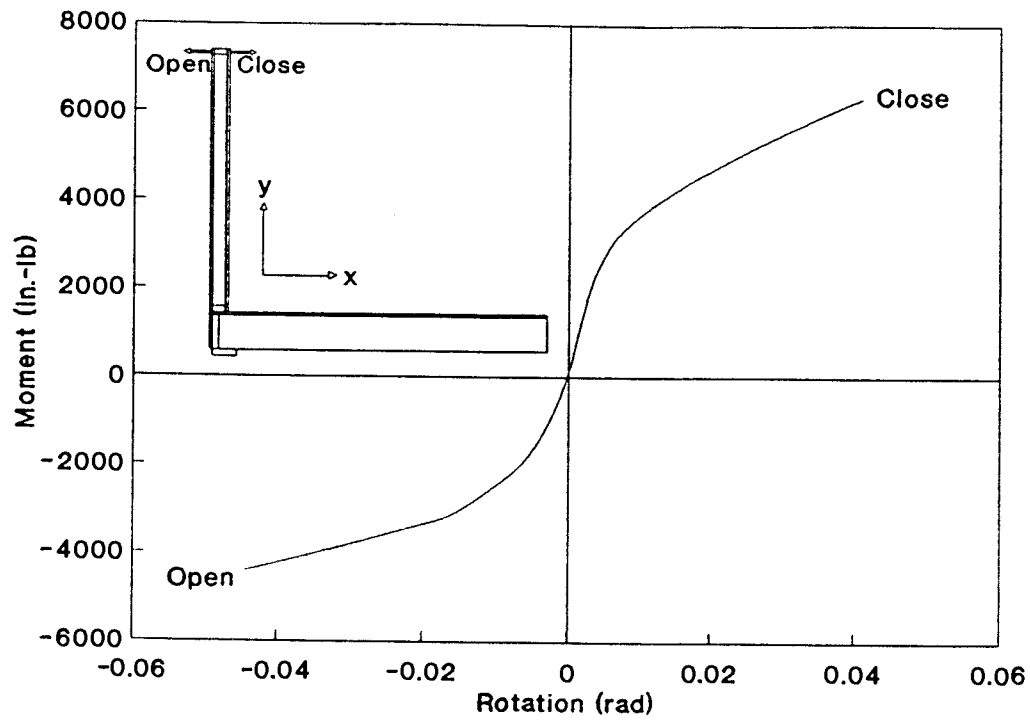
Figure 4-10. Characteristic moment-rotation curve for the exterior wall-to-foundation connection used in the full-scale structure.

Looking at the displaced structure in Figure 4-11 it can be seen that the separation of the floor joist from the sill plate was a major contributor in the load-uplift relation. The separation of the sole plate from the floor and stud was also a significant contributor. These separations were a result of nail withdrawal and the slip of the T-strap connecting the sill plate to the rim joist.

The load-uplift relation is shown in Figure 4-12. The first quadrant of the curve shows the translation of node A (in Figure 4-7) in the y-direction. Without the T-strap, the maximum withdrawal load would be governed by the withdrawal of the toe-nailed joint and would fail at about 388 lb. Since the wall and the foundation could not overlap, the compressive stiffness is considered very large in comparison to the uplift resistance. This is shown as the steep line in the third quadrant.

Reduced Model

By combining the moment-rotation and load-uplift relations, the detailed exterior wall-to-foundation connection that was used in the full-scale structure can be represented by a set of two springs. The first spring is a nonlinear moment-rotation spring that will model the opening and closing of the connection. The spring is piece-wise-linear and follows the curve in Figure 4-10. The second

y

x

b)

a)

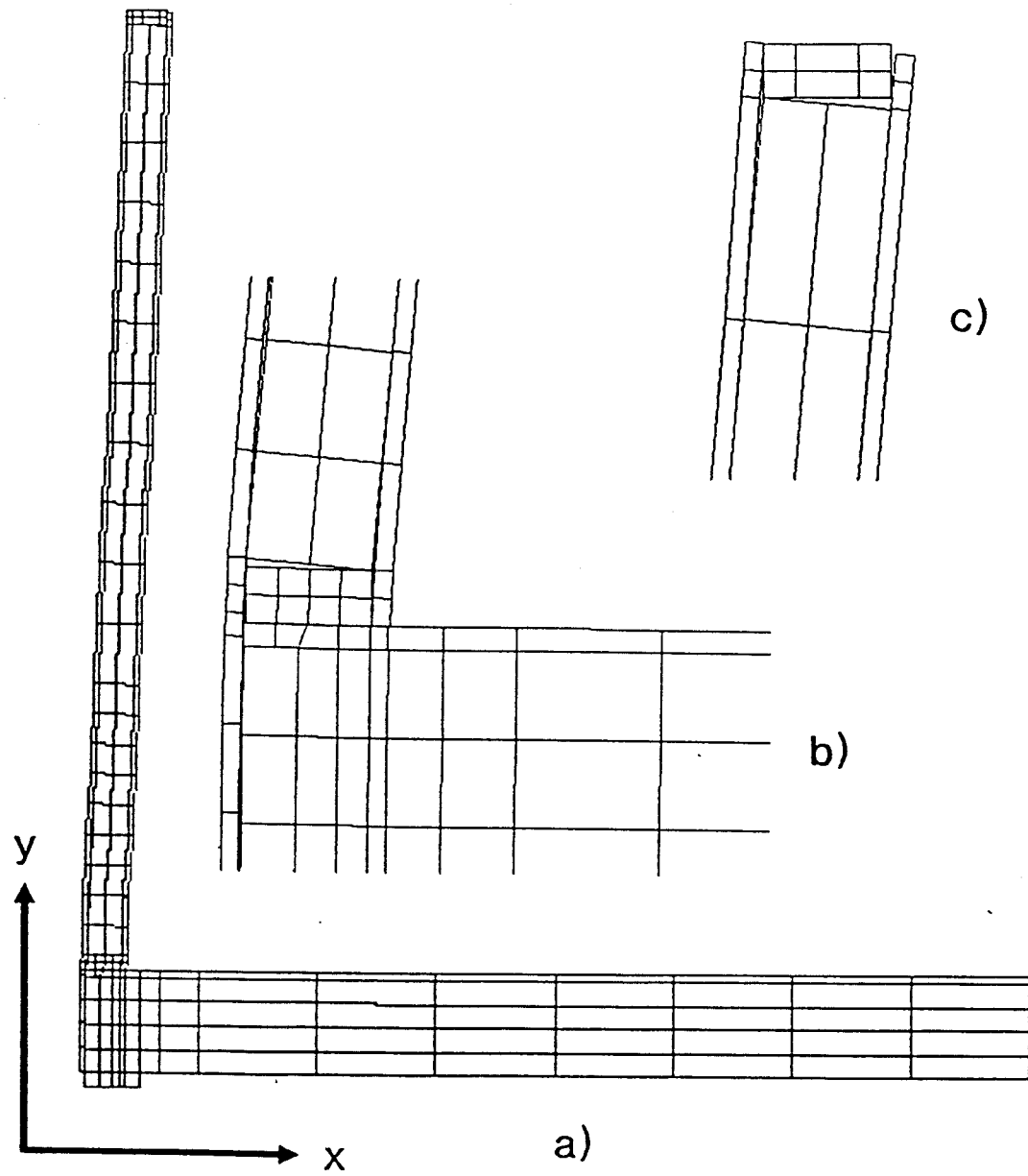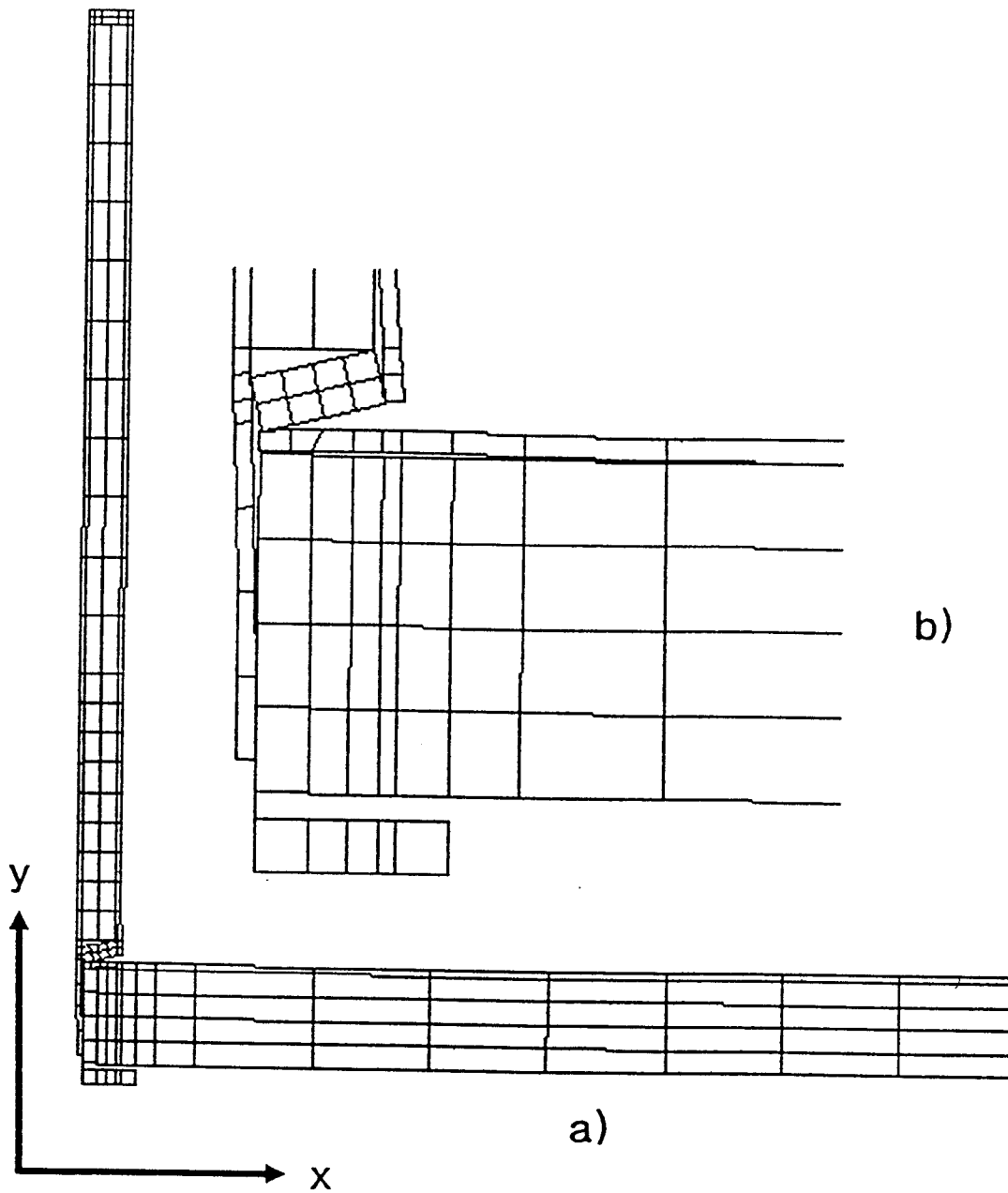Figure 4-11. Displaced structure for the uplift of the full-scale structure. a) full model, displacement scale = 25. b) wall-to-foundation detail, displacement scale = 25.
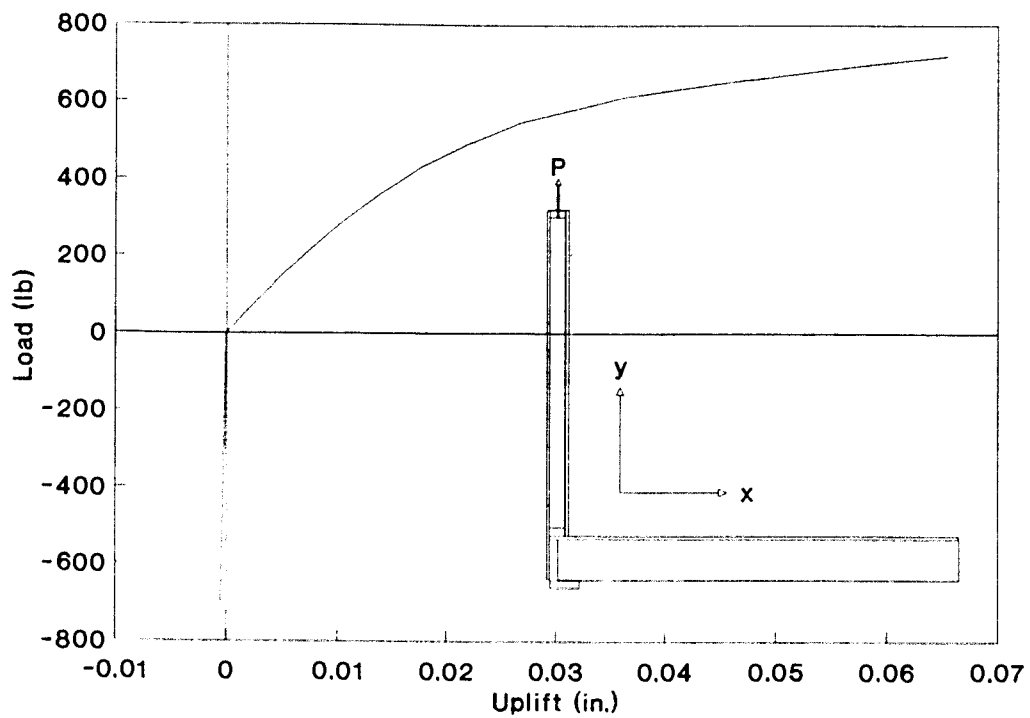
Figure 4-12. Characteristic load-uplift curve from the finite-element model for the exterior wall-to-foundation connection used in the full-scale structure.

spring is a nonlinear load-displacement spring that follows
the relationship of Figure 4-12.

5. ROOF TRUSS-TO-WALL CONNECTION

The structure tested by Phillips (1990) and Lafave (1990) had roof trusses that were fastened to four walls. The interior walls were connected to the bottom chord of the truss with a metal framing anchor (Simpson A34) shown in Figure 5-1. Two rotational resistances along with three translational resistances were required to model the connection in the full structure (Kasal 1992). The two rotational resistances needed were those of rotations about the global x and z-axes. The translations refer to the sliding of the truss in the x and z-directions along with the uplift from the top wall plates of the bottom chord of the roof truss.

This chapter presents the procedures used in the testing of the connection in two rotational tests. The results of these tests were compared to a finite-element model with the purpose of verifying the finite-element model. Once the model was verified, the overall objective was resolved by reducing the detailed finite-element model to a set of energetically-equivalent nonlinear load-deflection and moment-rotation springs.
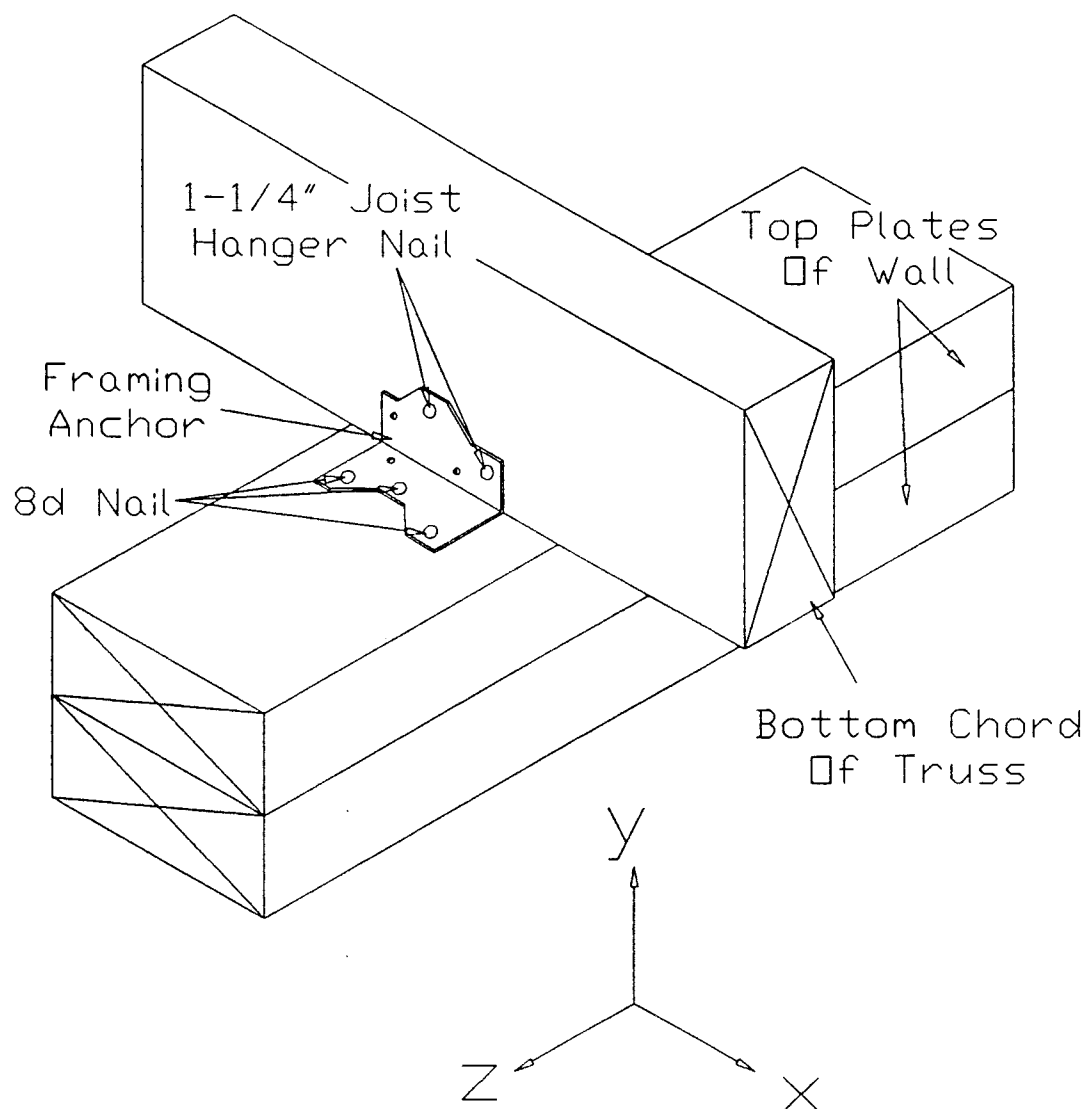
Figure 5-1. Interior wall-to-roof truss connection.

Experimental Procedure

Materials

These tests were performed at the same time as the nail shear tests discussed in Chapter 3. The wood used for the rotational tests was from the same lot as the nail shear tests, and therefore had the same material properties.

The anchors used were metal framing anchors (Simpson A34) purchased from a local supplier. They are made from 18-gauge galvanized steel. The framing anchors were fastened to the wood with 8d nails and $1\frac{1}{4}$-in. JHN.

Testing Arrangement

The basic test configurations for the truss chord rotation about the global x and z-axes are shown in Figures 5-2 and 5-3 respectively. Fifteen replicates of the intercomponent connection were tested in each rotation.

For these tests, the double top-plate of the wall was built up by fastening two wood blocks together with a pair of lag screws ($\frac{1}{2} \times 2\frac{1}{2}$ in.). Holes were pre-drilled for the lag screws so that there would be no splitting of the wood.

The specimen was attached to the test fixture by a two $\frac{3}{8}$-in. bolts, which passed through the bottom member of the top plate. Displacements were measured by two LVDTs located
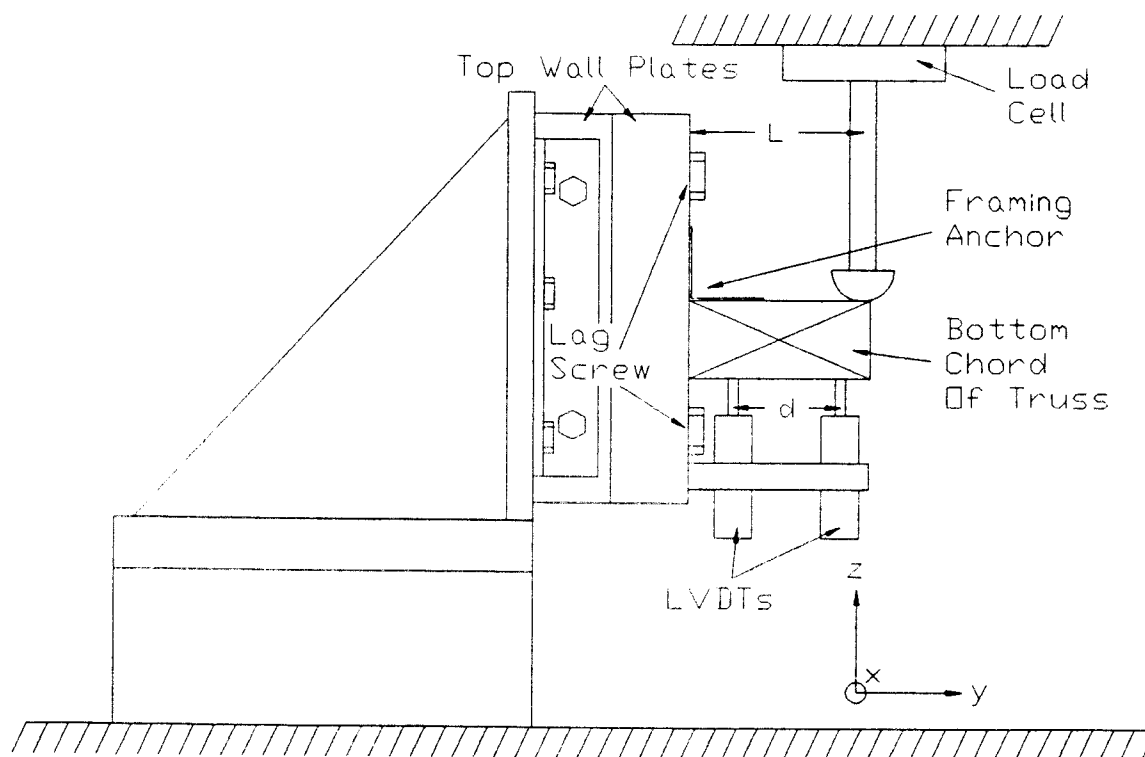
Figure 5-2. Testing apparatus used for the rotational tests about the x-axis of the interior wall-to-roof truss connection.
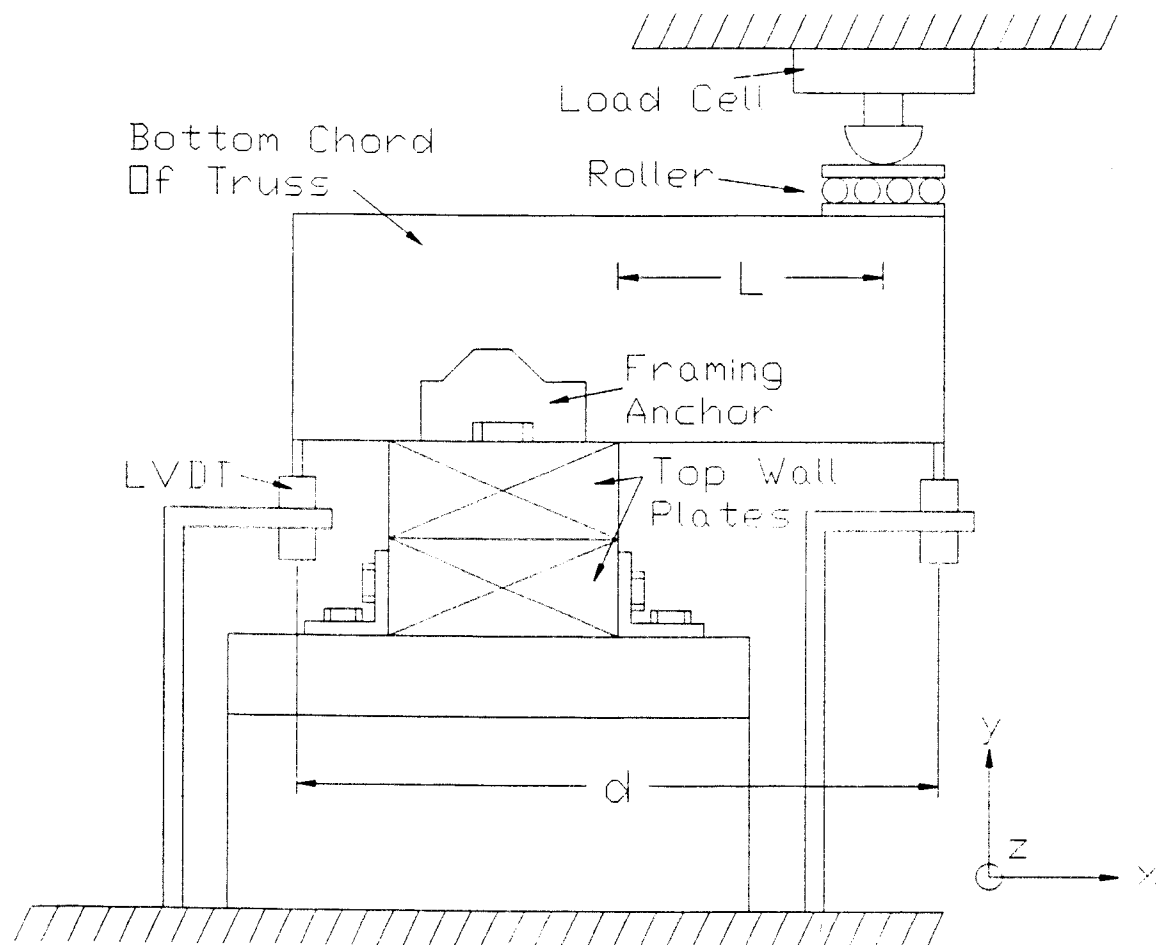
Figure 5-3. Testing apparatus used for the rotational tests about the z-axis of the interior wall-to-roof truss connection.

at a distance d from each other. Rotations in radians were obtained by dividing the difference of the LVDT readings by the distance d. Moment was expressed as the product of load as measured by the load cell and length (L) of the moment arm.

The load cell and data acquisition system were the same as that used for the nail shear tests in Chapter 3. The tests were conducted at a constant rate of 0.1 in./min. of crosshead travel until the rotation could no longer be qualified as "small."

Moment-rotation relationships were plotted after each test, and are shown in Appendix B. The curves for each rotation were collected and a regression performed on both sets. The results of the tests are shown as a dashed line in Figures 5-4 and 5-5. Since the behavior of the nails in shear are close to linear in the early portion of the load-slip curve, and in withdrawal, are nonlinear up to a certain yield point, the linearity of the dashed lines in Figures 5-4 and 5-5 suggests that most of the rotation was a result of the bending in the steel framing anchor. A small contribution of the nails in shear and withdrawal are present, and this gives the moment-rotation curve the slight nonlinearity present in Figures 5-4 and 5-5.
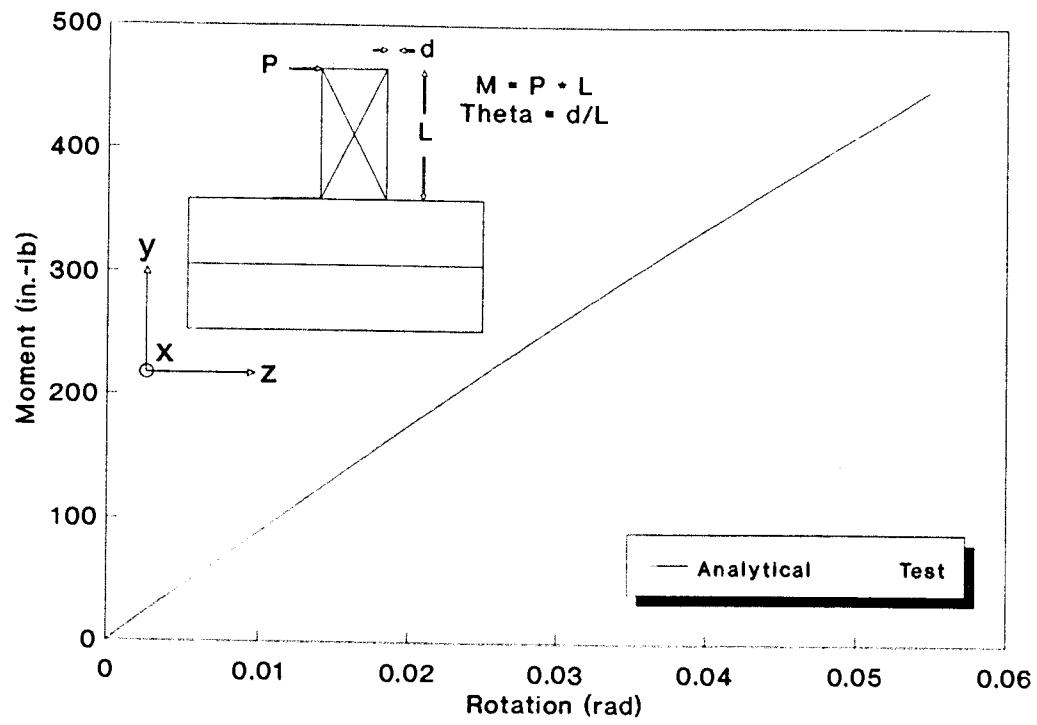
Figure 5-4. Experimental and analytical results of the
interior wall-to roof truss connection rotating about the x-
axis
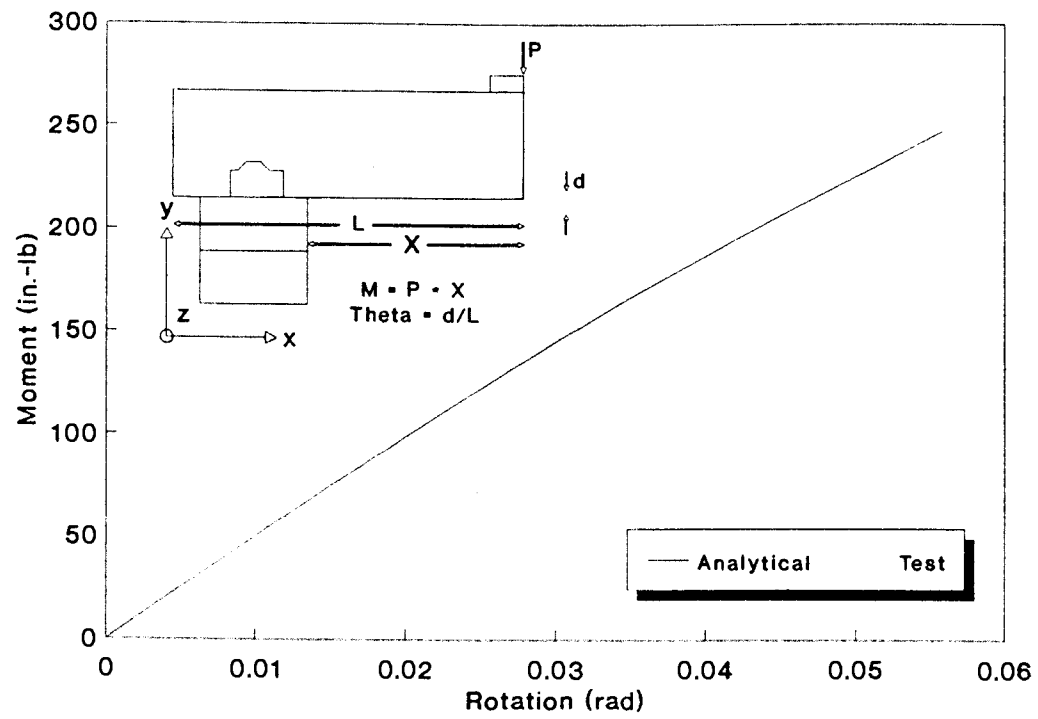
Figure 5-5. Experimental and analytical results of the interior wall-to-roof truss connection rotating about the z-axis.

Analytical Procedure

Recalling again that the objective was to establish a set of properties for the continuum being used as an intercomponent connection in a global full-structure analysis, the detailed three-dimensional model for the intercomponent connection included all essential details and degrees of freedom.

The Wood

The wood was modeled with eight-node, three-dimensional, isoparametric solids, shown in Figure 5-6. For this type of element, each node had three degrees of freedom, displacements in the nodal x, y, and z directions (DeSalvo and Gorman 1989). Material properties consisted of three moduli of elasticity (E_x, E_y, and E_z) calculated based on the longitudinal E and equations 4-1 and 4-2, three Poisson ratios (μ_{xy}, μ_{yz}, and μ_{xz}) provided by Bodig and Jayne (1982), and three shear moduli (G_{xy}, G_{yz}, and G_{xz}) calculated internally by equations 4-3 through 4-5.

The Framing Anchor

The light-gauge, metal framing anchor was modeled with four-node, quadrilateral shell elements, shown in Figure
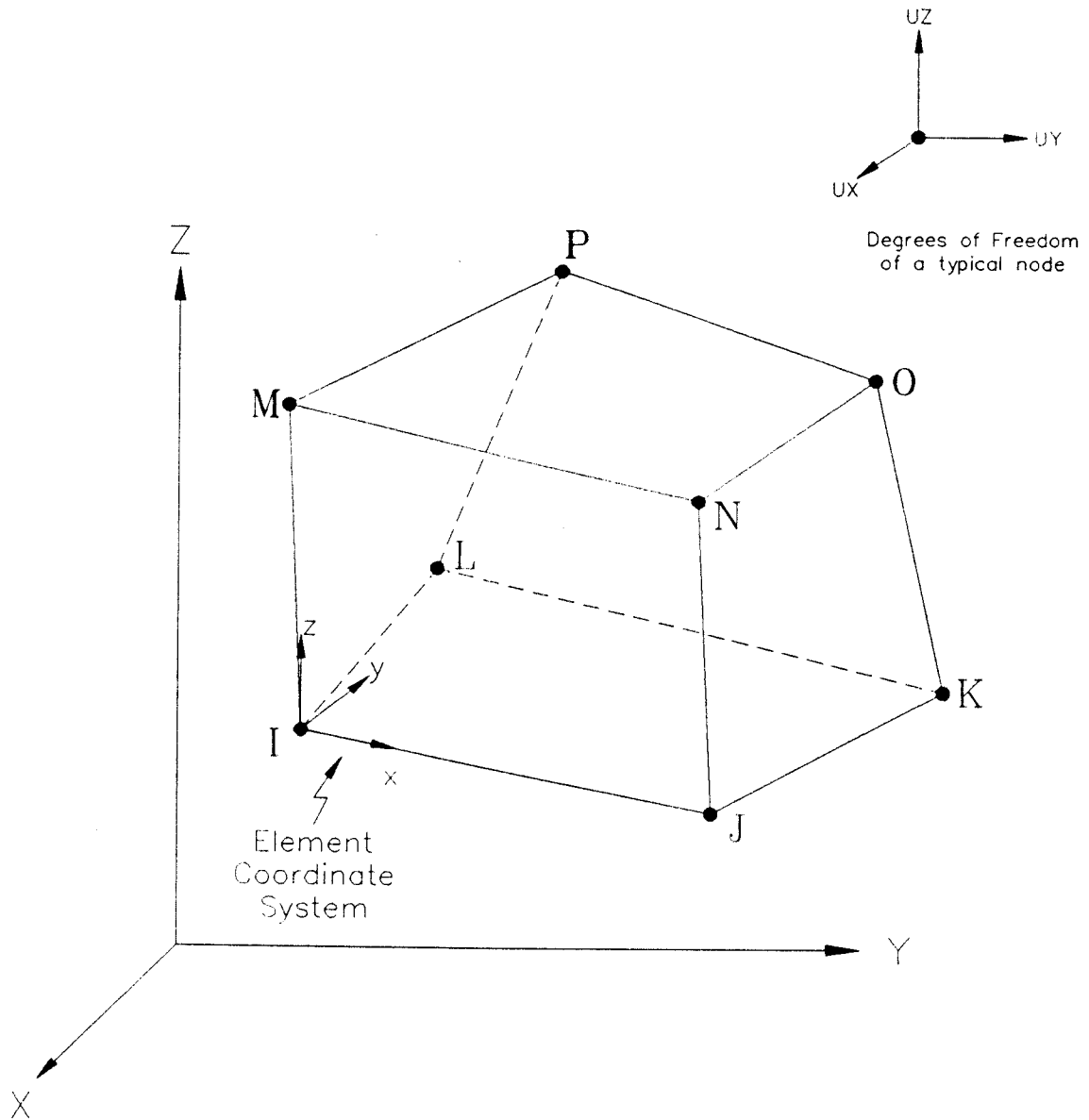
Figure 5-6. Eight-node isoparametric solid used in the model for wood.

5-7. Each node has six degrees of freedom, translations in the nodal x-, y-, and z-directions, and rotations about the x-, y-, and z-axes (Desalvo and Gorman 1989). Since the framing hanger was steel, the material properties were isotropic, and therefore only three material properties were required, $E = 29.0 \times 10^6$ psi, $\mu = 0.3$, and $G = 12.2 \times 10^6$ psi).

The Nails

Each nail was modeled with two-node, nonlinear, load-deflection elements. The behavior and definition of the element was discussed in Chapter 4. Five nails were used in the real connection, two JHN and three 8d nails. Load-slip curves from the experimental analysis were input for the 8d nails and the joist hanger-nails for shear values parallel and perpendicular to the grain. The withdrawal curves from Chapter 3 were also input. Carroll (1988) gave the properties for lag screws.

The Gaps

Gap elements, as described in Chapter 4, were used to separate the different materials of the finite-element model. These were nonlinear load deflection elements with a high stiffness in compression (1×10^7 lb/in.) which ensured the materials did not overlap, and low stiffness in tension

UZ

ROTZ

ROTY
UY

UX ROTX

Degrees of Freedom
of a typical node

Z

L

Thickness

I

K

J

Y

X
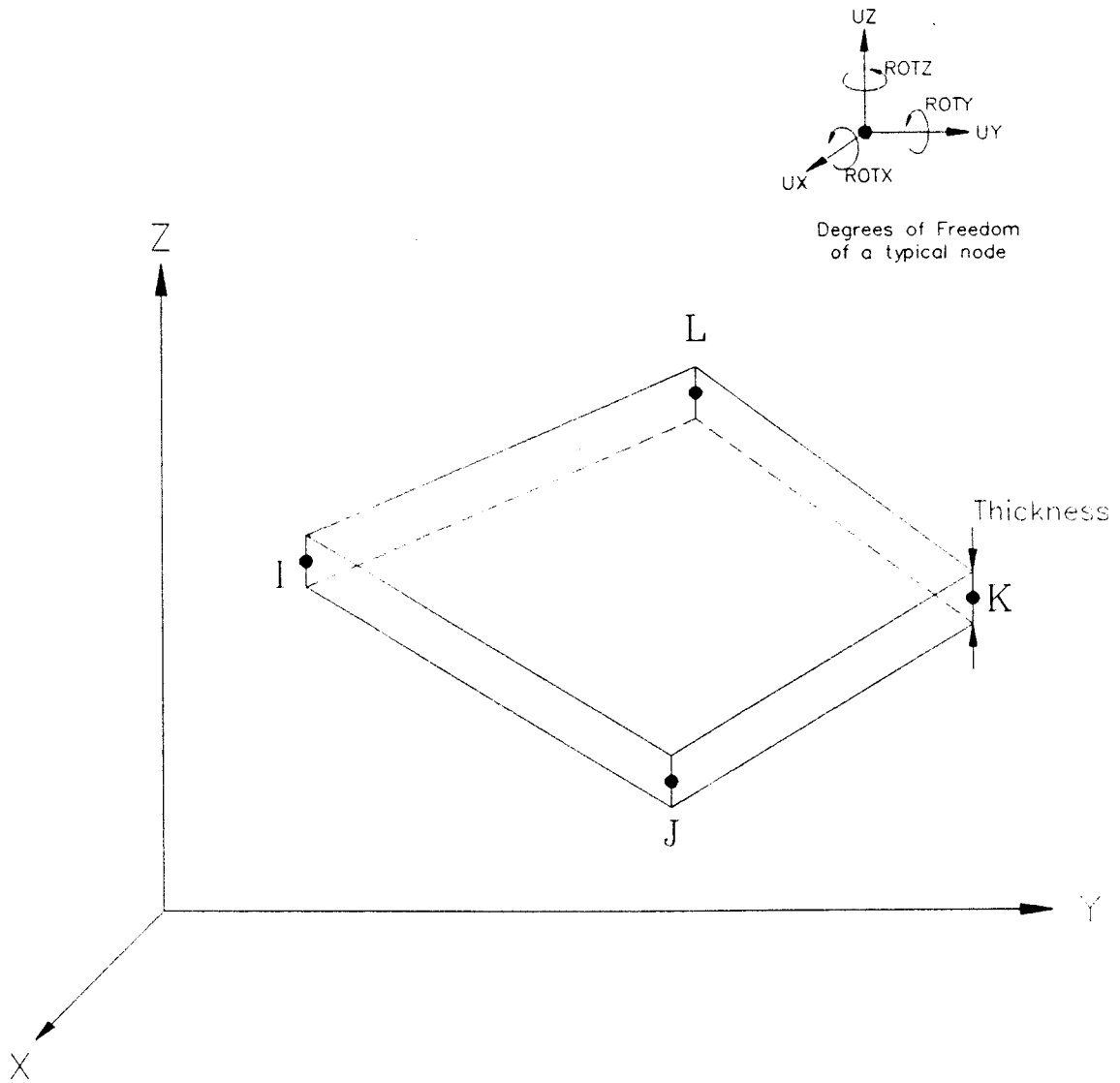
Figure 5-7. Four-node, quadrilateral shell element used in
the model for the metal framing anchor.

$(1 \times 10^{-3}$ lb/in.), which allowed the materials to separate.

Crushing

As the lower truss chord pivots about the top wall plate, a high bearing stress occurs at the wood-wood interface. Since the interface along the edges of this connection is so small, the resulting bearing stresses perpendicular to the grain will be large enough to contribute a significant amount of rotation due to the crushing of the interface. Loferski and Gamalath (1989) predicted the crushing stiffness of a wood-wood interface at a corner perpendicular to the grain. They found the crushing resistance for several species of wood and correlated the resistance to the specific gravity of the wood.

To simulate crushing of the wood due to high bearing stresses at the corners, nonlinear load-deflection elements were inserted along the contacts where a corner met solid wood. The load-deflection elements were the same as the gap elements with the exception that the stiffness of the spring used corresponded to the crushing resistance of the wood, as opposed to the high compressive resistance of the gap element. The stiffness used in the model was obtained from the work Loferski and Gamalath (1989). Based on the specific gravity of the Douglas-fir, the stiffness used for

the finite-element models was 1820 lb/in. per lineal inch of contact.

The Assembled Model

The model, shown in Figure 5-8, consisted of 565 elements made up of the following: 262 eight-node isoparametric solid elements modelling the wood, 174 four-node quadrilateral shell elements modelling the framing anchor, 129 nonlinear load-deflection elements modelling the gaps (99), nails (15), crushing along the edges (13), and lag screws (2). When the elements were assembled in the finite-element model, a total of 848 nodes were present, each of which had up to 6 degrees of freedom. When assembled the model had a 1938 degrees of freedom without the boundary conditions imposed.

The three 1¼-in. JHN that fixed the metal framing anchor to the lower truss chord were modeled with 9 nonlinear load-deflection elements (3 for each nail). These elements modeled the shear resistance parallel and perpendicular to the grain, as well as the withdrawal of the nail shank from the wood. Likewise the two 8d nails that fixed the metal framing anchor to the top wall plate were modeled with 6 nonlinear load-deflection elements. The two top plates of the wall were attached with just two nonlinear load-deflection elements that modelled withdrawal resistance

Wedge
element

y

x

z
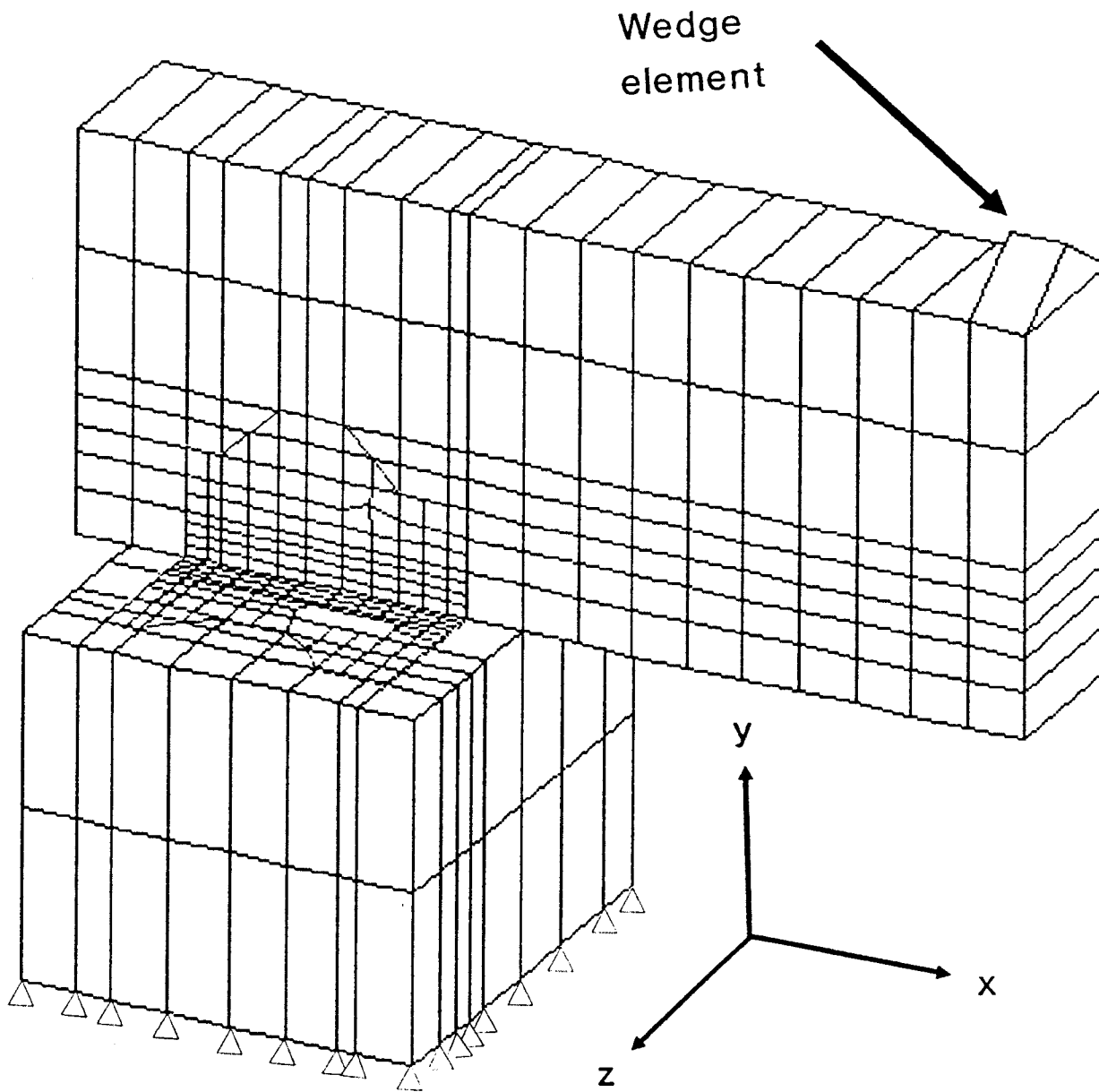
Figure 5-8. Assembled model of interior wall-to-roof truss
connection.

of the two lag screws. The shear effects of the lag screws were neglected, and therefore, only one element was needed for each lag screw.

The boundary conditions imposed on the model fixed the bottom plane of nodes of the lower top wall plate. This reduced the degrees of freedom by 243 (81 nodes × 3 DOF/node) for a total of 1695 degrees of freedom. Any other imposed displacement or load was applied as a form of loading the structure in rotation or shear.

This finite-element model can be loaded to simulate the conditions of the rotational tests covered earlier in this chapter. The resulting moment-rotation relations obtained from these simulations can be compared to the experimental results and used to verify the finite-element model. Once the model is verified, the material properties of the full structure can be entered to perform the necessary computations for the required moment-rotation and load-displacement relations for the full structure finite-element model.

Verification Model

The finite-element model was loaded in two ways for verification. The loadings were chosen to simulate the two rotational tests presented earlier. The first case consisted of loading the lower chord of the truss in such a way that a clockwise rotation about the x-axis was obtained

when looking from the positive x-axis. The second case
consisted of a clockwise rotation about the z-axis, when
looking from the positive z-axis, of the lower chord of the
truss.

Rotation about the x-axis. The moment-rotation
relationship for this load case was obtained by forcing two
nodes at the top of the lower truss chord in the negative z-
direction. The two nodes chosen were separated by $3\frac{1}{2}$-in.
and were directly over the sides of the top wall plates.
This corresponded to the $3\frac{1}{2}$-in. width of the loading head
used in the tests. Twelve load steps were required to
obtain a smooth curve.

Because of the large number of degrees of freedom and
the nonlinear characteristics of the finite-element model,
each load step took approximately 1 hour to run on a
microcomputer having an 80386 processor and a math
coprocessor.

The resulting moment-rotation curve is shown as the
solid line in Figure 5-4. The moment was obtained by
multiplying the resultant loads (P) of the forced nodes by
the lever arm (L). The rotation, in radians, was found by
dividing the relative displacement of a node at the top of
the wall truss to a node at the bottom of the wall truss (d)
by the separation (L) of the two nodes.

The analytical results showed excellent agreement for
the entire moment-rotation range. The maximum error

occurred at the finish of the curve. For a rotation of 0.055 radians, the test showed a moment of 447.1 in.-lb, and the finite-element model 448.8 in.-lb, which is a deviation of only 5.9%.

Rotation about the z-axis. During the experimental tests with this connection, it was noticed that during the rotational test about the z-axis, the lower chord of the truss had a tendency to twist slightly about the x-axis as well. For that reason the extra wedge-shaped element was placed on the top of the lower truss chord. The moment rotation relation was obtained by forcing the top edge node of the wedge element through a series of displacements in the y-direction. By loading that way, the lower truss chord in the model was also allowed to twist slightly about the x-axis.

A smooth moment-rotation curve was obtained by using seven load steps. The load was obtained by recording the reaction loads of the displaced node of the wedge element. The resulting moment-rotation curve is shown as the solid line in Figure 5-5. The moment was obtained by multiplying the resultant load P by the distance X, which was the distance from the edge of the top plates of the wall to the applied load. The rotation, in radians, was obtained by dividing the distance d by the length of the lower truss chord. The distance d represents the change in y-displacements of the ends of the lower truss chord. The

endpoints of lower truss chord were chosen since the LVDTs were attached at the same location.

When comparing the test and analytical moment-rotation curve, the two showed excellent agreement for the initial portions of the curves. In the latter portions of the curves, some deviation occurs, with a maximum error occurring at the end-point. At the rotation of 0.056 rad the test showed a moment of 208.1 in.-lb and the finite-element model 247.6 in.-lb, which is in error by 19.0%.

Full-Structure Connection Model

Once the finite-element model was verified by comparison with experimental data, the model was used to produce the relationships needed in the full-structure model. Five relationships were necessary for the connection to be useful in the full-structure model (Kasal 1992). The first two were the moment-rotation curves about the global x and z-axes, and the other three were load-displacement curves along all three axes.

Rotation about the x-axis. The moment-rotation relationship was defined by obtaining the relative rotation of the lower chord of the truss to the upper wall plate, which differed from the verification finite-element model where the gross rotation of the lower chord of the truss was determined. The relative rotation was determined by simply subtracting the rotation of the top wall plate from the

gross rotation of the truss chord.

Figure 5-9 shows the characteristic moment-rotation relation from the finite-element model of the lower truss chord when rotating about the top plate of the interior wall. A positive rotation corresponds to a clockwise (CW) rotation of the lower truss chord when looking down the positive x-axis. Likewise a negative rotation corresponds to a counter-clockwise (CCW) rotation. It can be seen from Figure 5-9 that the connection offered very little resistance to rotation in the CCW direction with respect to the CW direction. Rotation in the CCW direction caused the framing anchor to bend closed with the center of rotation at the right angle bend of the framing anchor. Hence the only resistance against rotation was the bending of the 18-gauge framing anchor. However, rotation in the CW direction caused the framing anchor to bend open while the center of rotation was at the lower edge of the truss chord away from the framing anchor. Thus, not only was the framing anchor contributing to the rotational resistance, but the shear stiffness of the JHN as well as the withdrawal stiffness of the 8d nails contributed to the overall moment-rotation relationship.
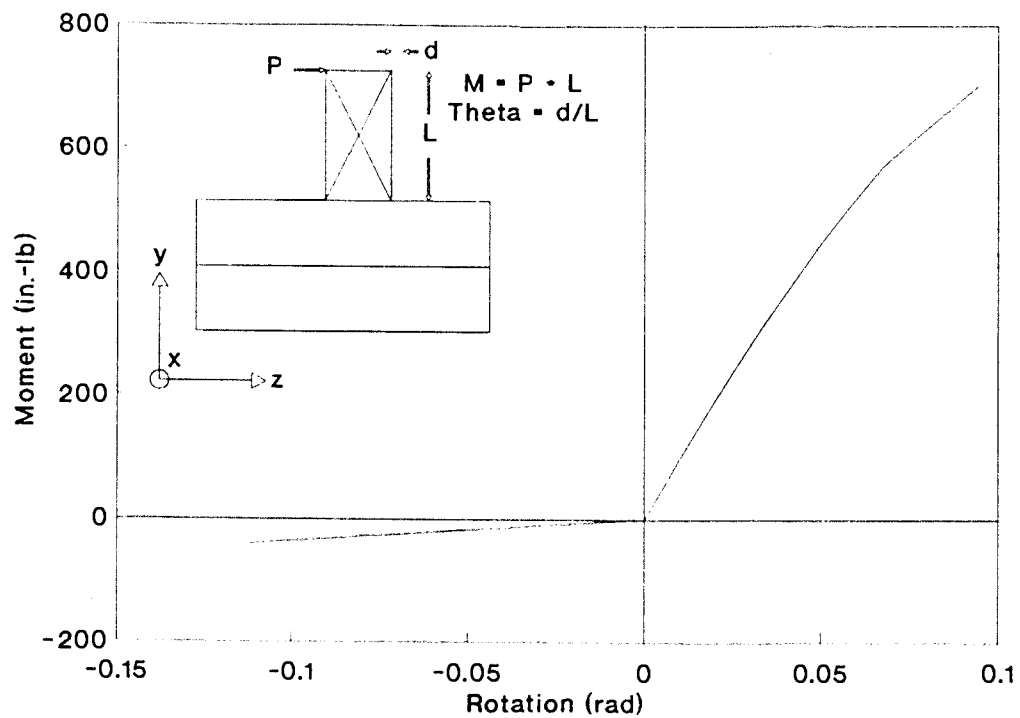
Figure 5-9. Characteristic moment-rotation relation for the finite-element model of the lower truss chord when rotating about the top plate of the interior wall (rotation about the global x-axis).

Rotation about the z-axis. The characteristic moment-rotation relation developed from the finite-element analysis is shown in Figure 5-10. The relation was found in a manner similar to the analysis of the verification model. However, the rotation of the lower truss chord was relative to the wall top plates. Thus, the top plate rotation was subtracted from the gross rotation of the truss chord.

When the lower truss chord was rotated in the CCW (when looking from the positive z-axis) direction the mesh was redefined such that the overhang and loading wedge occurred on the opposite side of the top wall plates. This way the loading was applied in the same manner for each direction of rotation.

Displacement along the x-axis. The load-displacement relationship in the x-direction is shown in Figure 5-11. To ensure that the lower truss chord remained horizontal it was subjected to equal displacements along the x-axis as well as restrained against displacements in the y and z-directions at all eight corners of the lower truss chord. Since the load-displacement relationship between the upper member of the top wall plates and the lower truss chord was desired, the lower of the top wall plates was fixed at every node. This in turn reduced the degrees of freedom and reduced the run time of the model.

Although the curve appears to be symmetric, there are subtle differences due to the asymmetric nail pattern and
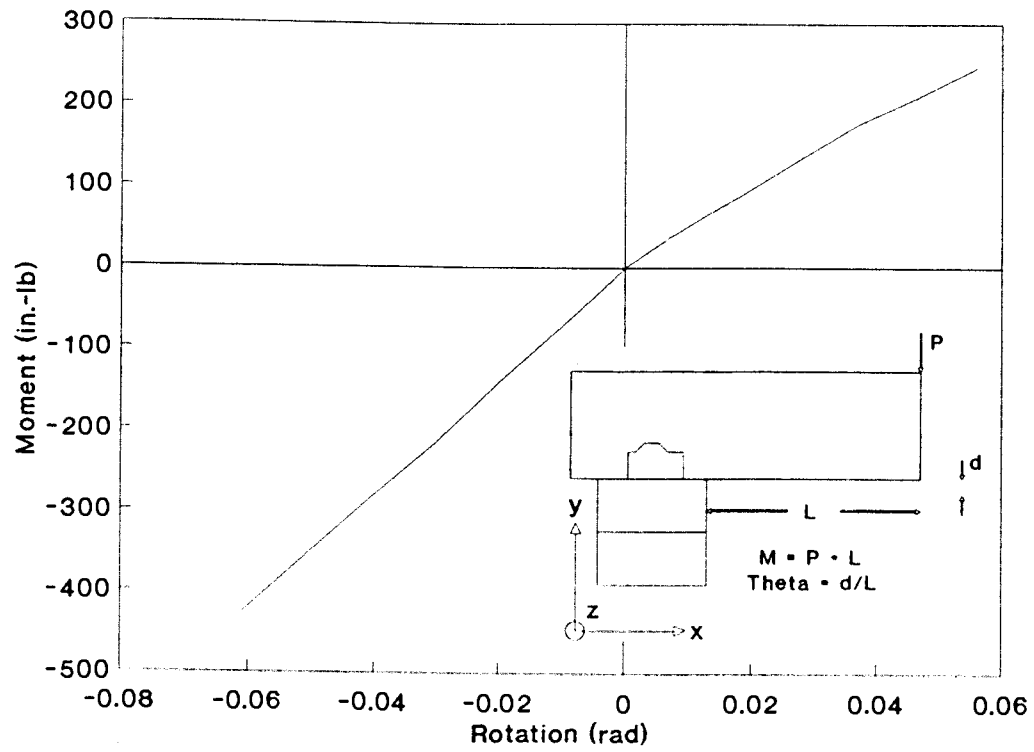
Figure 5-10. Characteristic moment-rotation relation from the finite-element model of the lower truss chord rotating about the top plate of the interior wall (rotation about the global z-axis).
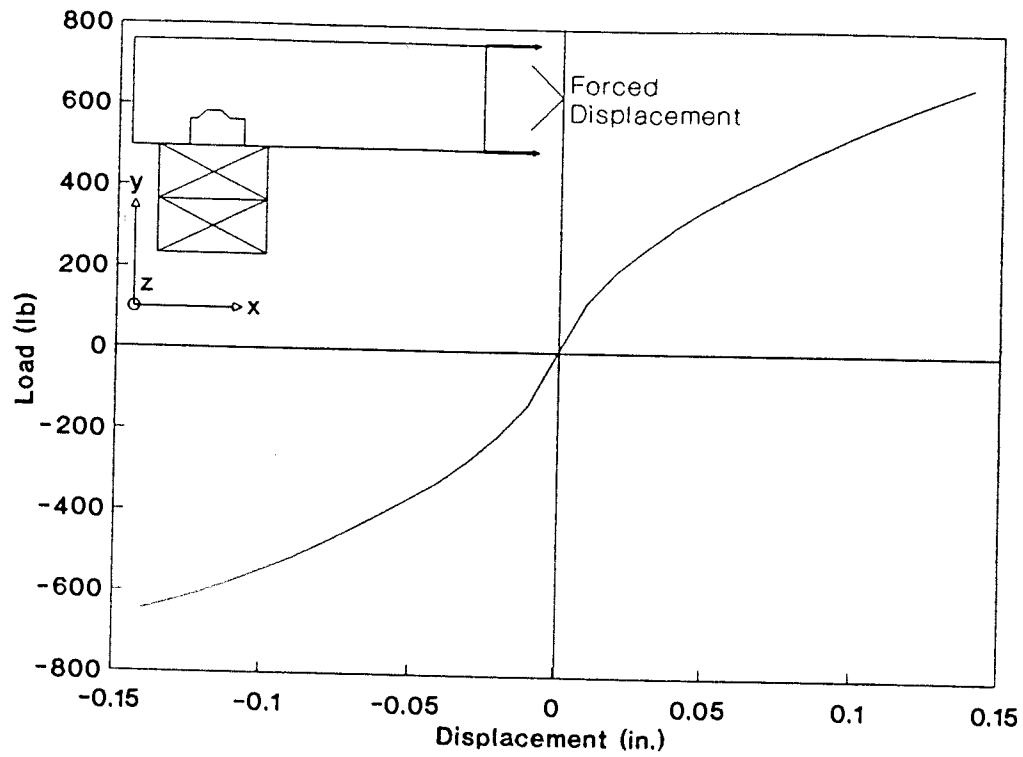
Figure 5-11. Characteristic load-displacement relation from the finite-element model of the lower truss chord sliding on the top wall plate along the global x-axis.

shape of the framing anchor. For a 0.14-in. displacement in the negative x-direction, a 646 lb load was required compared to a 665 lb load to produce the same displacement in the positive x-direction.

Uplift along the y-axis. The characteristic uplift load-displacement relation of the truss-to-wall connection is shown in Figure 5-12. Only one quadrant of the curve is shown since the displacement in the negative y-direction would cause crushing of the wood, and for practical purposes can just be assumed infinitely stiff. The uplift load-displacement relationship was found by displacing four nodes of the lower truss chord, two at the front face of the truss and two at the back. By applying the displacement at four nodes, the lower truss chord experienced only translation in the positive y-direction. Again, since only the relationship between the lower truss chord and the upper top wall plate was needed, the bottom member of the top wall plate was fixed at every node.

The load-uplift relation in Figure 5-12 has a slight nonlinearity to it, although it appears linear. Most of the displacement was a result of the metal framing anchor bending under load. The slight kink near the end of the curve corresponds to the first slope change of the 8d nail in withdrawal.

Figure 5-12. Characteristic uplift load-displacement relation from the finite-element model of the lower truss chord separating from the top wall plate along the global y-axis.

Displacement along the z-axis. The characteristic load-displacement relation in the z-direction for the roof truss-to-wall connection is shown in Figure 5-13. The connection stiffness was greater when displacements occurred in the direction of the framing anchor (positive z-direction) as opposed to away from the framing anchor (negative z-direction). When the truss was displaced in the positive z-direction the resistance was a result of the nail slip between the framing anchor and the top wall plate. The framing anchor was pushed by the roof truss and deformation of the framing anchor did not affect the characteristic load-displacement relation.

When displacements occurred away from the framing anchor though, the resistance was much weaker. The primary cause of displacement was the deformation of the framing anchor. Being only 18 gauge, the framing anchor offered relatively little resistance in bending.
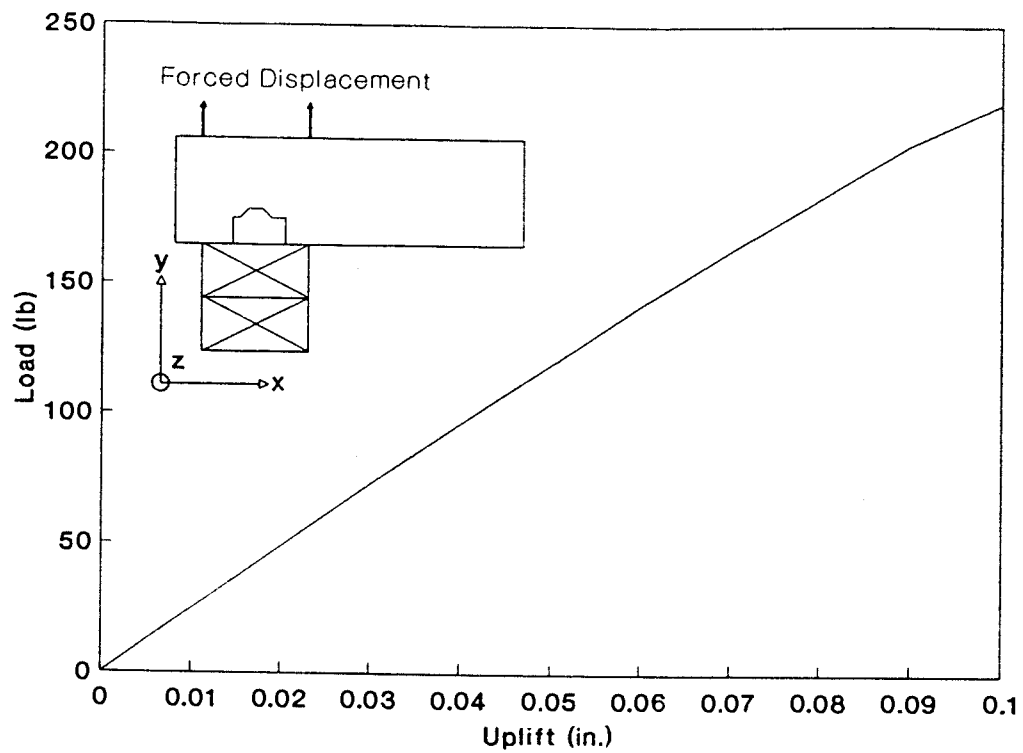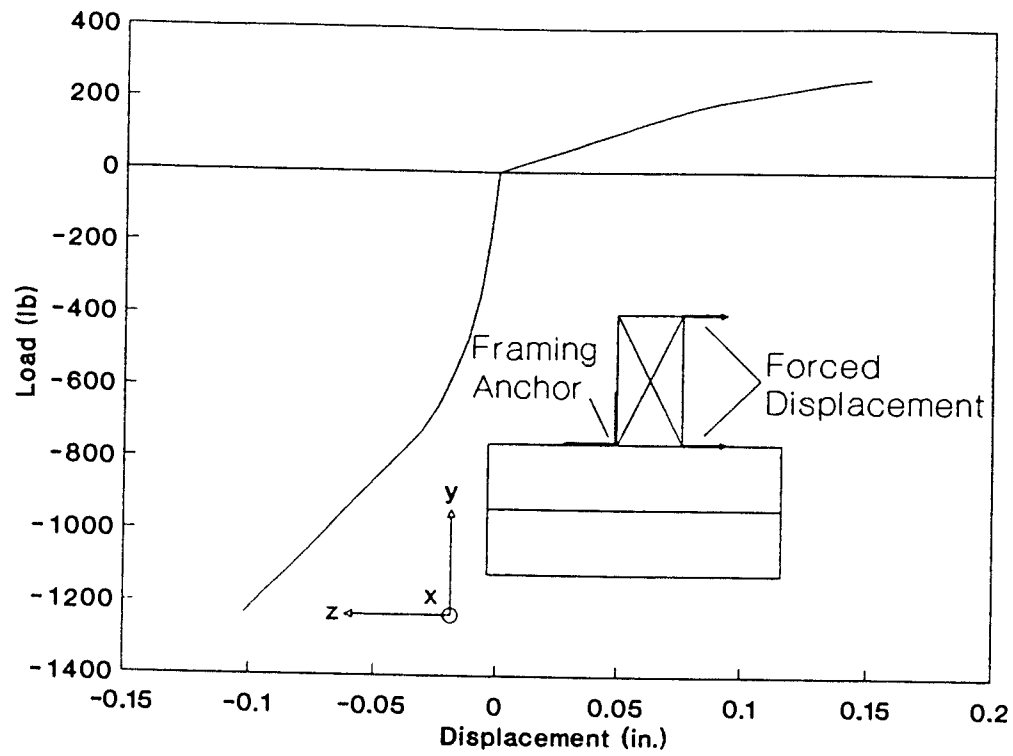
Figure 5-13. Characteristic load-displacement relation from the finite-element model of the lower truss chord sliding on the top wall plate along the global z-axis.

6. EXTERIOR WALL-TO-EXTERIOR WALL CONNECTION

The plan of the structure erected and tested at WSU was such that the structure consisted of four exterior walls, all at right angles. Each of the four corners were fastened together in a similar manner, and therefore one model of the exterior wall to exterior wall connection was sufficient to provide the needed nonlinear springs for the full-structure model.

A drawing of the connection is shown in Figure 6-1. The actual connection consisted of three Douglas-fir studs, T1-11 exterior sheathing, and gypsum board sheathing on the interior portion of the walls. Figure 6-1 shows the connection as well as the next adjacent stud on each wall. Wall 1 was the end wall (Phillips 1990), and was oriented parallel to the plane of the applied loads in the structural tests. Wall 5 was the wall the loads were applied to in the full-structure tests.

The stiffnesses required from this connection included the rotational stiffness, as the connection was both opened and closed (Kasal 1992). Separation stiffnesses as wall 1 was pulled away from wall 5, and as wall 5 was pulled away from wall 1 were also required to make the model complete.
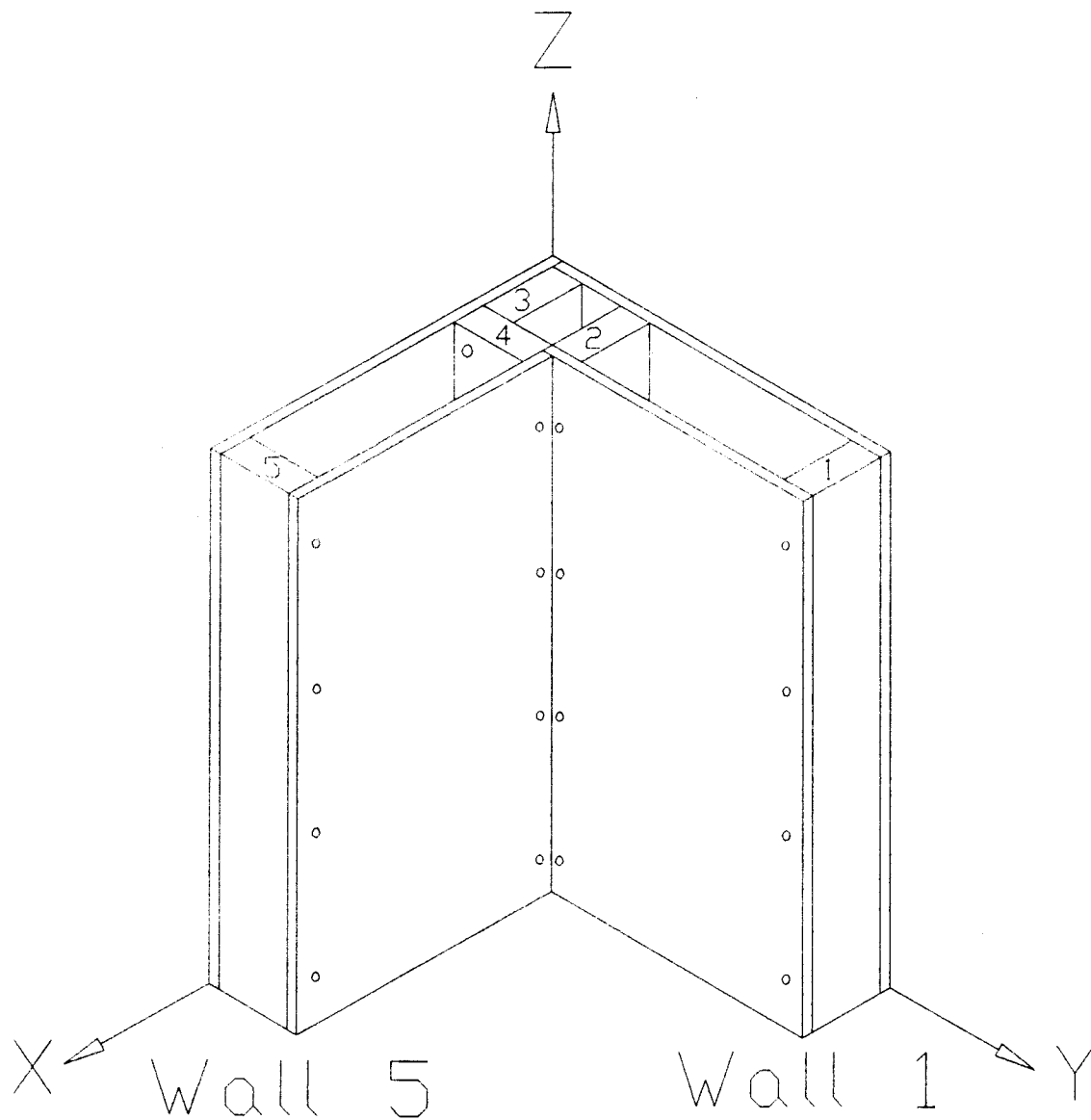
Figure 6-1. Exterior wall-to-exterior wall connection used in full-scale structure test at WSU (Phillips 1990) and intercomponent connection test at OSU.

A similar approach to that used for the roof truss-to-wall connection was used for this connection. First, the connection was built and tested. The test specimen was then modeled using the finite-element model to verify the computational procedure, which yielded characteristic load-displacement and moment-rotation relationships. The material properties of the finite-element model were then modified to represent the properties of the actual structure (Phillips 1990), and the finite-element method was used to obtain the characteristic properties for the reduced system which were nonlinear springs.

Experimental Procedure

Materials

The connections tested were fabricated from a combination of Douglas-fir studs, ½-in. gypsum board sheathing, ½-in. exterior plywood sheathing, drywall nails, 6d nails, and 16d nails. All the materials were purchased from a local supplier.

The plywood and gypsum board were tested in bending to establish the necessary material properties for the finite-element model. The setup for bending tests of the sheathing materials is shown in Figure 6-2. The method followed the guidelines outlined in ASTM D 3043-87 (ASTM 1989), Standard
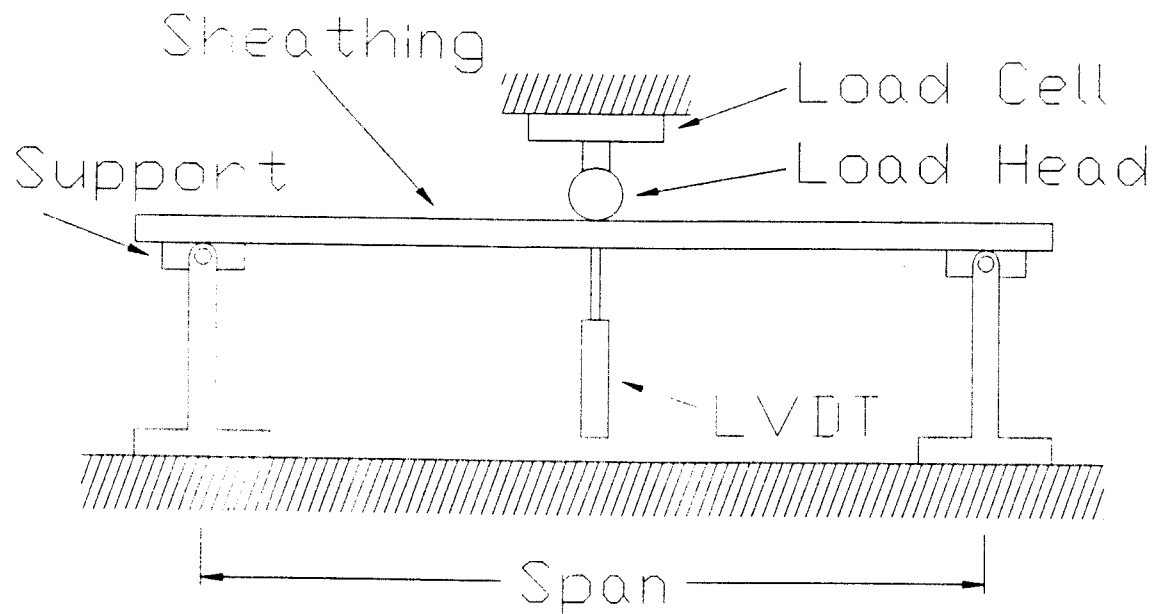
Figure 6-2. Apparatus used to determine the bending properties of the $\frac{1}{2}$-in. exterior plywood sheathing and $\frac{1}{2}$-in. gypsum board used in the exterior wall-to-exterior wall connection.

Methods of Testing Structural Panels in Flexure. This

method was used for both the exterior sheathing and the

gypsum board, since ASTM C 473-87a (ASTM 1990), Standard

Test Methods for Physical Testing of Gypsum Board Products

and Gypsum Lath, does not provide test methods for

determining the E of gypsum board sheathing.

Plywood Testing

Three 4×8 ft sheets of the plywood were used to

assemble the six connections. Six coupons were taken from

each sheet. Three were taken with the outer layer of veneer

grain oriented in the longitudinal direction, with the

remaining three oriented in the perpendicular direction.

The load head was lowered at midspan at a constant rate

of 0.118 in./min. until the coupon failed. An LVDT recorded

the midspan deflection, while a load cell recorded the

applied load. The resulting E values were obtained from

basic mechanics.

$$E = \frac{P L^3}{48 \delta I}$$
6-1

Where:
  P = Load applied at midspan
  L = Span of specimen (14.5 in.)
  δ = Midspan deflection
  I = Moment of inertia based on gross cross section

The resulting load-midspan deflection curves are shown in Appendix C. The first set of curves shows the results of the bending longitudinal to the outer fibers. The slope of the linear portion of the load-midspan deflection curves represents the modulus of elasticity of the coupon. The second set of curves shows the results when bending took place perpendicular to the outer fibers. A summary of the results are given in Table 6-1.

Table 6-1. Bending properties of the ½-in. exterior plywood used in the exterior wall-to-exterior wall connection tests performed at OSU, n=9.

Fiber Direction	MC (%)	SG	E (lb/in^2)
Longitudinal	10.83(0.73)[a]	0.50(0.04)	$9.48 \times 10^5 (1.34 \times 10^5)$
Perpendicular	10.89(0.67)	0.50(0.04)	$6.21 \times 10^5 (1.64 \times 10^5)$

[a] Parenthesis indicate standard deviation.

Gypsum Board

Two coupons were taken from each connection tested. One coupon had the paper fiber running in the longitudinal direction and the other ran perpendicular. The tests were conducted in the same manner as those for plywood with the exception that the spans of the specimens were reduced to 12-in.

The load-midspan deflection curves are also shown in Appendix C. It can be seen from the graphs that both the bending longitudinal and perpendicular to the paper grain

have similar properties. When the specimens were tested
with the paper fibers oriented longitudinally, the bending
modulus (E) was found to be 2.66×10^5 lb/in.^{2} with a standard
deviation of 4.01×10^4 lb/in.^{2}. When tested with the paper
fiber oriented perpendicular, the bending modulus (E) and
standard deviation were 2.56×10^5 lb/in.^{2} and 4.13×10^4 lb/in.^{2}
respectively.

Testing Arrangement

The testing setup used to evaluate the exterior wall-
to-exterior wall connection is shown in Figure 6-3. The
test was developed to rotate the intercomponent connection
so that the two walls opened and closed relative to one
another.

The studs (numbered 1-5 in Figure 6-3) were cut to a
length of 24-in., and ran the full length of the connection.
Studs 3 and 4 were fastened together with five 16d nails
spaced at 6-in. o.c. The two sheets of gypsum board were
fastened to the studs with four drywall nails spaced at 6-
in. o.c., per row. There were six rows of 6d nails used to
fasten the exterior sheathing to the studs. Studs 1, 2, 5
and the longer edge of stud 3 had four 6d nails spaced 6-in.
o.c. The shorter side of stud 3 and 4 each used five 6d
nails spaced 6-in. o.c. to fasten the exterior sheathing to
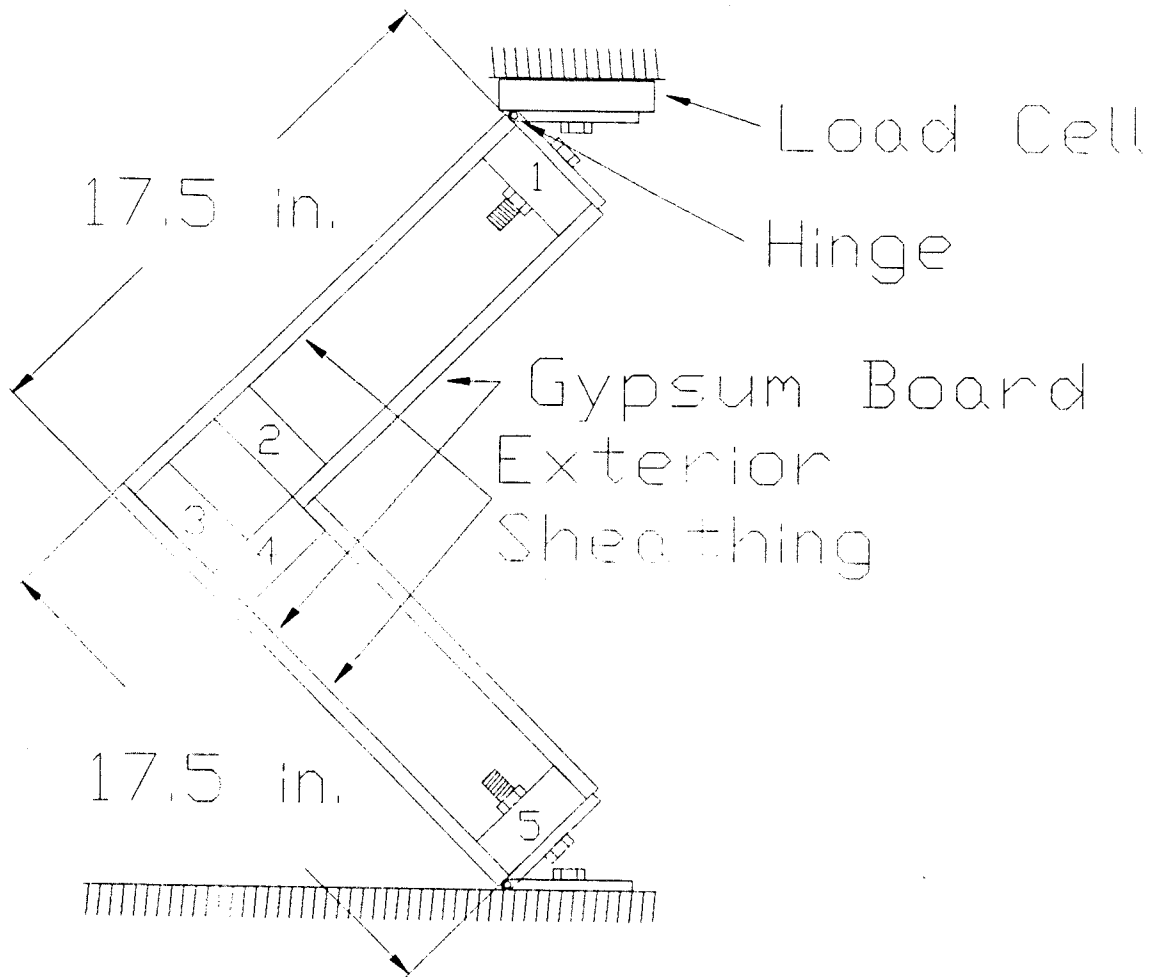them. All the nails used in the connection were hand driven

Figure 6-3. Testing apparatus used to test the exterior wall-to-exterior wall connection when subjected to an opening and closing cyclic loading.

without the use of pilot holes. The outer layer of the exterior sheathing and the paper on the gypsum board both had the fibers running parallel to the length of the studs.

The load was monitored by a load cell mounted between the hinge and the crosshead of the testing machine. The displacement measured was that of the crosshead as it was lowered or raised to load the connection. The crosshead was raised and lowered at a constant rate of 0.1 in./min.

Although the global model of the complete structure did not require cyclic behavior, a load and fully reversed load was applied.

A total of six assembled connections were tested. The first was loaded in closing until the crosshead was lowered about 0.5 in. Then the crosshead was raised 1.0 in. to open the connection and give a net crosshead movement of 0.5 in. Finally the crosshead was brought back to the original unloaded position to complete the hysteresis loop. The next connection was loaded in just the opposite order. It was first loaded to open the connection, then closed, and finally brought back to the neutral position.

The results of the testing are shown in the six hysteresis loops that make up Figure 6-4 to 6-9. From these six figures, it can be seen that Figure 6-6 has very low load values and a shape which does not compare to the other five graphs. For those reasons it was decided to ignore the results of this test and use the results of the other five.
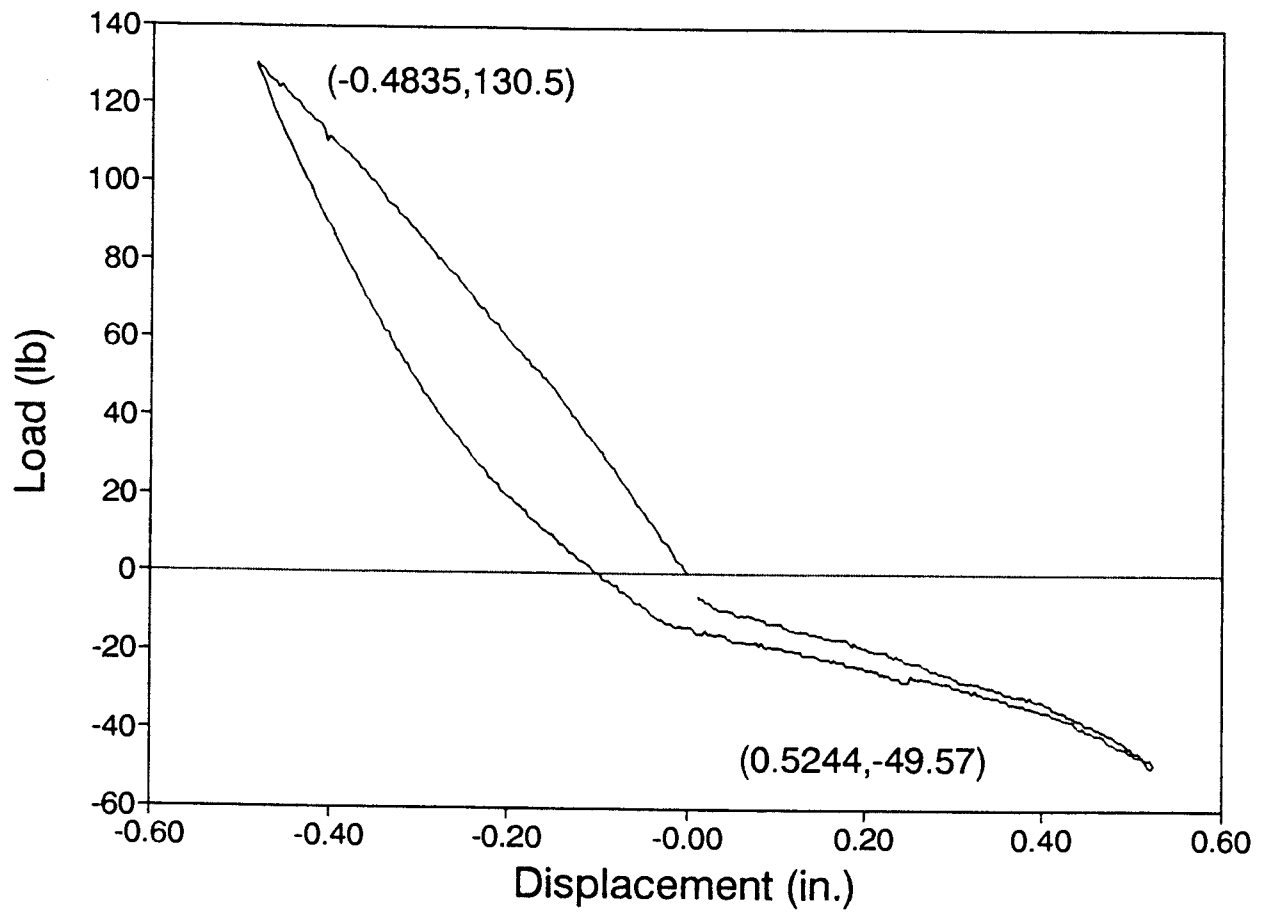
Figure 6-4. Load vs load head movement (close-open-close) for test 1 of the exterior wall-to-exterior wall connection.
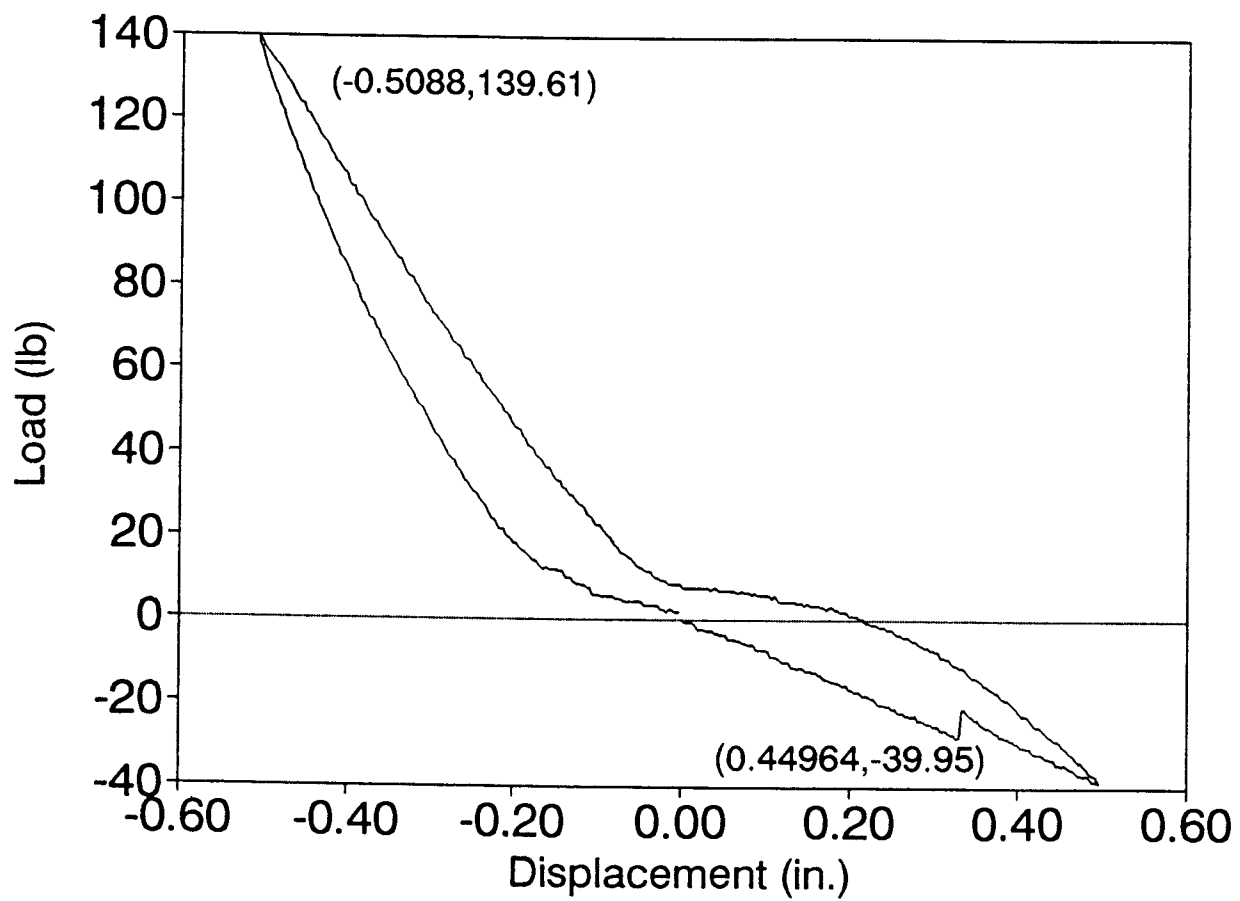
Figure 6-5. Load vs load head movement (open-close-open) for test 2 of the exterior wall-to-exterior wall connection.

Figure 6-6. Load vs load head movement (close-open-close) for test 3 of the exterior wall-to-exterior wall connection.

Figure 6-7. Load vs load head movement (open-close-open) for test 4 of the exterior wall-to-exterior wall connection.

Figure 6-8. Load vs load head movement (close-open-close) for test 5 of the exterior wall-to-exterior wall connection.

Figure 6-9. Load vs load head movement (open-close-open) for test 6 of the exterior wall-to-exterior wall connection.
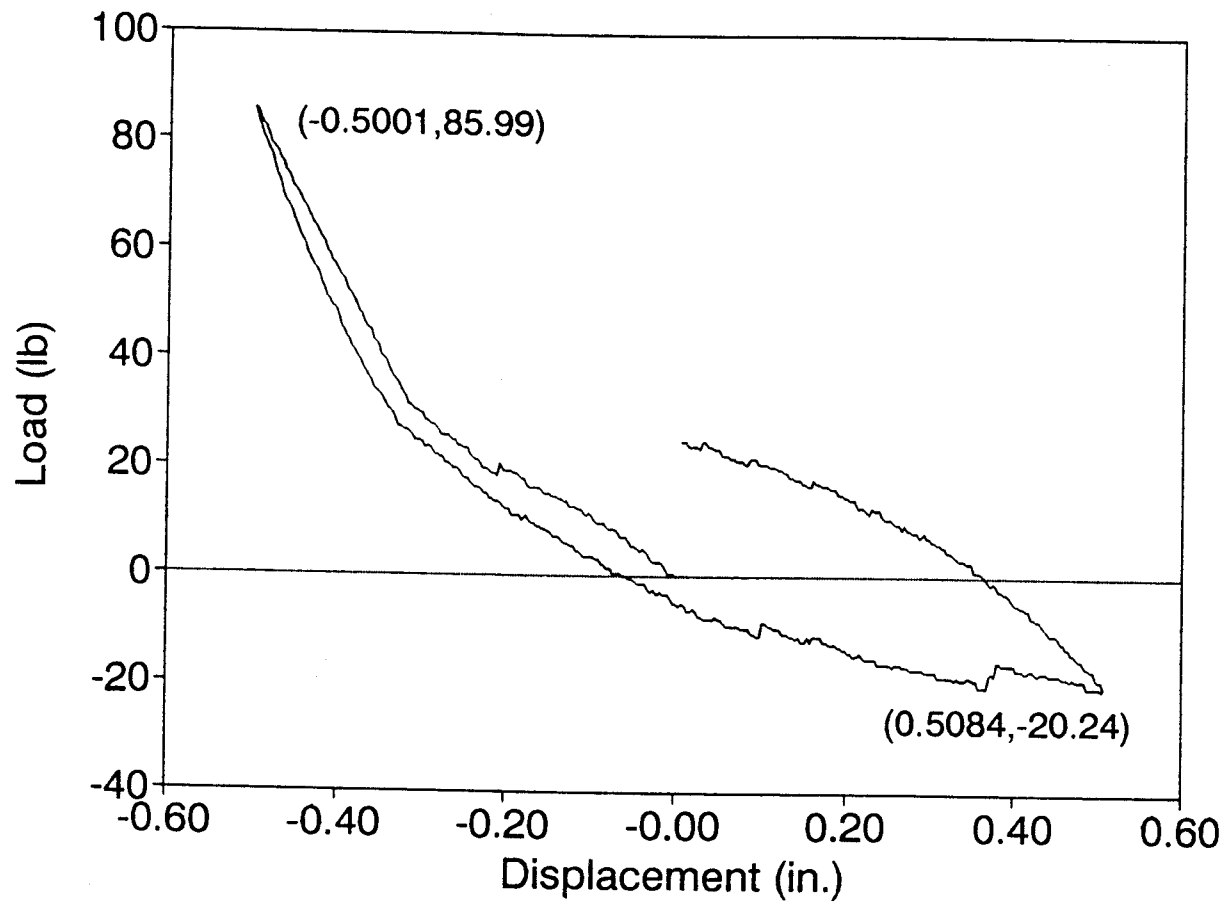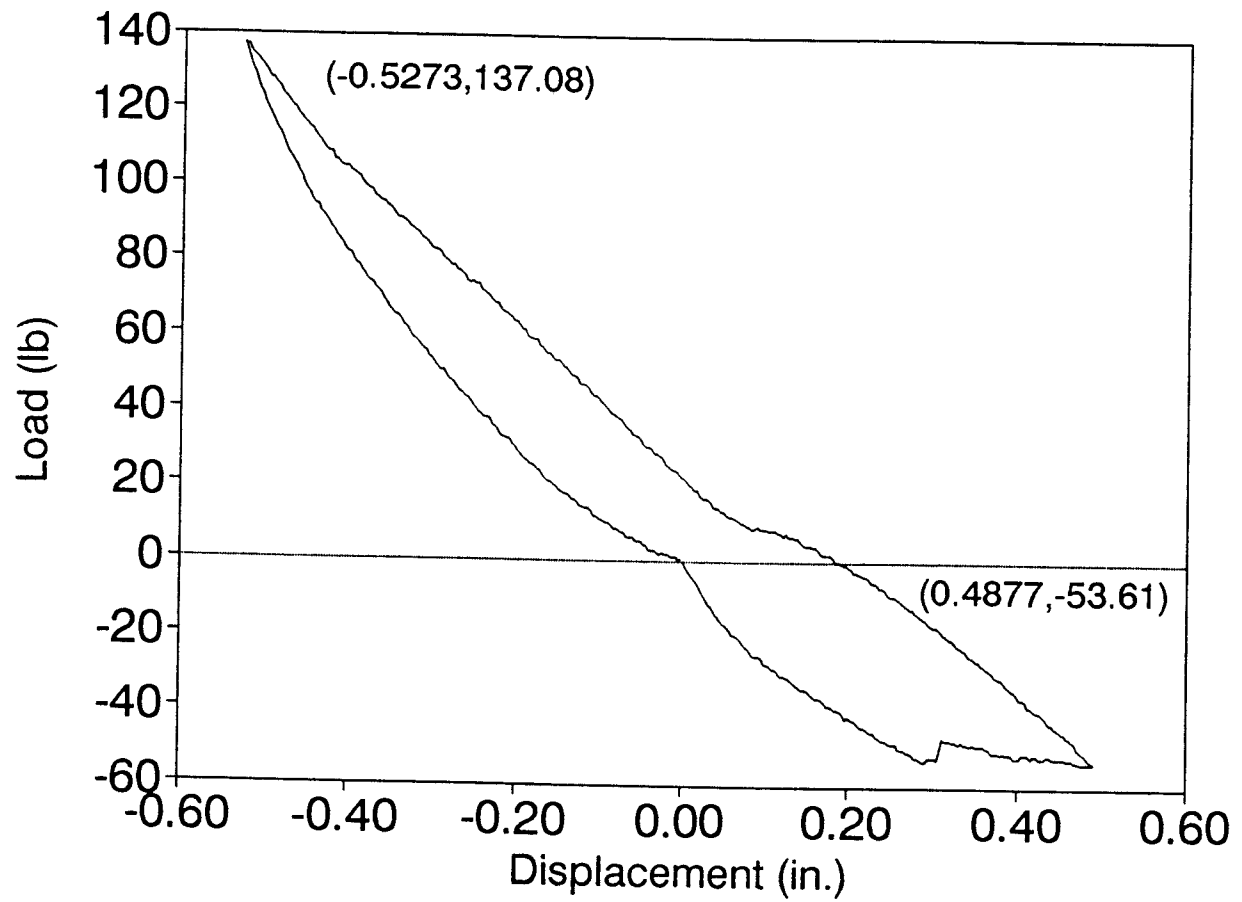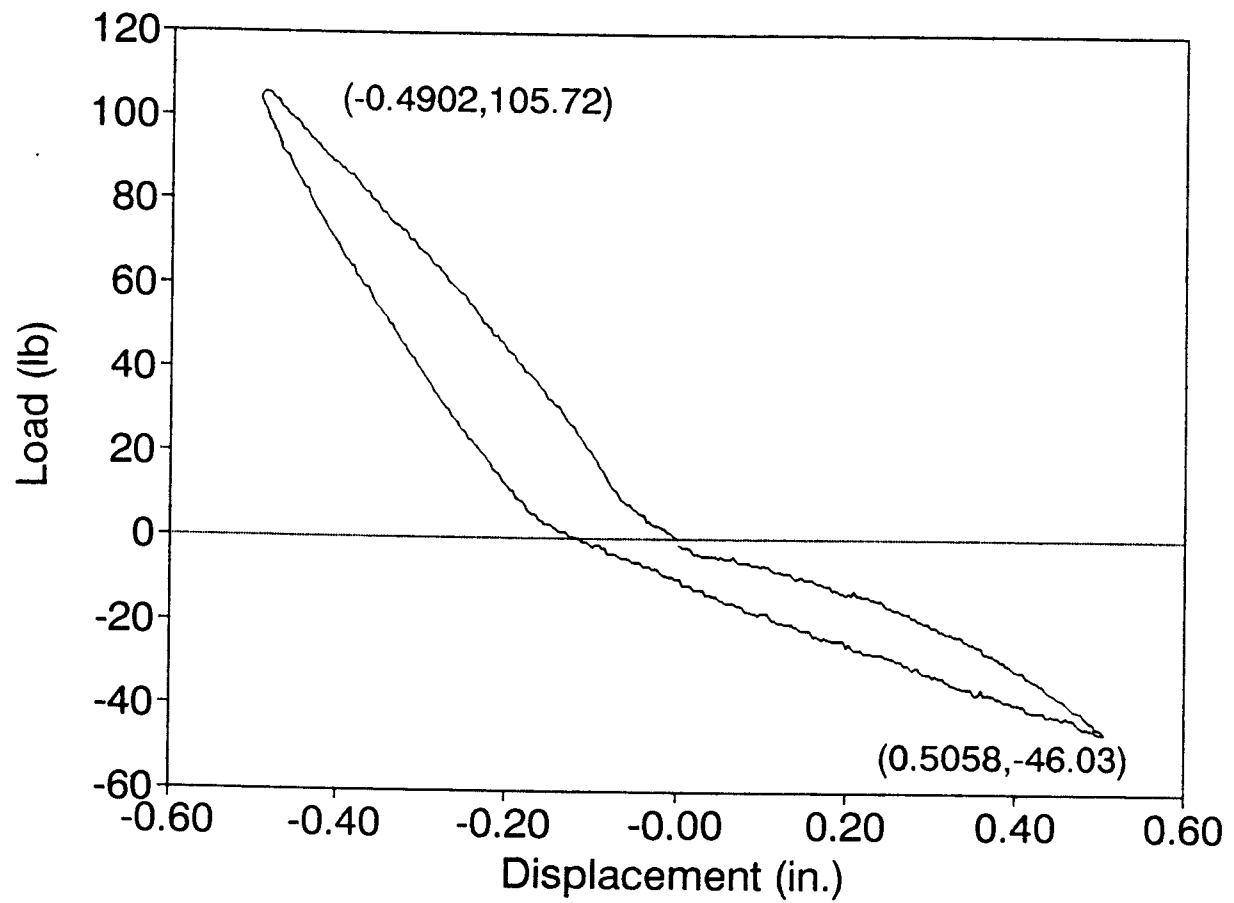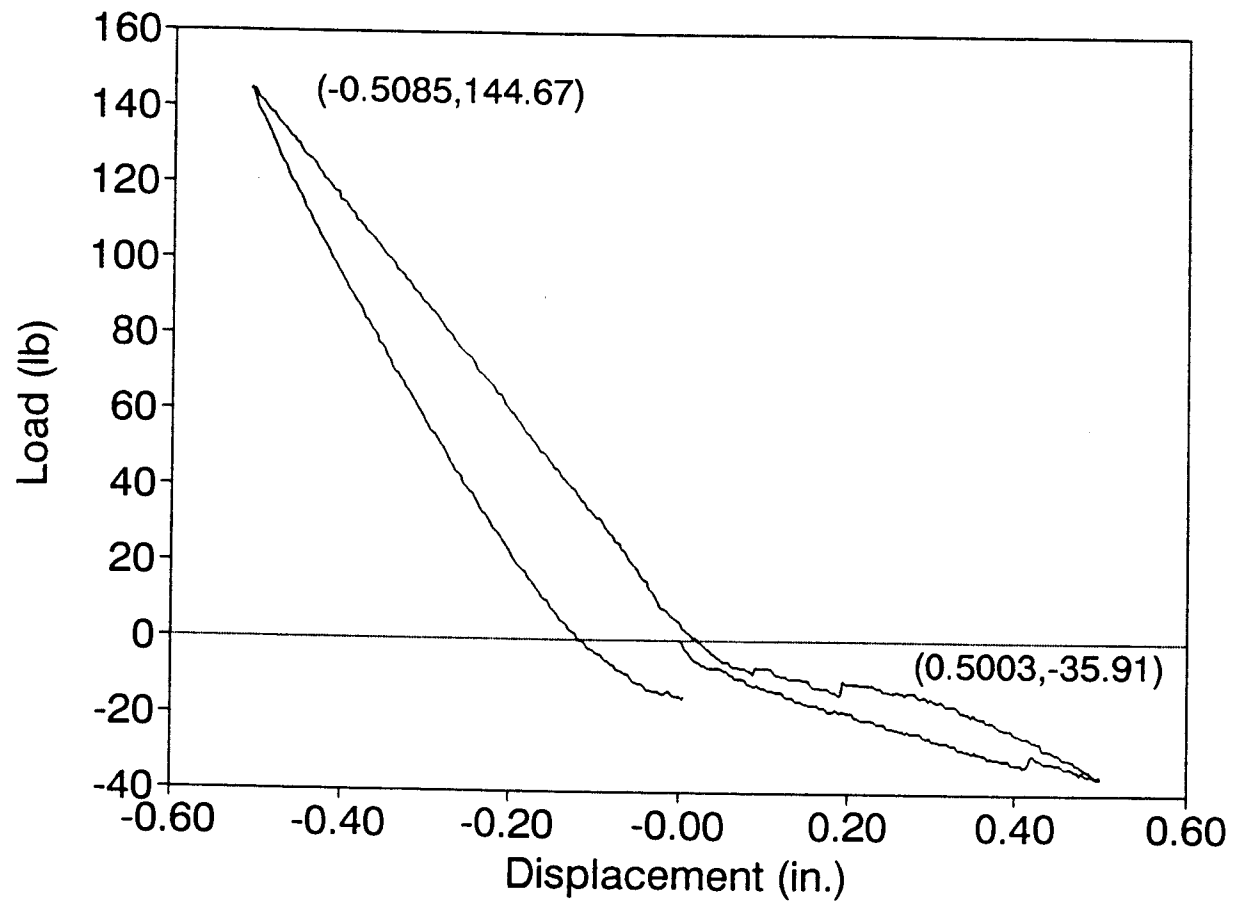
These hysteresis loops of the exterior wall-to-exterior wall connection will be used in the analytical procedure to verify the finite-element model.

Analytical Procedure

The relationships required to verify the experimental procedure and those that are to be used in the full-structure model (Kasal 1992) can be obtained from a two-dimensional finite-element model. One finite-element model was set up to predict the behavior of the exterior wall-to-exterior wall connection tests just described. This finite-element model served as the verification of the finite-element method. The material properties and nailing schedule were modified to model the full-structure connection as assembled by Phillips (1990), and the finite-element model was then used to obtain the characteristic load-displacement and moment-rotation relationships required for the full-structure finite-element model.

Wood and Gypsum board

The wood and gypsum board were modeled in a manner similar to the other two-dimensional models, with a four-node plane stress isoparametric solid element (Figure 4-4). The material properties from the plywood and gypsum board

bending tests were used in the verification finite-element model, and handbook values were used to obtain the relationships that were used as the nonlinear springs in the full-structure model.

Nails

The nails in this model were represented with a pair of two node, nonlinear, load-deflection elements (Figure 4-5). The load-slip relationships for the nails were obtained from two sources. Phillips (1990) provided load-slip results for tests performed on a 16d nail joint fastening two Douglas-fir studs. The load-slip relationships for the drywall and 6d nails used to fasten the gypsum board and exterior sheathing to the studs were provided by Polensek and Bastendorff (1987). The load-withdrawal curve that was used for the 16d nail was taken from Table 3-2, and corresponded to the 16d nail with $1\frac{1}{2}$ in. of shaft exposed. The separation of the sheathing from the studs was handled with a curve made up from the withdrawal-load curves of Table 3-2 and the pull-through curves of Tables 3-3 and 3-4. The two curves were combined in series so that each part carried the same load and could displace independently of each other, to model the actual behavior of the sheathing joint.

The Assembled Models

Both the verification model and the model used to obtain the final connection stiffness relationships utilized the same finite-element mesh. The only differences occurred in the different material properties, boundary conditions, and number of nails used. The mesh used for both models is shown in Figure 6-10.

Verification Model

To accurately model the boundary conditions of the verification model, only one node was fixed against translation. Node A in Figure 6-10 was the corner node of stud 1 (Figure 6-3). This node was fixed in the x- and y-directions but was allowed to rotate about the z-axis. This simulated the hinge action of the test fixture. The finite-element loading was accomplished by forcing node B, which is the corner node of stud 5, in a straight line toward node A. The reaction loads at node B were recorded, and the resultant load in the line of the imposed displacement represented the load recorded by the load cell.

Closing resistance. The first loading case simulated the corner subjected to hysteresis loading initiated by closing the connection. The hysteresis loop in Figure 6-11 is the result of 40 load steps. Ten load steps closed the corner a total of about 0.5-in. Twenty load steps then proceeded through the zero displacement point and continued
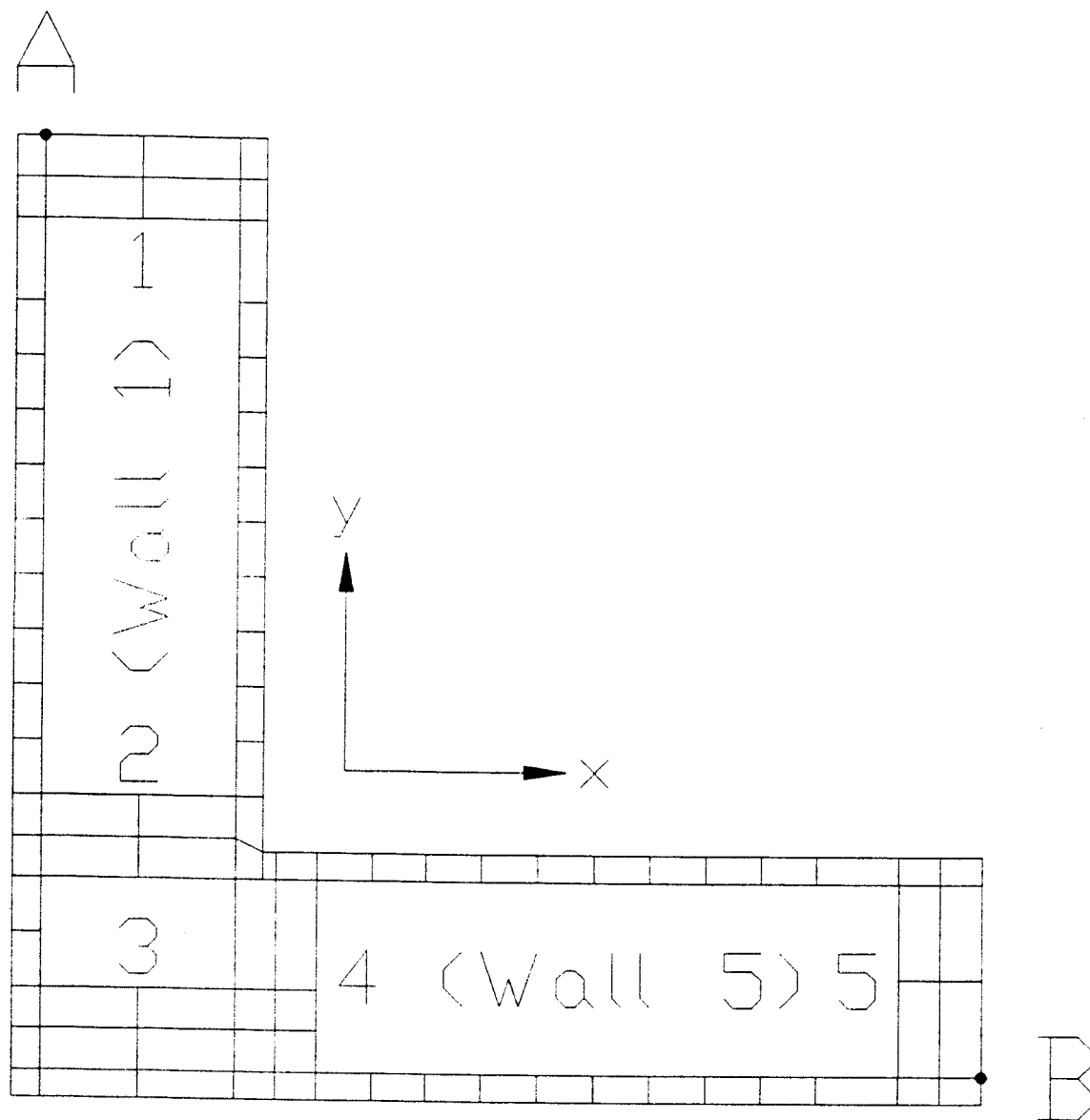
Figure 6-10. Finite-element mesh used in the exterior wall-to-exterior wall corner connection model.
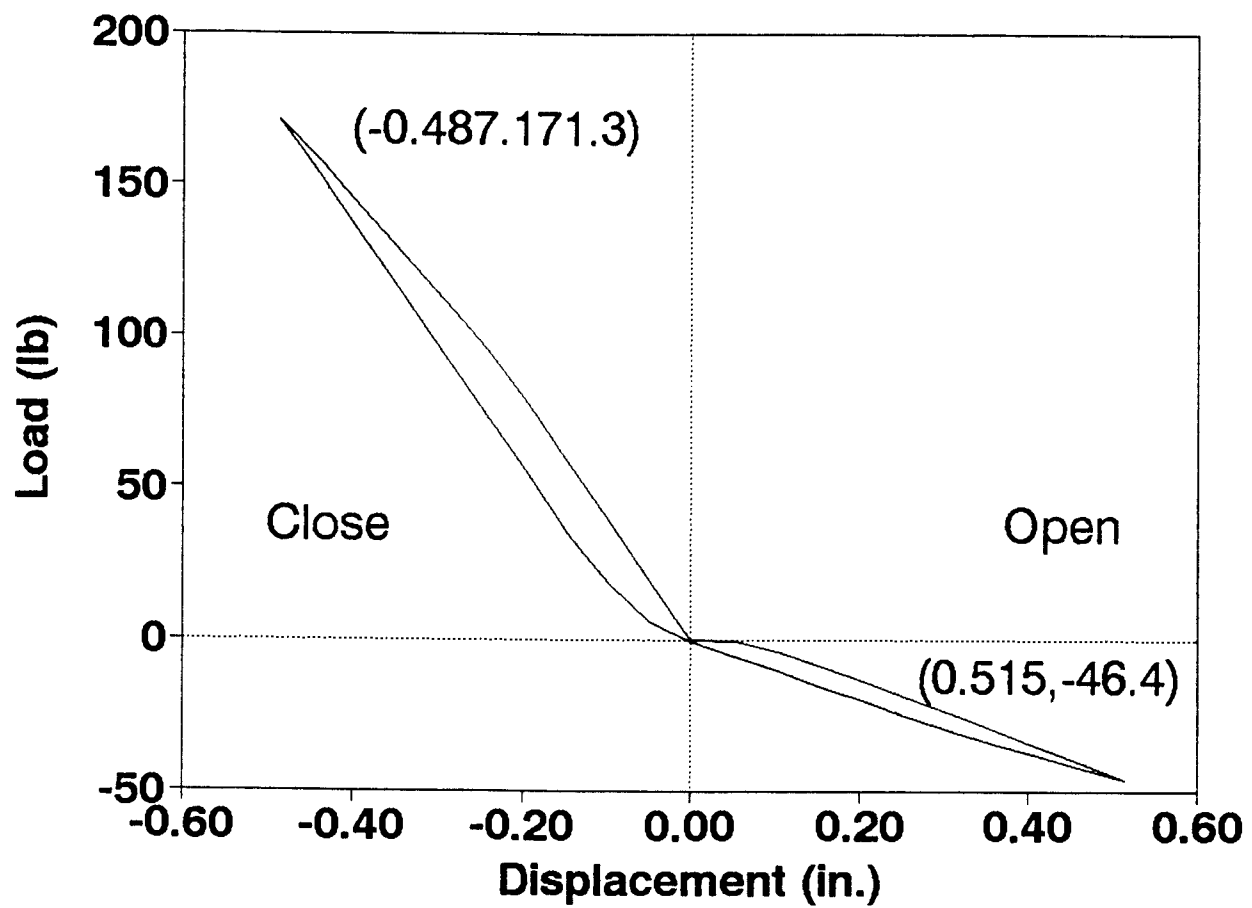
Figure 6-11. Load vs load head displacement relation obtained from a finite-element model of the exterior wall-to-exterior wall connection when the loading sequence is close-open-close.

until the connection was open a distance of 0.5-in. Finally, the connection was brought back to the starting position to complete the hysteresis loop.

Figure 6-11 shows the load-displacement relationship of the loadhead movement as the model was loaded. When this curve is compared to Figures 6-4, and 6-8, (tests which were initiated by closing the corner) it compared fairly well in shape, however the load values tended to be low when comparing the opening portion of the curves. The average loadhead displacement and load for Figures 6-4 and 6-8 were .487-in. at 118.1 lb in closing and .515-in. at 47.8 lb in opening. At the same displacement values, the finite-element model predicted a closing load of 171.3 lb (45.0% error), and an opening load of 46.4 lb (2.9% error).

An explanation for the large error in closing and small error when opening can be found in the model where all gaps between the materials were assumed to be zero. Therefore, when the model was forced into closure, the gypsum board and studs that made up the corner assembly were instantaneously opposing the movement, and began resisting from the start of the test. The true behavior of the connection was different. When the connection was forced into closure, it had initial gaps between the materials that were a result of imperfect construction. These can arise from warped or twisted members, cuts that are not perfectly straight, and misalignment of the materials during construction.

Therefore, when the connection was closing, not all the materials were making contact from the start. As a result, the resisting load of the connection was lower then that of the finite-element model. When the model was loaded in tension, forcing the connection to open, the status of the initial gaps did not play a role since the materials were continuously separating.

Opening resistance. The second case simulated with the finite-element model was that of the corner connection being subjected to a hysteresis loading initiated by opening the connection. The boundary conditions for this case were identical to the previous case. The loading was accomplished in a similar way with the exception that the load path started by opening the connection as opposed to closing it. Forty load steps were used to open, close, and return the connection to the unloaded position.

Figure 6-12 shows the load-displacement relationship. The curve begins at the origin, and as the connection opened, the curve proceeds until a displacement of 0.495-in. and a load of 46.2 lb was reached. The average of the three tests (Figures 6-5, 6-7 and 6-9) that were loaded in the same sequence produced a load of 42.8 lb (7.9% error) for the same displacement. The model was then loaded in compression, closing the connection until the loadhead movement reached 0.515-in. past the starting position. That displacement required a load of 175.8 lb for the finite-
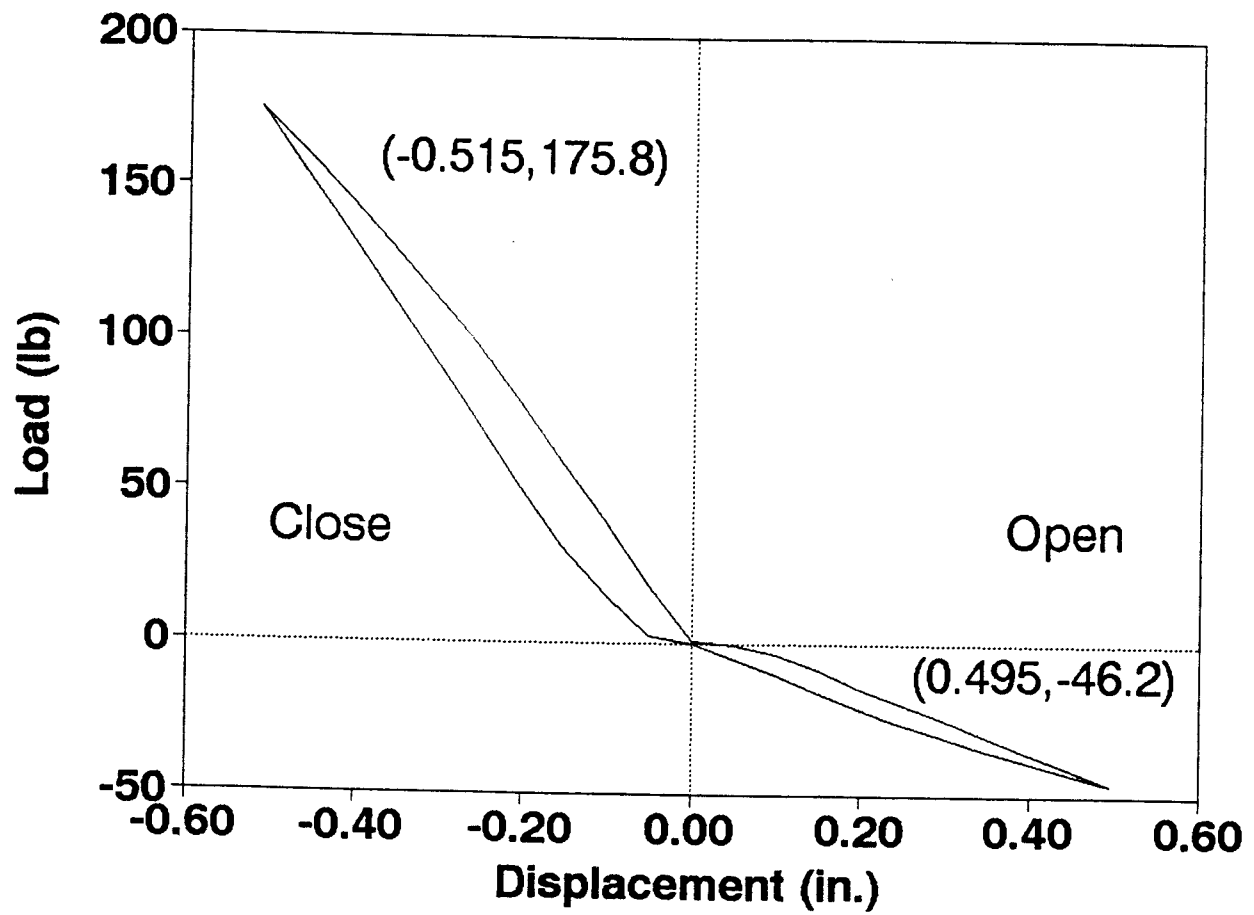
Figure 6-12. Load vs load head displacement relation obtained from a finite-element model of the exterior wall-to-exterior wall connection when the loading sequence is open-close-open.

element model and 140.5 lb (25.1% error) for the average
load of the three tests. Again it was obvious that the
model performed more like the experimental specimens when
loaded in tension than in compression due to the affects of
the gaps in the test.

Full-Structure Connection Model

There were three relationships needed for the exterior
wall-to-exterior wall connection in the full-structure model
(Kasal 1992). The first one was the separation stiffness of
the transverse wall (wall 1) from the longitudinal wall
(wall 5) in the y-direction. Secondly, the separation
stiffness of the longitudinal wall from the transverse wall
in the x-direction. Finally, the rotational stiffness of
the connection was needed as the connection was loaded in
both closing and opening.

The finite-element mesh used in the full-structure
connection model was not altered. However, changes were
made to the material properties and the nail properties and
locations. Phillips (1990) provided longitudinal bending
moduli (E_L) for the studs used in the connection. With E_L
and equations 4-1 to 4-5, the other material properties for
the studs were found. However, Phillips did not provide any
material properties for the sheathing properties used in the
structure therefore the material properties from our testing
were used. The load-slip values for the 16d nails that

Phillips (1990) provided were used rather than the properties found by Polensek and Bastendorff (1987).

The nailing schedule for the connection (Phillips 1990) was as follows: the gypsum board sheathing had drywall nails placed at a 7-in. spacing on all framing members. To handle this spacing with a 24-in. section of the connection, the nails were assumed to be spaced at 6-in. in the model, but their stiffnesses were multiplied by 6/7. The exterior sheathing had 6d nails placed every 6-in. along the perimeter framing members, and 12-in. along interior framing members. Unlike the verification model, this model did not have any nails fastening the exterior sheathing to studs 2 or 4. This corresponded to the nail schedule used in the connection of the experimental structure. The framing members (studs 3 and 4) were fastened with 16d nails spaced 6-in. along their lengths. All withdrawal and pull-through values for the nails remained the same as the verification model.

Separation of wall 1 from wall 5 in the Y-direction. The load-displacement relationship of wall 1 separating from wall 5 was obtained by moving wall 1 and holding wall 5 stationary. The load was applied by pulling the edge corners of stud 1 in the positive y-direction and recording the resultant loads. Fifteen load steps were applied in 0.01-in. increments, for a total of 0.15-in. The outside faces of studs 4 and 5 were held fixed to prevent the

framing of wall 5 from translating.

The results of the finite-element model, along with the loading and boundary conditions are shown in Figure 6-13. Figure 6-14 shows a plot of the displaced structure as it was loaded. The separation was found by recording the translation of the center of stud 2 in the y-direction as the load was applied. It should be noted that these results were for a 24-in. section of the connection. If these results were to be expressed as springs in a model every 12-in., the value of the load would be divided by two to make the input valid.

Separation of wall 5 from wall 1 in the X-direction. This relationship was obtained in a manner similar to the one described above. The corner nodes of the edge of stud 5 were forced through fifteen displacement steps in the x-direction of 0.01-in.

The resultant loads were totaled after each step and compared to the slip of the exterior sheathing. The final results of the run, along with the boundary conditions are shown in Figure 6-15. A plot of the displaced structure is shown in Figure 6-16. In this plot, studs 3 and 4 are not going to separate since the exterior sheathing is nailed to stud 3, therefore stud 3 is pushing against stud 4 and will remain in contact. The displacement occurs between the exterior sheathing and stud 3. Again, it should be noted
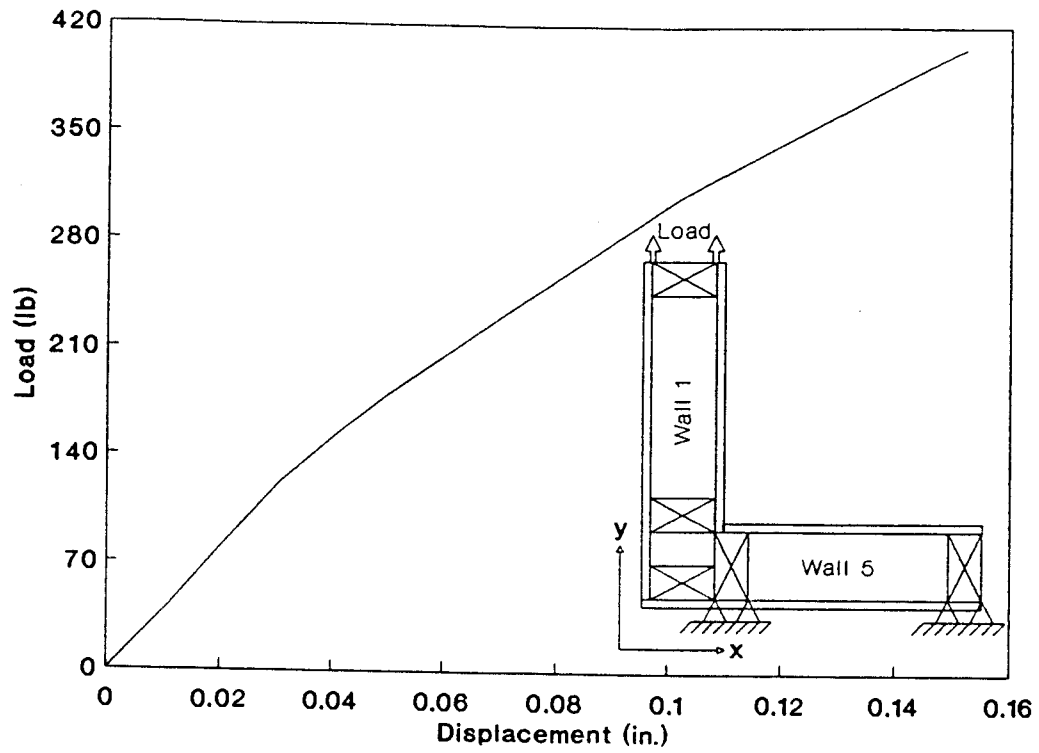
Figure 6-13. Characteristic load-displacement relation obtained from a finite-element model of wall 1 moved in the y-direction away from wall 5.
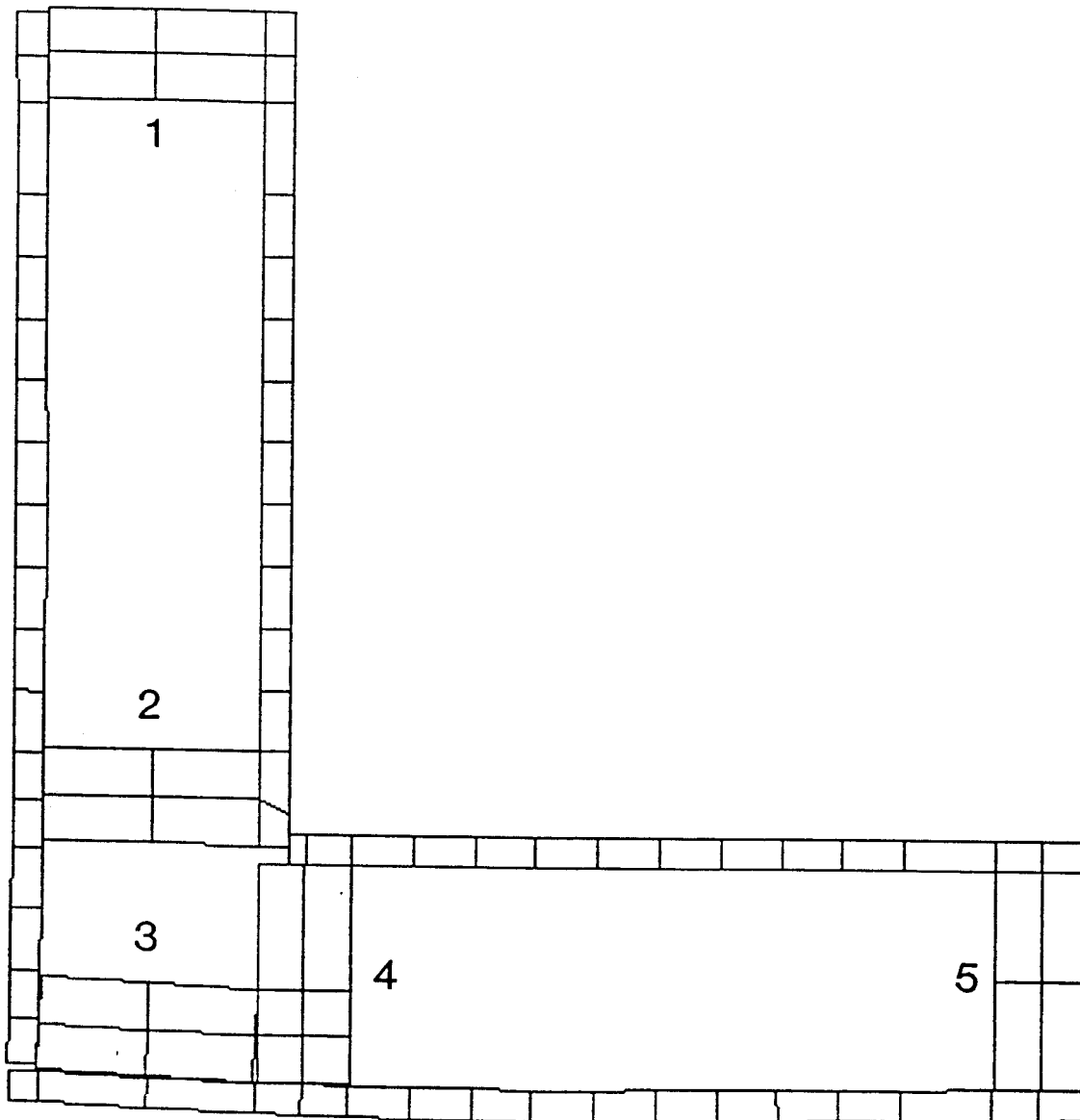
Figure 6-14. Displaced structure of the exterior wall-to-exterior wall connection as wall 1 is separating from wall 5 in the y-direction (Load = 406 lb, displacement of stud 2 in the y-direction = 0.152 in., displacement scale = 2).
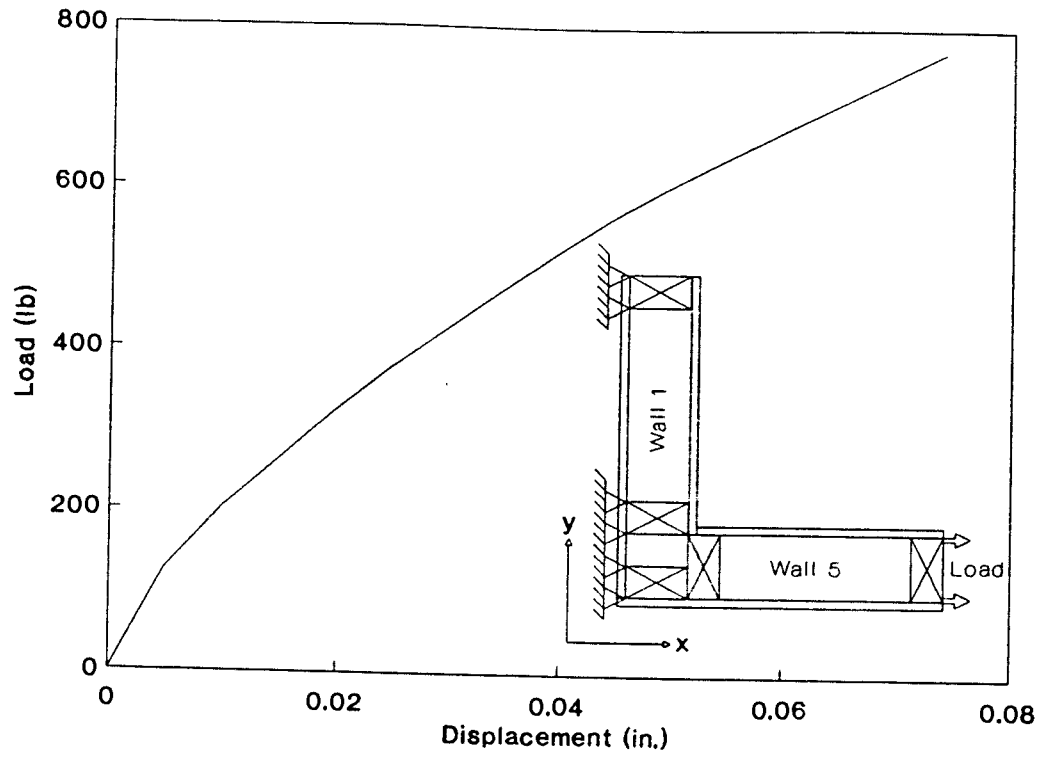
Figure 6-15. Characteristic load-displacement relation obtained from a finite-element model of wall 5 being pulled in the x-direction away from wall 1.
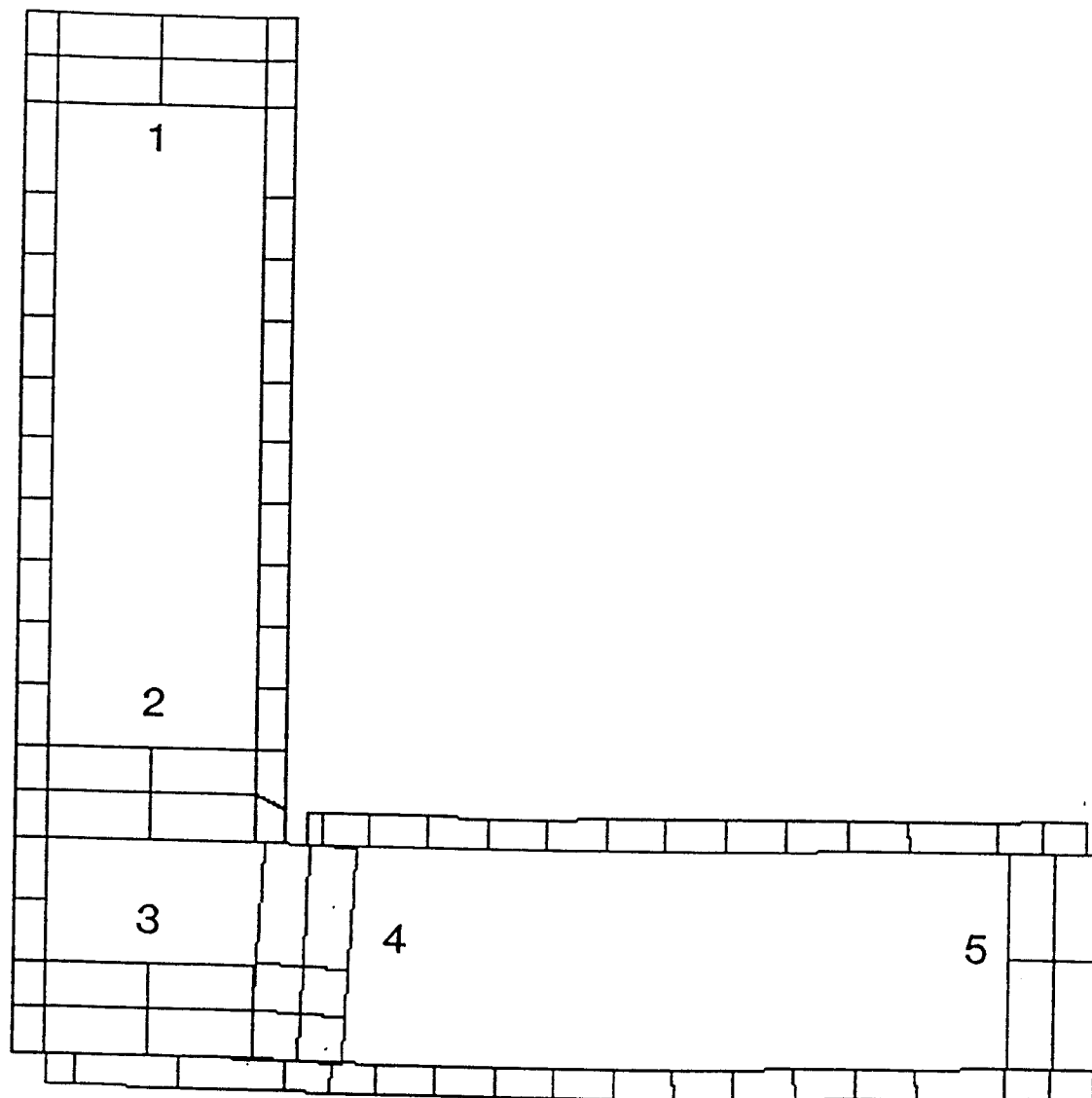
Figure 6-16. Displaced structure of exterior wall-to-exterior wall connection as wall 5 is separating from wall 1 in the x-direction (Load = 772 lb, displacement of exterior sheathing in the x-direction = 0.074 in., displacement scale = 2).

that these represent the separation stiffness for a 24-in. section.

Rotational stiffness of the exterior wall-to-exterior wall connection. For this finite-element model, the boundary conditions and loading situation were identical to the verification model. Node A (Figure 6-10) was fixed against translation, but free to rotate as node B was displaced toward and away from it.

Unlike the verification model, this model was only loaded in one direction. It was first loaded in such a way as to close the connection. The characteristic stiffness results of the closing and opening of the exterior wall to exterior wall connection are shown in Figure 6-17. As with the verification model, the connection was much stiffer in closing. Figure 6-18 shows how the connection looked when node B was moved 0.283-in. toward node A. The model was then run again with the connection opening with node B being pulled away from node A. Figure 6-18 shows the connection when node B was moved 0.283-in. away from node A.

The rotation for the moment-rotation relationship was obtained by following the paths of the mid-side nodes located in the short side of studs 2 and 4. For stud 2, these two nodes were followed in the y-direction and divided by 3.5-in. to give a rotation in radians. A similar procedure was followed to acquire the rotation of stud 4.
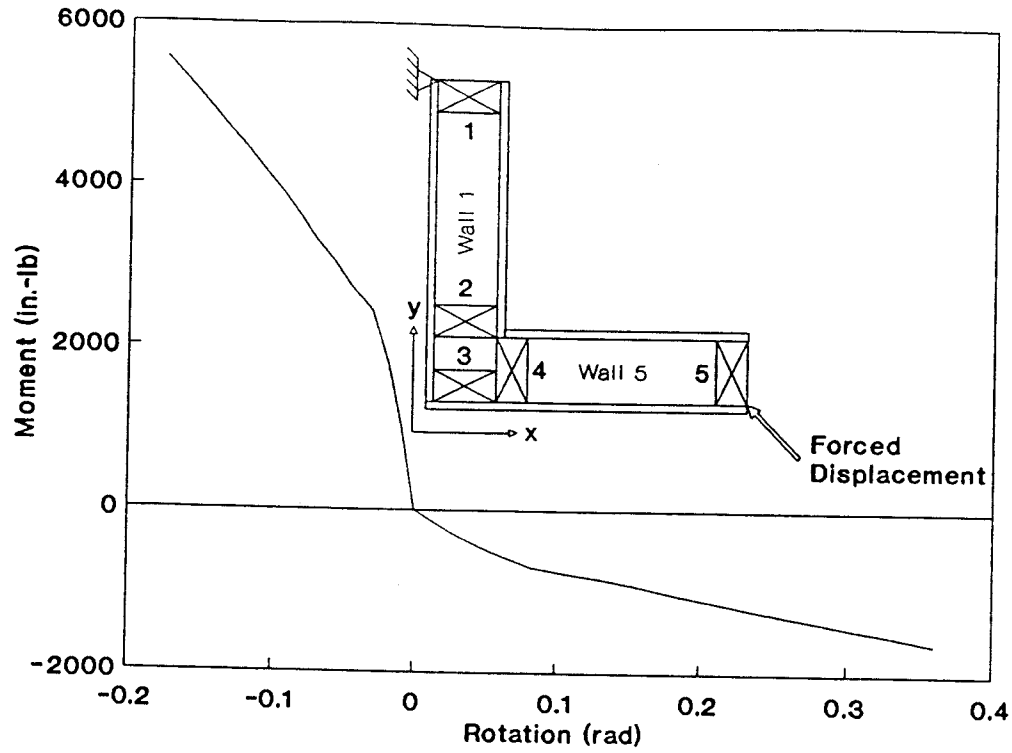
Figure 6-17. Characteristic moment-rotation relation obtained from a finite-element model between the moment applied to the connection, and the relative rotation of studs 2 and 4.
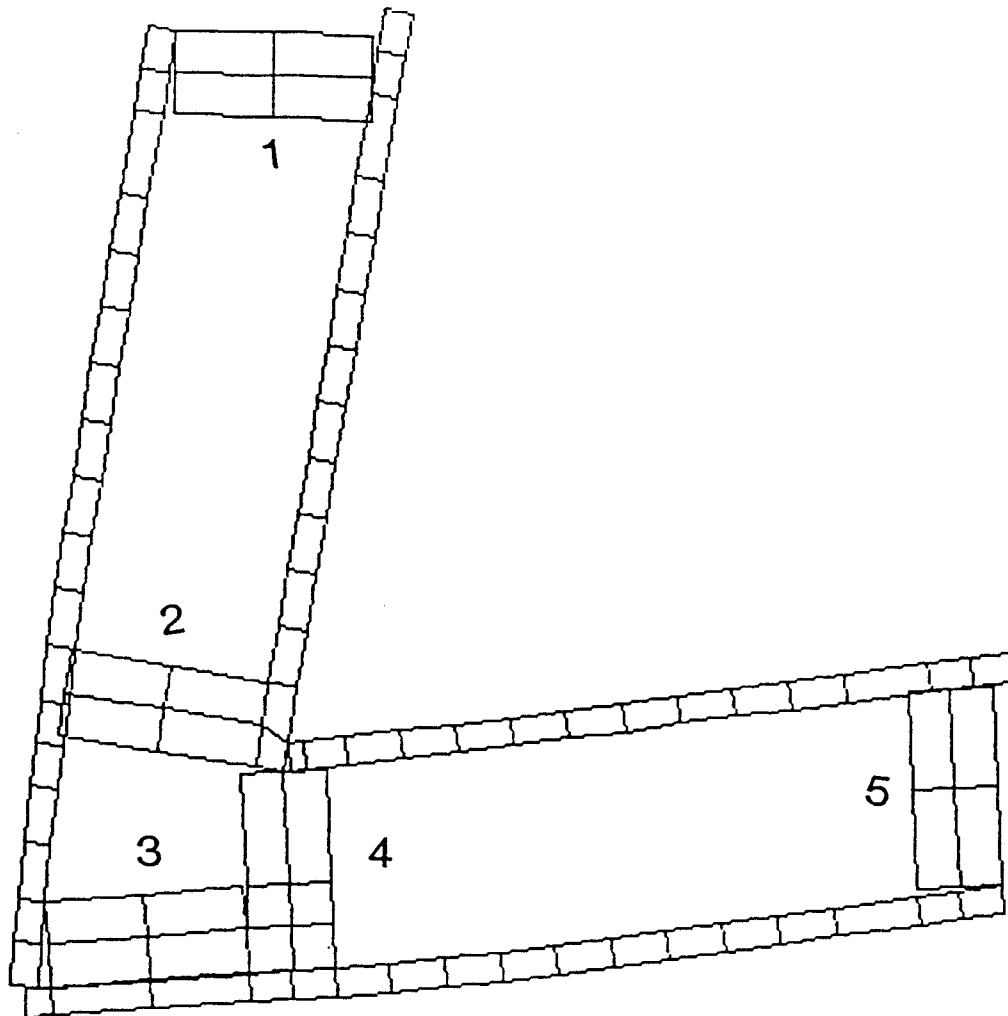
Figure 6-18. Displaced structure of the exterior wall-to-exterior wall connection loaded such that the corner closes (Moment = 4461 in.-lb, rotation = -0.121 rad, displacement scale = 1).

The two rotations were combined to find the rotation of one stud relative to the other.

Comparing Figures 6-18 and 6-19 it is obvious that the connection pivots about two separate points. When the connection is closing, the connection pivots about the point where studs 2 and 4 meet. However, when the connection is opening, the pivot point is about the outside corner of stud 3. Because of this, the moments for the each load case were found in a different way. The load was always in the same location and acting in the same direction, at node B acting on the line from A to B. The moment arm for each case was the distance from the pivot point to where it intersected the line of force at a right angle. This was 11.3 in. when the connection was closing, and 12.7 in. when the connection was opening.

The relationship in Figure 6-19 can now be entered into the model as a nonlinear spring. It can be incorporated into the full-structure model to represent the rotational stiffness of a 24-in. section of the intercomponent connection.
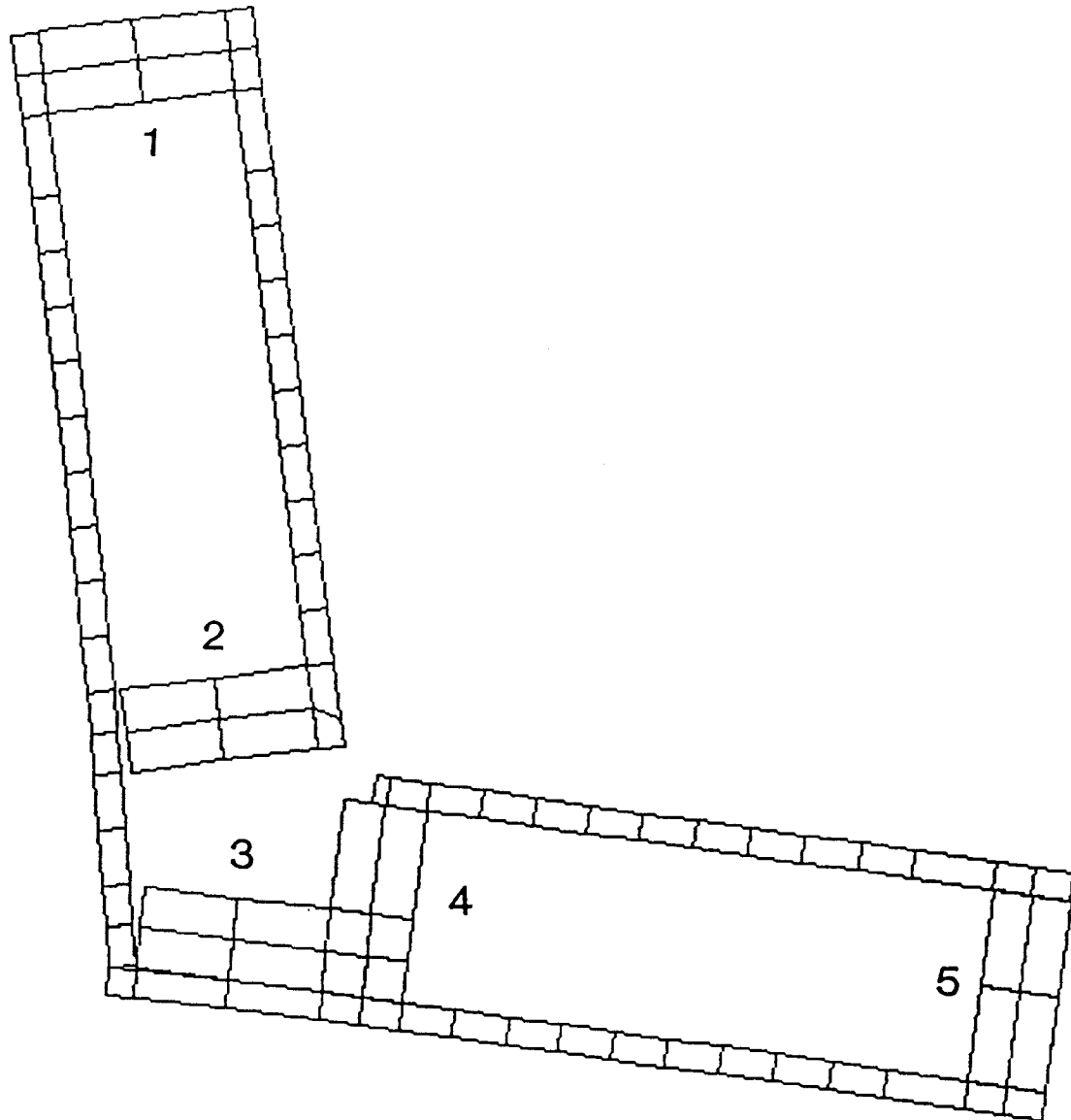
Figure 6-19. Displaced structure of the exterior wall-to-exterior wall connection loaded such that the corner opens (Moment = -1292 in.-lb, rotation = 0.259 rad, displacement scale = 1).

7. EXTERIOR WALL-TO-INTERIOR WALL CONNECTION

The full-scale structure that was built and tested by Phillips (1990) was assembled in such a way that the exterior wall-to-interior wall connection offered resistance only at the wall top plates.

The top assembly for the exterior wall-to-interior wall connection is shown in Figure 7-1. The connections consisted of a double layer of studs, the upper top plates and the lower top plates. The upper top plates consisted of a continuous 2×4 oriented along the exterior wall, with the end of the interior wall 2×4 lying flush against its side grain. The lower top plates had a 2×4 running along the top of the interior wall with one edge flush against the exterior sheathing. The 2×4's of the exterior wall were flush against the side grain of 2×4 of the interior wall. The connection was fastened together with 10d nails spaced at 6-in. intervals.

Only two relationships were needed for the finite-element model of the full structure. The first was the rotational resistance as a load was applied to the end of the interior wall, in a direction parallel to the exterior wall. The second was the separation stiffness of the connection as a load was applied at the end of the interior
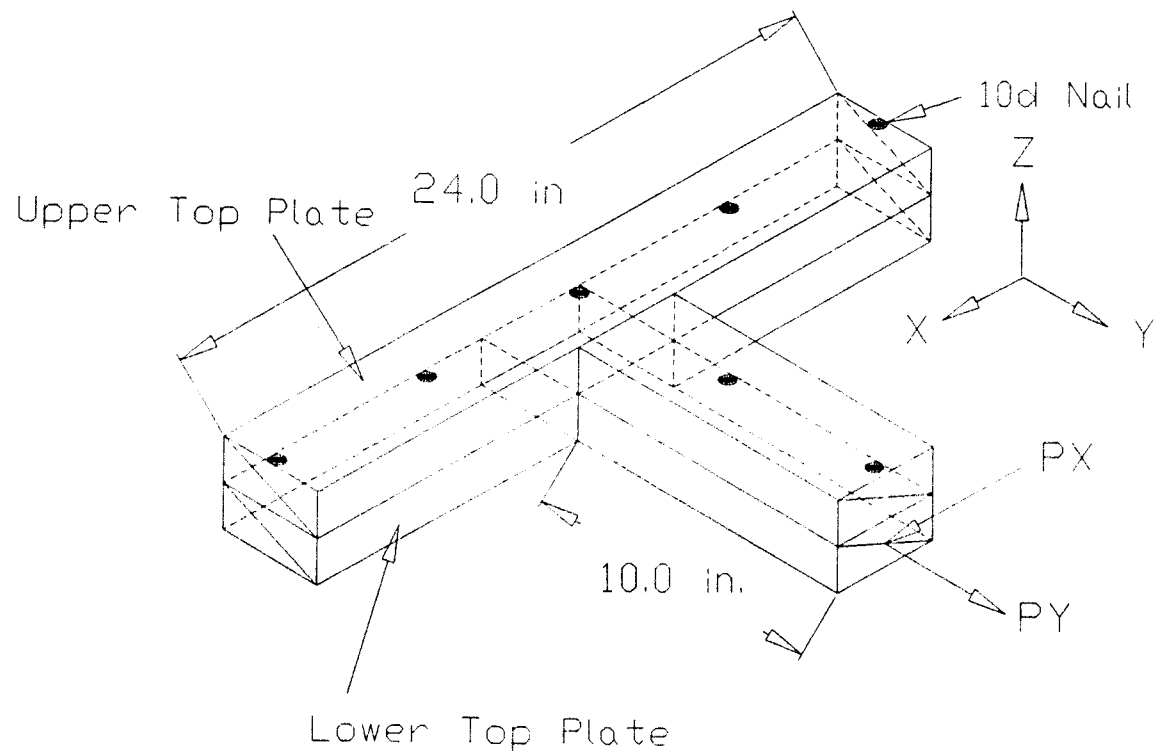
Figure 7-1. Exterior wall-to-interior wall connection with 10d nails spaced 6 in. on center.

wall, along the line of the interior wall.

No testing was performed on this connection, and therefore only theoretical results are presented here. It was decided to use the same two dimensional procedure used for the exterior wall-to-foundation connection, since that connection had excellent agreement between the analytical and experimental results.

Analytical Procedure

Since the two relationships required lie in the same plane, a two-dimensional model provided the needed information. Three types of elements were used in the finite-element model.

The Wood

The wood was represented in the same way as in the finite-element model of the exterior wall-to-foundation connection. Four-node (Figure 4-4) and eight-node plane stress isoparametric solids were used to model the 2x4's.

There were four connections of this type used in the full structure. Each connection consisted of 5 members. The material properties used in the model were based on the average longitudinal bending modulus E_L found by Phillips (1990). Poisson's ratios were obtained from Bodig and Jayne

(1982). The remaining moduli of elasticity and the three shear moduli were obtained from equations 4-1 to 4-5.

The nails

Each 10d nail was modelled with a pair of two-node, nonlinear, load-deflection elements (Figure 4-5). Phillips (1990) provided one load-slip curve, parallel to the grain, for the 10d nails. Since a load-slip curve for a nail loaded perpendicular to the grain was not provided by Phillips, the curve for a nail loaded parallel to the grain was used for both directions. While load-slip results by Polensek and Bastendorff (1987) were available for the perpendicular to grain relationship, they differed from the load-slip data given by Phillips (1990). A small error was accepted by assuming the nail acted the same in both directions. The alternative was to accept the results of Polensek and Bastendorff (1987), but the error associated with those data may have been greater.

The relationship used in the model for the 10d nail parallel and perpendicular to the grain was:

$$\text{Load(lb)} = 792 * \text{Slip(in.)}^{0.6191} \qquad 7\text{-}1$$

The gaps

The gaps were modelled with a load-deflection element with a high compressive resistance (1×10^7 lb/in.) and very little tensile resistance (1×10^{-3} lb/in.). This permitted the free separation of materials , but allowed no overlap.

The Assembled Model

The fully assembled finite-element model is shown in Figure 7-2. The model consisted of 416 nodes to define the 5 structural members. There were 264 four-node, 8 eight-node isoparametric solid elements, 86 nonlinear load-deflection elements used for the nails and 15 gap elements used for a total of 373 elements.

Since the model is plane stress, and therefore two dimensional, the elements have been stacked on top of one another. The model obtained the needed bending stiffness when the $1\frac{1}{2}$-in. thickness of the wood was input. The exterior wall extended 118-in. on both sides of the interior wall giving a total length 239.5-in. in the x-direction when the interior wall is included. The exterior wall was extended half the distance to the next wall or partition to get the full affect of the sliding action between the upper and lower top plates along the exterior wall. The small section of the interior wall extends 10-in. from the
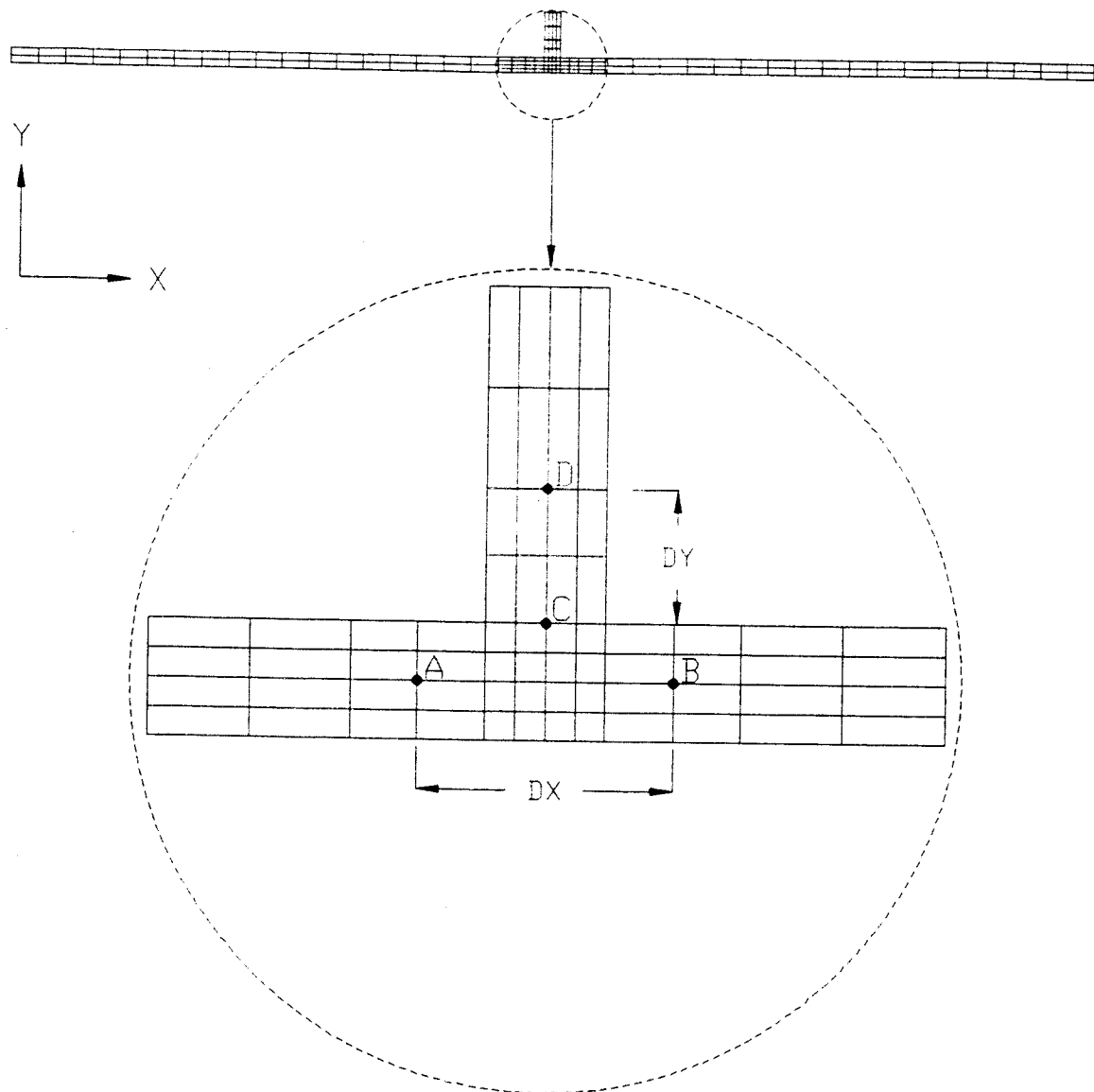
Figure 7-2. Finite-element mesh used in the model of the exterior wall-to-interior wall connection.

exterior wall for a total length of 13.5-in. in the y-direction.

Boundary conditions were applied at each end. The ends of the lower top plates were fixed in both the x and y-directions, while the upper top plate was fixed only in the x-direction to allow the upper top plate to slide relative to the lower top plate in the y-direction.

Figure 7-2 shows the segment of the model where the mesh is finer. The mesh here is four elements wide and two elements deep, as opposed to two wide and two deep for the majority of the top plate of the exterior wall. This segment of the mesh represents the portion of the connection depicted in Figure 7-1.

Rotation

Since the model was symmetric, to obtain a full moment-rotation relationship, the model needed only to be loaded in one direction. This was accomplished by applying a load to the positive y-end of the lower top plate and recording the displacements. The result is shown in Figure 7-3. The displaced structure is shown in Figure 7-4. Notice in the displaced structure that both layers of the model become noticeable.

The moment was obtained by multiplying the applied load (PX) by the lever arm length (L) as shown in Figure 7-1. The relative rotation was obtained from the upper top plate
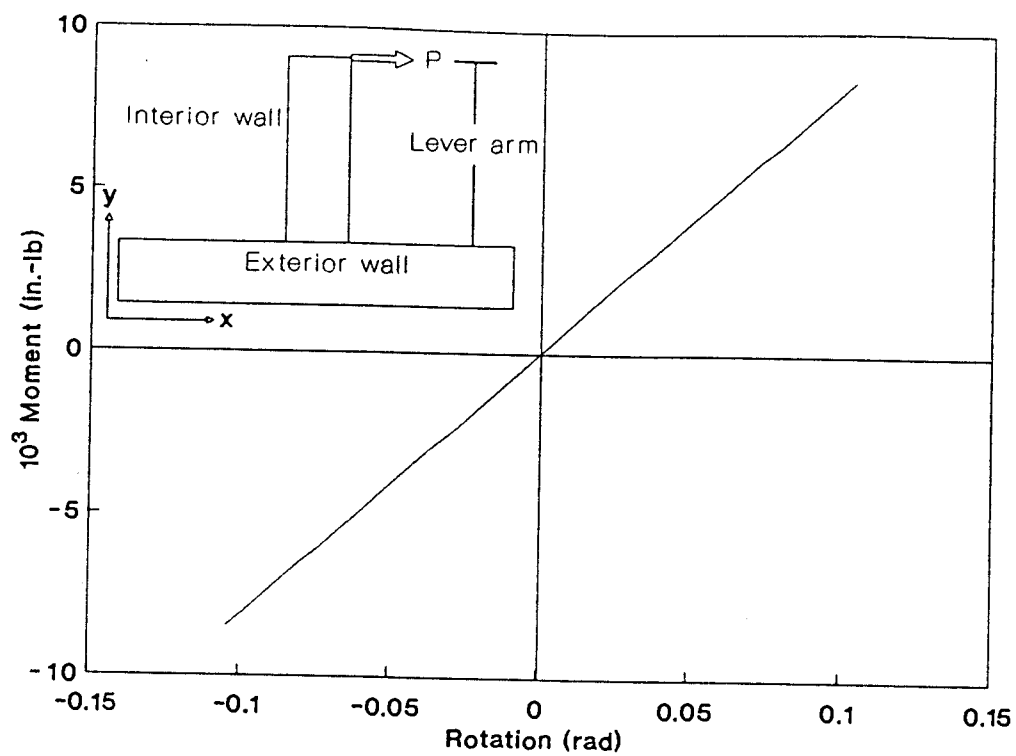
Figure 7-3. Characteristic moment-rotation relation obtained from a finite-element model of the exterior wall-to-interior wall connection.
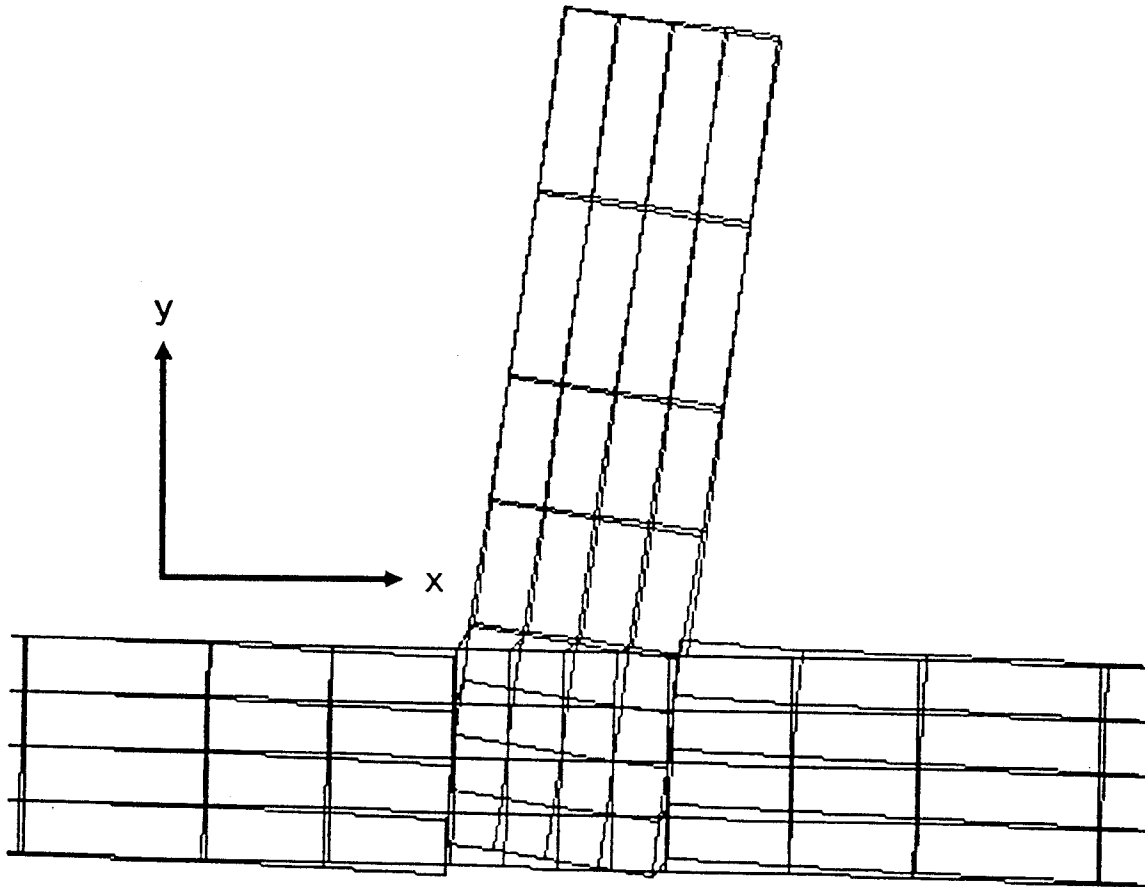
Figure 7-4. Displaced structure showing the exterior wall-to-interior wall connection subjected to a moment.

of the exterior wall and the lower top plate of the interior wall. These two members were selected because they extend the full length of the walls in question. The rotation of the exterior wall was found by recording the y-displacements of nodes A and B, shown in Figure 7-2, and dividing their differences by DX. Similarly, the rotation of the interior wall was found by dividing the differences of the x-displacements of nodes C and D by the distance DY.

Twenty-three load steps were performed on this model. A large number of load steps were used since the model had relatively few nonlinear elements and degrees of freedom, which meant each load step was solved quickly. The results of the rotational model are shown in Figure 7-3. Again, note that the model is symmetric, and therefore the third quadrant of the curve is simply the negative of the first quadrant.

Separation

Since the lower top plate of the interior wall was fastened to the upper top plate of the exterior wall with a single 10d nail, the separation stiffness of the joint should simply be the load-slip relationship input for the 10d nail. With this being the case, performing this run was only useful to do a minor check on the model.

Referring to Figure 7-1, the loading was accomplished by imposing a load in the y-direction (PY) on the lower top

plate of the interior wall. The characteristic load-displacement relation from the model is given in Figure 7-5. The separation was simply a measurement of the gap between the upper top plates of the exterior wall and the interior wall. The displaced structure is shown in Figure 7-6.

As expected, the results are nearly identical to the load-slip relation of the 10d nail in eq. 7-1.
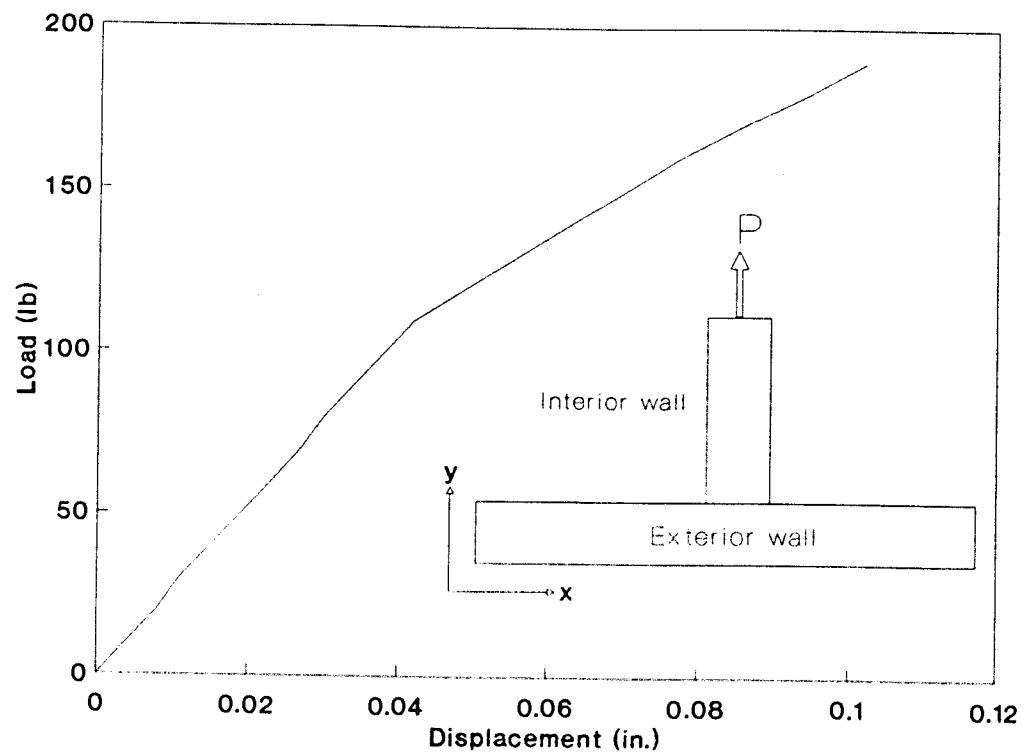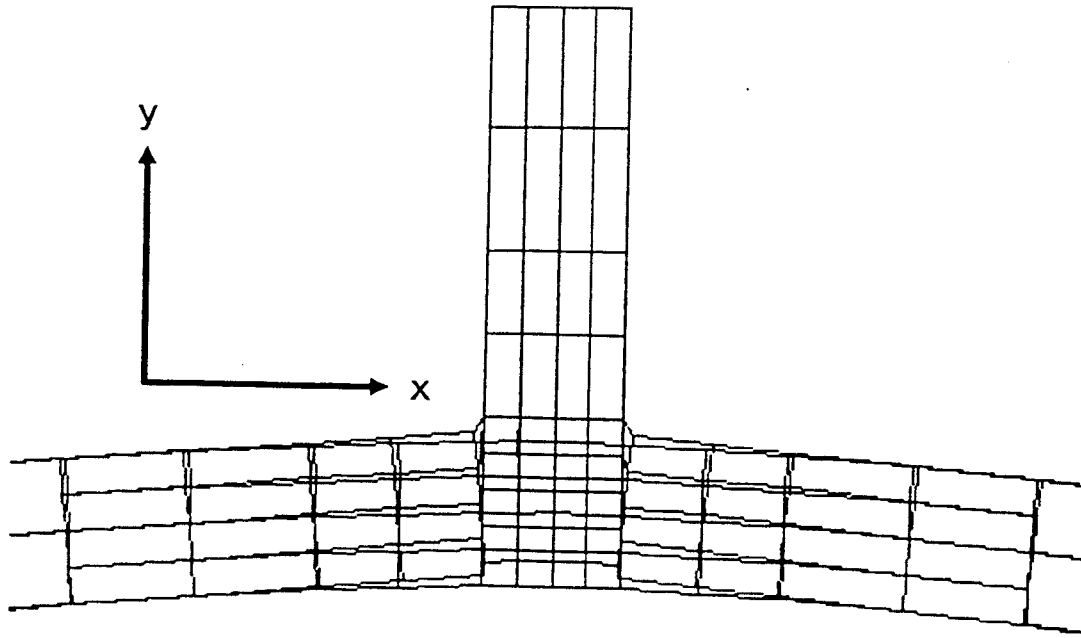
Figure 7-5. Characteristic load-displacement relation obtained from a finite-element model of the exterior wall-to-interior wall connection.

Figure 7-6. Displaced structure showing the exterior wall-to-interior wall subjected to a translational load.

8. SUMMARY AND CONCLUSIONS

Summary

The use of intercomponent connections in a light-frame wood structure allows the engineer to analyze the structure as a whole, as opposed to current design practices which treats each component as a separate design problem. Four intercomponent connections that are used in light-frame wood structures were analyzed by testing and nonlinear finite-element methods.

The main objective of this project was to model the intercomponent connections in a detailed fashion, and subject the models to various load scenarios to acquire either load-displacement or moment-rotation relationships. This way the detailed connection could be replaced by an energetically equivalent nonlinear spring and used in a larger global model of a full structure, thus reducing the total number of degrees of freedom in the global model.

The nail characteristics were nonlinear load-displacement relationships which were included in the finite-element models. Since the nails provided such a crucial role in the analysis, their characteristics had to be determined. Past literature provided some load-slip

curves for the nails used in the connections, however, some testing was performed for nails in shear. In addition, there was no literature found that provided nail withdrawal from framing or nail head pull-through with these sheathing materials and nail combinations, so tests were performed to determine these load-displacement characteristics.

The nail characteristics, along with material properties found by coupon testing, were used in the finite-element models. There were two categories of finite-element models, two dimensional and three dimensional. In the two-dimensional models the solid elements, which represented the wood and sheathing materials, were modeled with either four or eight-node isoparametric plane stress solid elements. The three dimensional model used an eight node anisotropic solid element. Both categories of models included the orthotropic behavior of the wood.

One model had a steel framing anchor used to connect two members together. The framing anchor was modeled with a four-node quadrilateral shell element. The materials in the model were prevented from overlapping by providing gap elements between the nodes of the different materials. These provided a very high resistance in compression and a negligible resistance in tension. The nonlinearity of the model was introduced by the nails. Each nail was modeled with two-node nonlinear load-deflection elements. Each node had only one degree of freedom, so two (three in the three-

dimensional model) elements had to be used to accommodate the load-displacement relationships of the nails in every direction. These elements were defined by a piece-wise linear load-deflection curve that could exhibit up to forty different slopes.

Conclusions

With the models verified, they were subjected to a series of loading scenarios to produce characteristic load-displacement and moment-rotation relationships. These relationships were assigned to energetically equivalent nonlinear springs and used in a global model (Kasal 1992) which was used to predict the load sharing characteristics of the experimental structure.

This technique of replacing a detailed model with a set of springs greatly reduces the degrees of freedom of the global model. The reduction of the degrees of freedom not only makes the analysis possible on microcomputers, but it reduces the amount of CPU time required to solve the global model. The connections were reduced from hundreds and even thousands of degrees of freedom to a total of twelve or fewer depending on how many springs were needed.

This procedure of modeling the intercomponent connections can be of great use to the engineer. With a library of connections available, an engineer can design a

wooden structure more efficiently by changing some of the variables in the model to see how the connection responds. For example, the engineer can vary the sheathing thickness in a model to determine if ⅜-in. or ½-in. sheathing will provide the rotational stiffness required.

BIBLIOGRAPHY

1. American Society For Testing and Materials (ASTM). 1985. Standard test methods for mechanical fasteners in wood, D1761. P. 294-305 in Annual Book of Standards, Vol. 04.09. ASTM, Philadelphia, PA.

2. American Society For Testing and Materials (ASTM). 1989. Standard methods of testing structural panels in flexure, D3043-87. P. 417-427 in Annual Book of Standards. Vol. 04.09. ASTM, Philadelphia, PA.

3. American Society For Testing and Materials (ASTM). 1990. Standard test methods for physical testing of gypsum board products and gypsum lath, C473-87a. P. 251-261 in Annual Book of Standards. Vol 04.01. ASTM, Philadelphia, PA.

4. Bodig, J and Jayne B. 1982. Mechanics of Wood and Wood Composites. Van Nostrand Reinhold Company, Inc., New York, NY.

5. Carrol, J.D. 1988. Withdrawal and Combined Load Capacity of Threaded Fasteners Wood Joints. MS thesis, Virginia Polytechnic Institute and State University, Blackburg, VA.

6. DeSalvo, G.J., and R.W. Gorman. 1989. ANSYS Engineering System User's Manual Version 4.4, Vol. I. Swanson Analysis Systems, Inc., Houston, PA.

7. Ehlbeck, J. 1979. Nailed Joints In Wood Structures. MS Thesis. Virginia Polytechnic Institute and State University, Blacksburg, VA. 147 p.

8. Faherty, K.F. 1982. Design of Connections. P. 367-431 in Wood: Engineering Design Concepts. (Freas, A.D., C.M. Moody, and L.A. Soltis). Materials Education Council. University Park, PA.

9. Falk, R.H., and R.Y. Itani. 1989. Finite-element modeling of wood diaphragms. Journal of Structural Engineering. 115(3):543-559.

10. Forest Products Laboratory. 1987. Wood Handbook: Wood as an Engineering Material. Agriculture Handbook 72. USDA-Forest Service, Washington, DC. 466 p.

11. Foschi, R.O. 1974. Load-slip characteristics of nails. Wood Science. 7(1):69-76.

12. Hilton, K.C., A. Polensek, and G.H. Atherton. 1976. Effect of nail spacing on rigidity of a plywood-wood joint. Wood Science. (8)4:234-236.

13. Hunt, R.D., and A.H. Bryant. 1990. Laterally loaded nail joints in wood. Journal of Structural Engineering. 116(1):111-124.

14. International Conference of Building Officials (ICBO). 1988. Uniform Building Code. ICBO, Whittier, CA. 926 p.

15. Jenkins, J.L., A. Polensek, and K.M. Bastendorff. 1979. Stiffness of nailed wall joints under short and long term lateral loads. Wood Science. 11(3):145-154.

16. Kasal, B. 1992. A Nonlinear Three-Dimensional Finite -Element Model of Light-Frame Wood Structure. PhD thesis. Oregon State University, Corvallis, OR.

17. Komatsu, K. 1989. Behavior of nailed timber joints with steel side plates. Proceedings P-89-94. Pacific Timber Engineering Conference. University of Auckland, New Zealand.

18. LaFave, K.D. 1990. Experimental and Analytical Study of Load Sharing in Wood Truss Roof Systems. MS thesis, Washington State University, Pullman, WA.

19. Liska, J.A., and B. Bohannan. 1973. Performance of wood construction in disaster areas. Journal of the Structural Division, Proceedings of the American Society of Civil Engineers. 99(ST12):2345-2354.

20. Loferski, J.R., and S. Gamalath. 1989. Predicting rotational stiffness of nail joints. Forest Products Journal. 39(7/8):8-16.

21. Loferski, J.R., and A. Polensek. 1982. Predicting inelastic moduli of sheathing to stud nail joints. Wood Science. 15(1):39-43.

22. Mack, J.J. 1966. The strength and stiffness of nailed joints under short-duration loading. Division of Forest Products Paper No. 40. CSIRO, Melbourne, Australia.

23. Mclain, T.E. 1976. Curvilinear load-slip relations in laterally loaded nailed joints. Proceedings P-76-16. Forest Products Research Society. Madison, WI.

24. National Forest Products Association (NFPA). 1988. National Design Specifications for Wood Construction. NFPA, Washington, DC.

25. Pellicane, P.J. 1991. Mechanical behavior of nailed joints with various side member materials. Journal of Testing and Evaluation. 19(2):97-106.

26. Phillips, T.J. 1990. Load Sharing Characteristics of Three-Dimensional Wood Diaphragms. MS thesis, Washington State University, Pullman, WA.

27. Polensek, A. 1978. Properties of components and joints for rational design procedure of wood stud walls. Wood Science. 10(4):167-175.

28. Polensek, A. 1988. Effects of testing variables on damping and stiffness of nailed wood-to-sheathing joints. Journal of Testing and Evaluation. 16(5):474-480.

29. Polensek, A., and K.M. Bastendorff. 1987. Damping in nailed joints of light-frame wood buildings. Wood and Fiber Science. 19(2):110-125.

30. Polensek, A., and B.D. Schimel. 1986. Rotational restraint of wood-stud wall supports. Journal of Structural Engineering. 112(6):1247-1262.

31. Tuomi, R.L., and W.J. McMutcheon. 1974. Testing of a full-scale house under simulated snowloads and windloads. Forest Service Research Paper FPL 234. Forest Products Laboratory, United States Department of Agriculture. Madison, WI.

32. Polensek, A. 1988. Predicting load sharing among substructures in light-frame wood buildings. United States Department of Agriculture (USDA), Grant Application. Oregon State University, Corvallis, OR.

33. Wilkinson, T.L. 1972. Analysis of nailed joints with dissimilar members. Journal of the Structural Division, Proceedings of the American Society of Civil Engineers. 97(ST9):2005-2013.

34. Wilkinson, T.L. 1974. Elastic bearing constants for sheathing materials. USDA Forest Service Research Paper FPL-224. Forest Products Laboratory, Madison, WI.

APPENDICES

APPENDIX A

Nail Slip, Withdrawal, and Nail-Head Pull-Through Curves
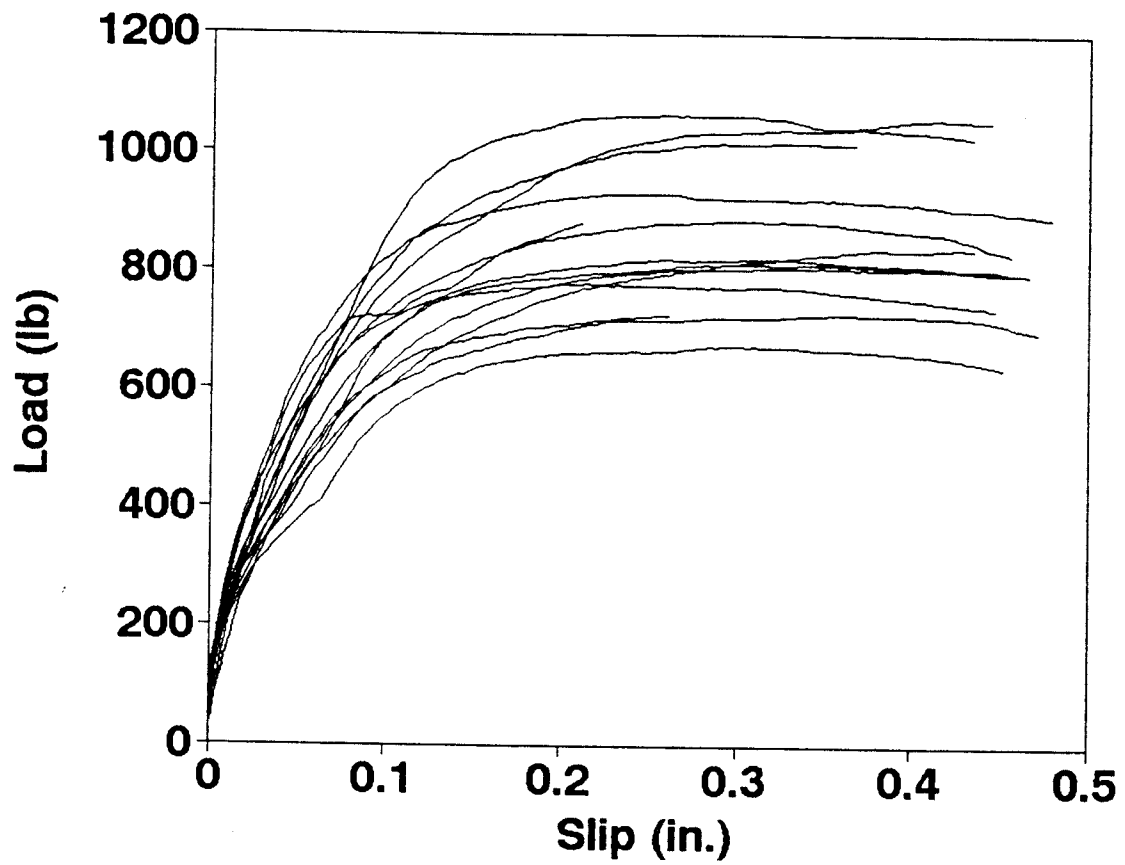
Figure A1. Combined results of the load-slip curves of three 1¼-in. JHN loaded in shear parallel to the fiber grain.
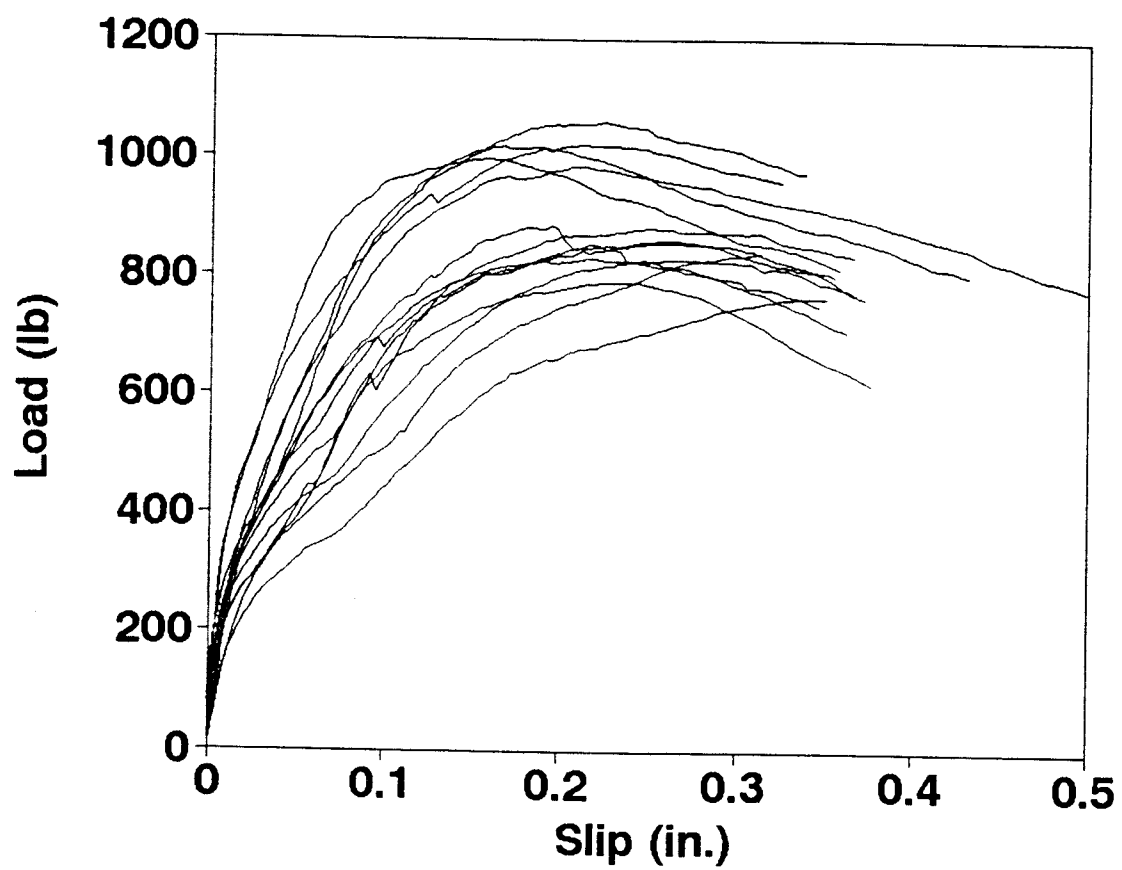
Figure A2. Combined results of the load-slip curves of three 1¼-in. JHN loaded in shear perpendicular to the fiber grain.
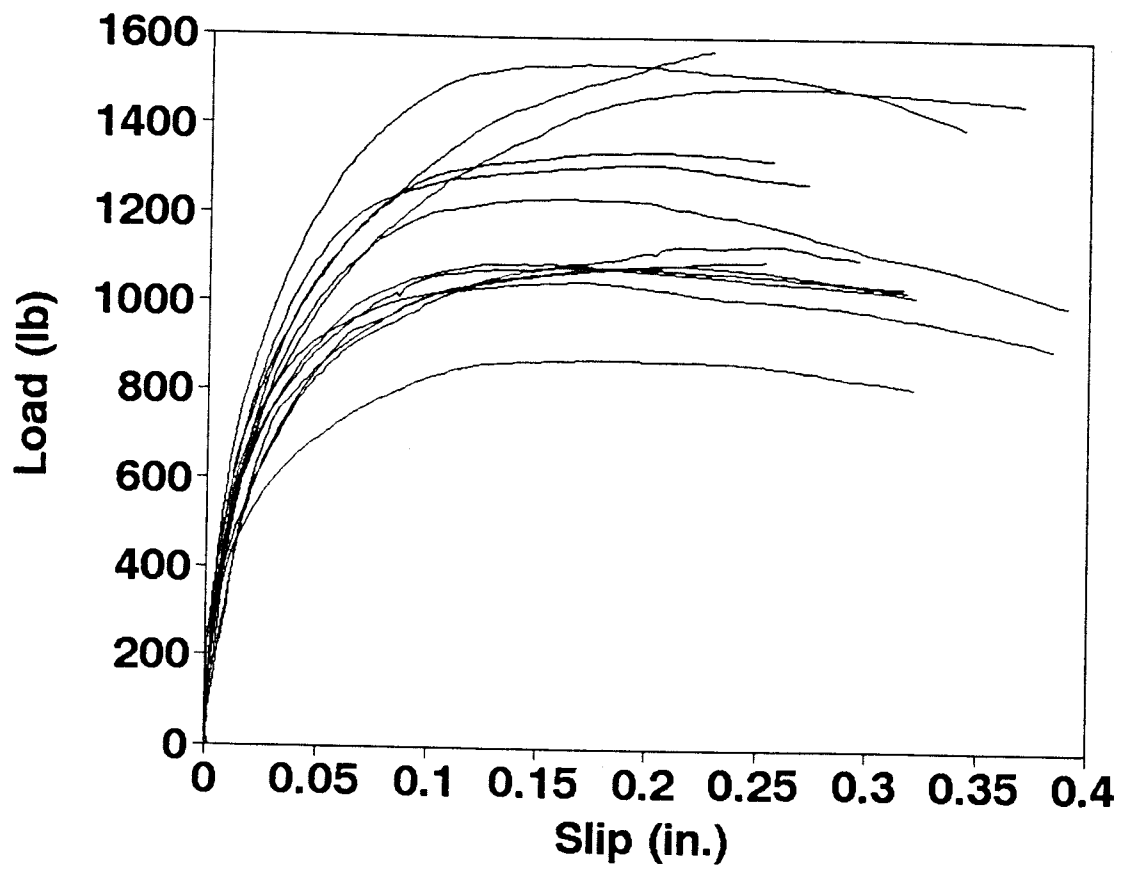
Figure A3. Combined results of the load-slip curves of two 8d nails loaded in shear parallel to the fiber grain.
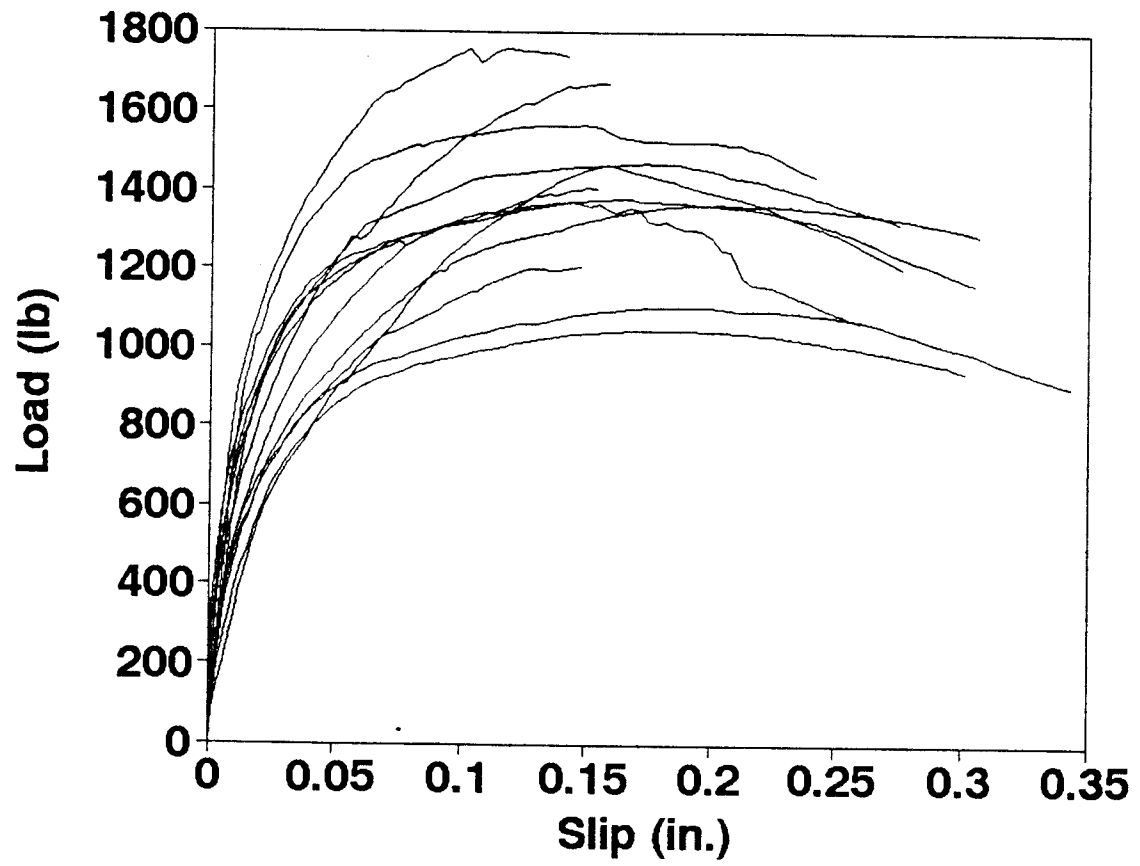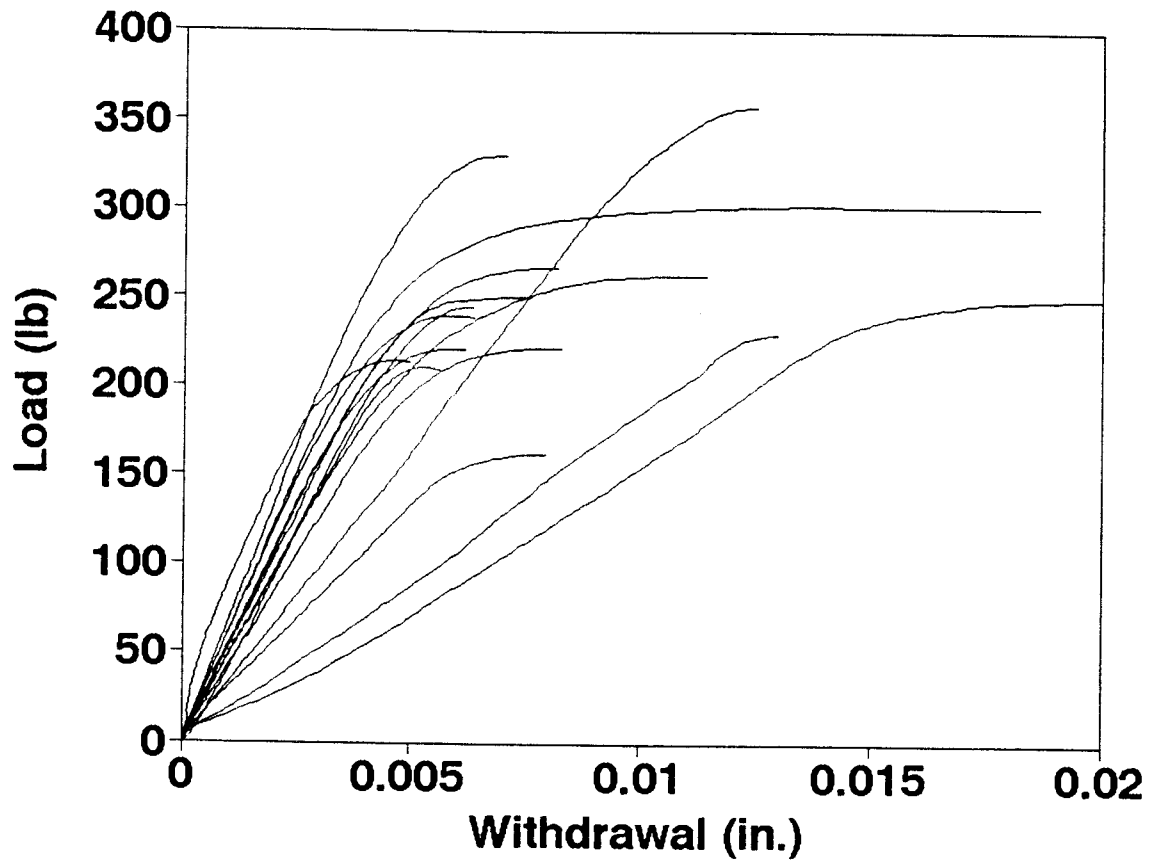
Figure A4. Combined results of the load-slip curves of two
8d nails loaded in shear perpendicular to the fiber grain.

Figure A5. Combined results of the load-withdrawal curves of a 1¼-in. JHN with 0.2 in. of the nail shaft exposed.
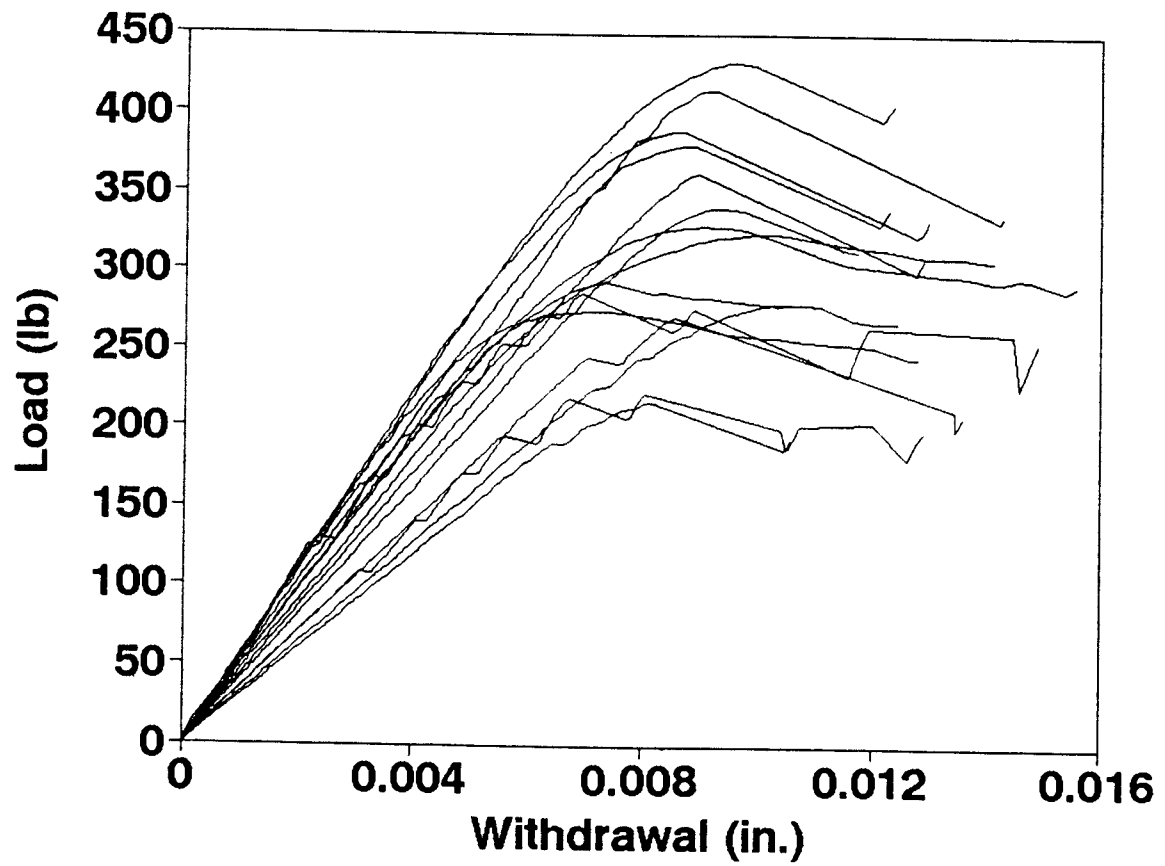
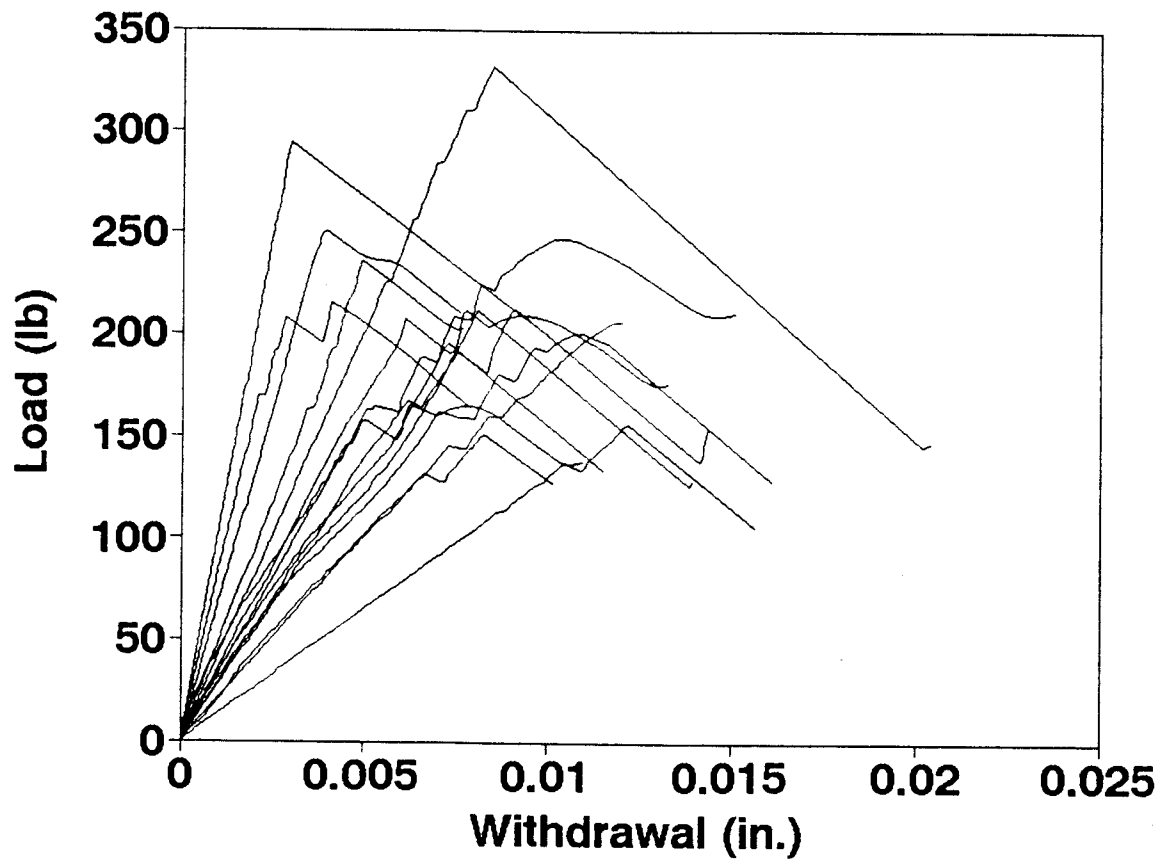Figure A6. Combined results of the load-withdrawal curves of a 6d nail with ½ in. of the nail shaft exposed.
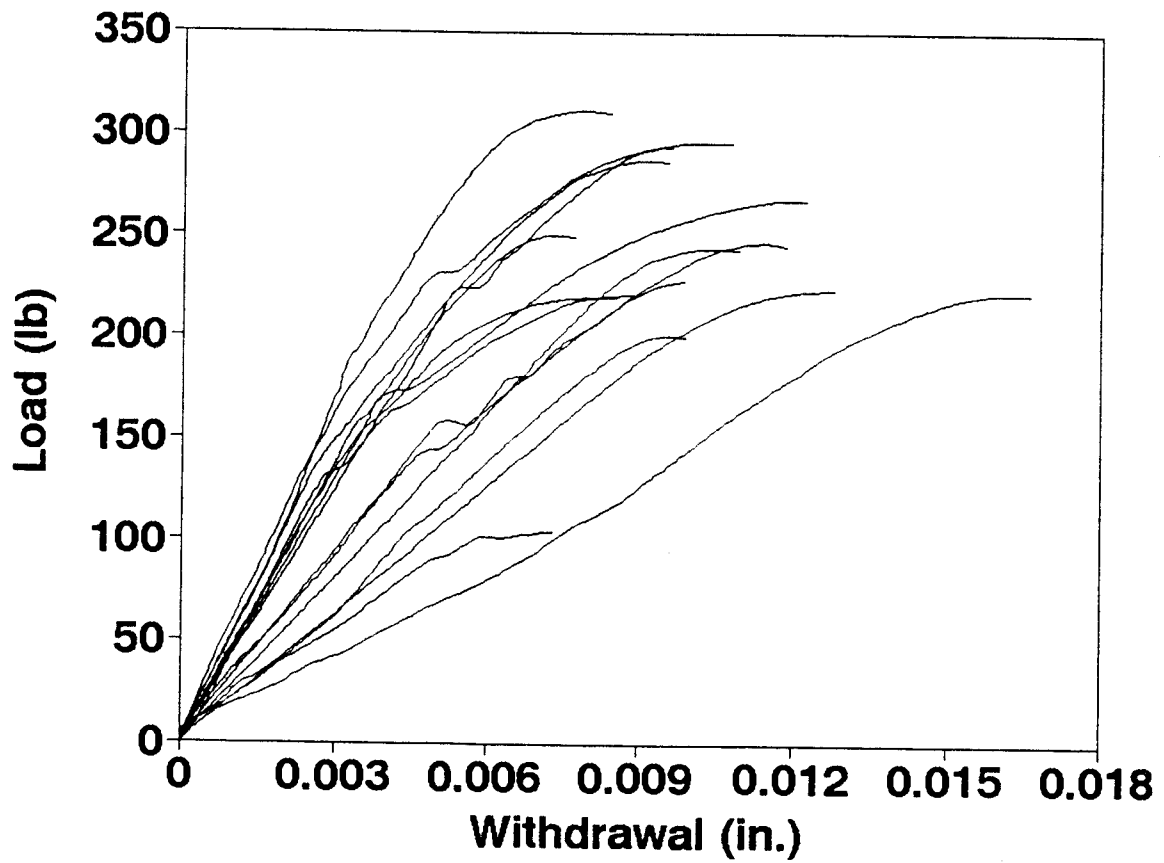
Figure A7. Combined results of the load-withdrawal curves of an 8d nail with 0.2 in. of the nail shaft exposed.
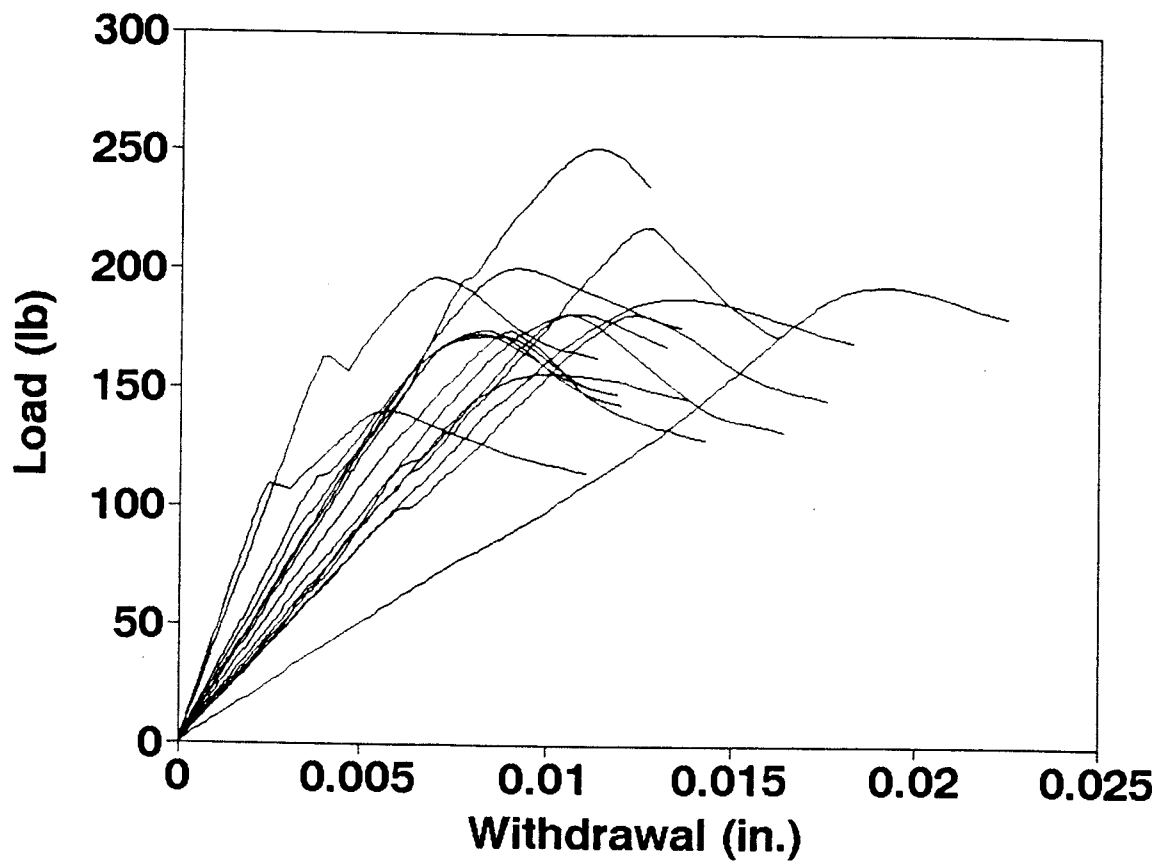
Figure A8. Combined results of the load-withdrawal curves of an 8d nail with ½ in. of the nail shaft exposed.
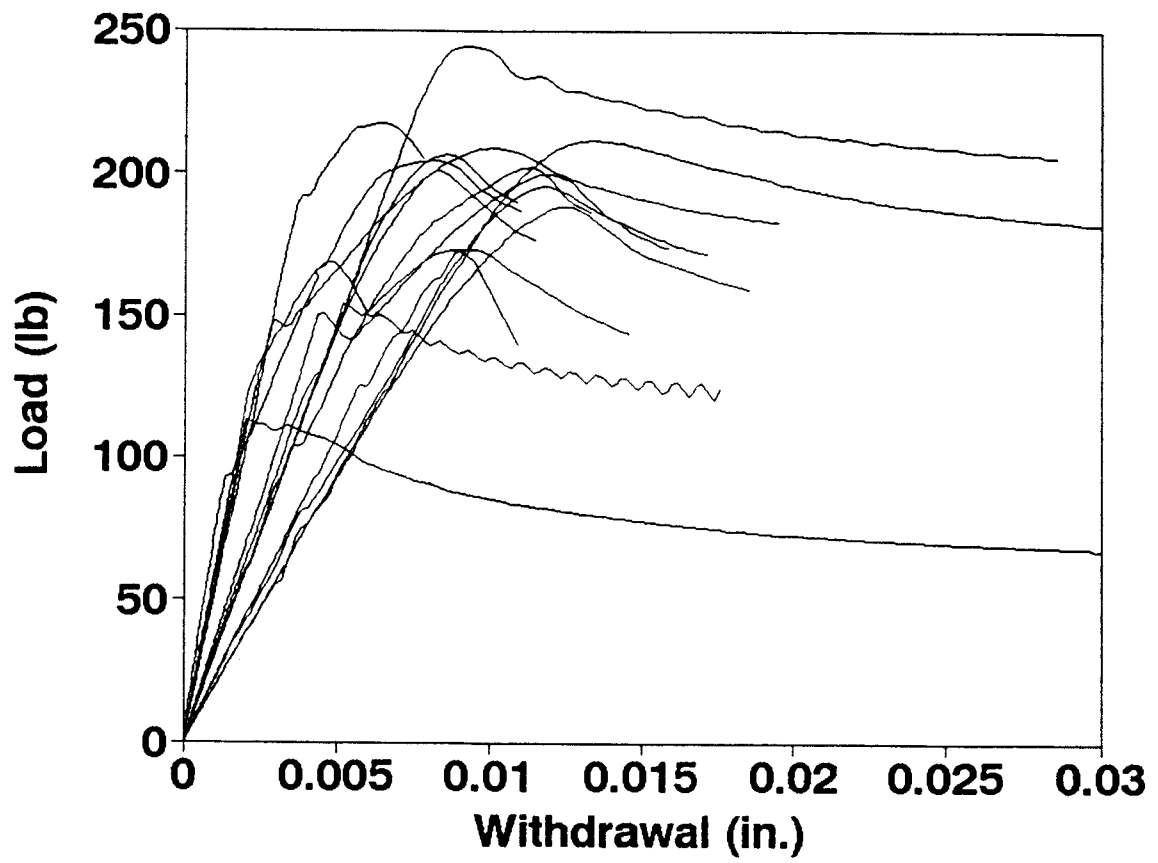
Figure A9. Combined results of the load-withdrawal curves of a 10d with 1½ in. of the nail shaft exposed.
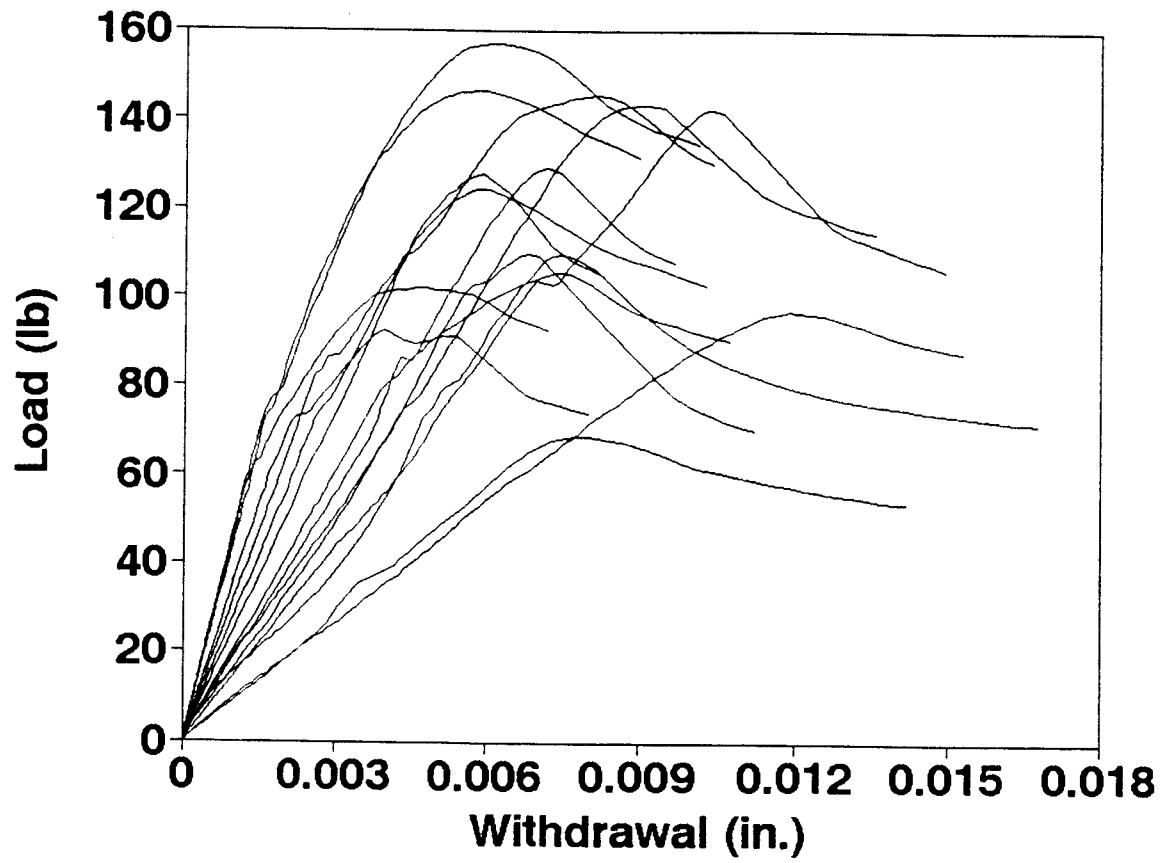
Figure A10. Combined results of the load-withdrawal curves of a 10d nail with 2 in. of the nail shaft exposed.
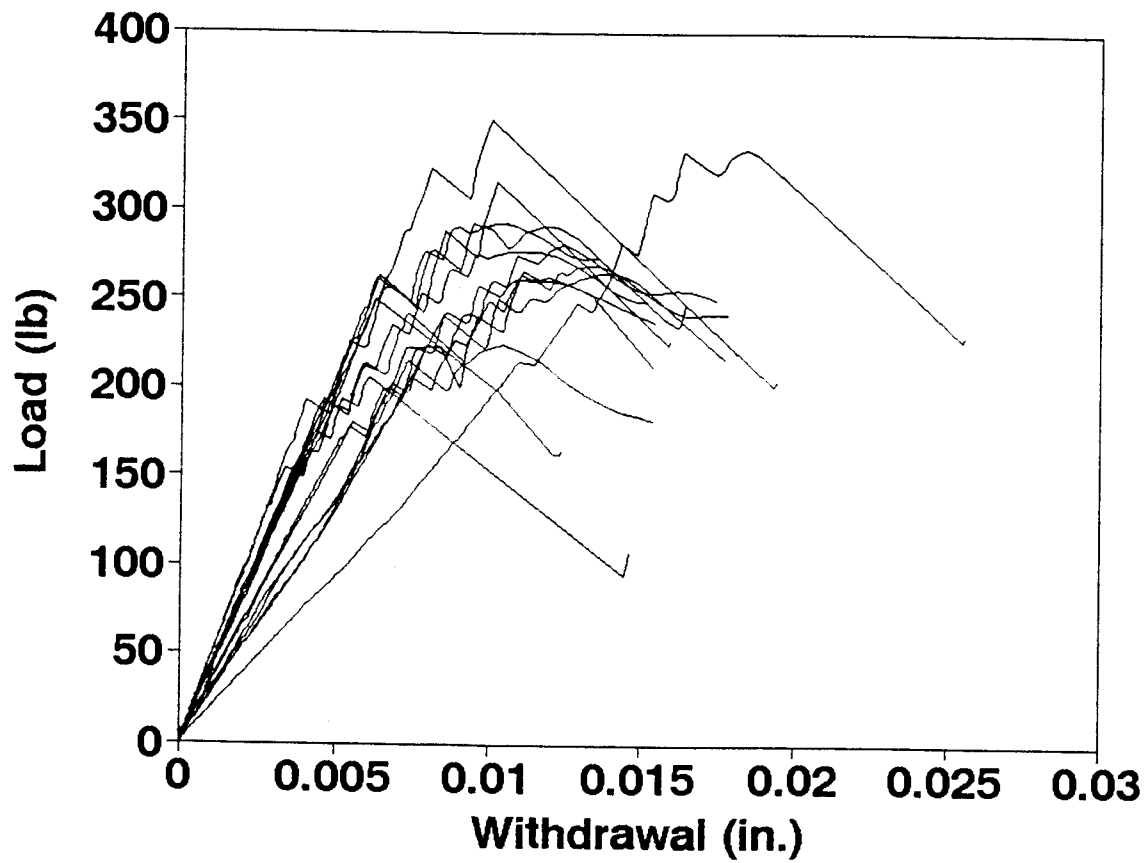
Figure A11. Combined results of the load-withdrawal curves of a 16d nail with 1½ in. of the nail shaft exposed.

Figure A12. Combined results of the load-withdrawal curves of a 16d nail with 2 in. of the nail shaft exposed.
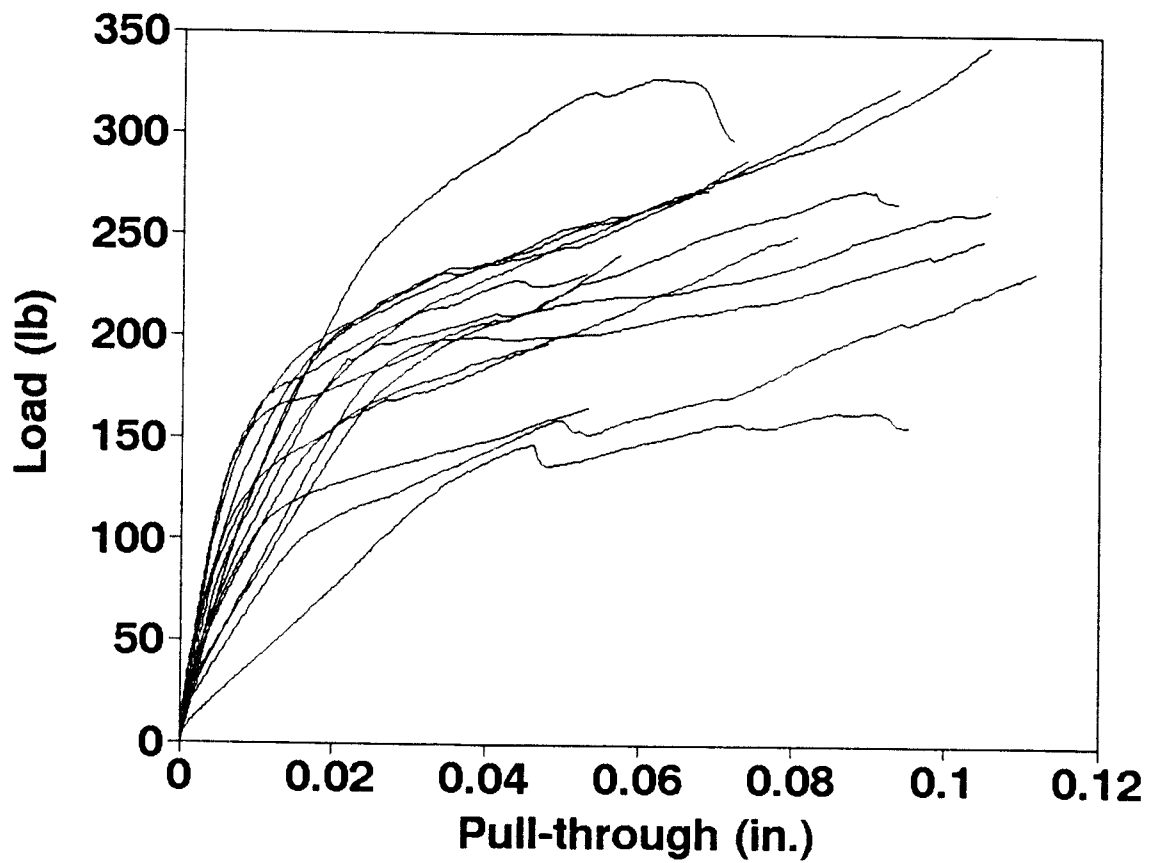
Figure A13. Combined results of the nail-head pull-through curves of a 6d nail passing through ½ in. of exterior plywood sheathing.

Figure A14. Combined results of the nail-head pull-through curves of an 8d nail passing through ½ in. of exterior plywood sheathing.
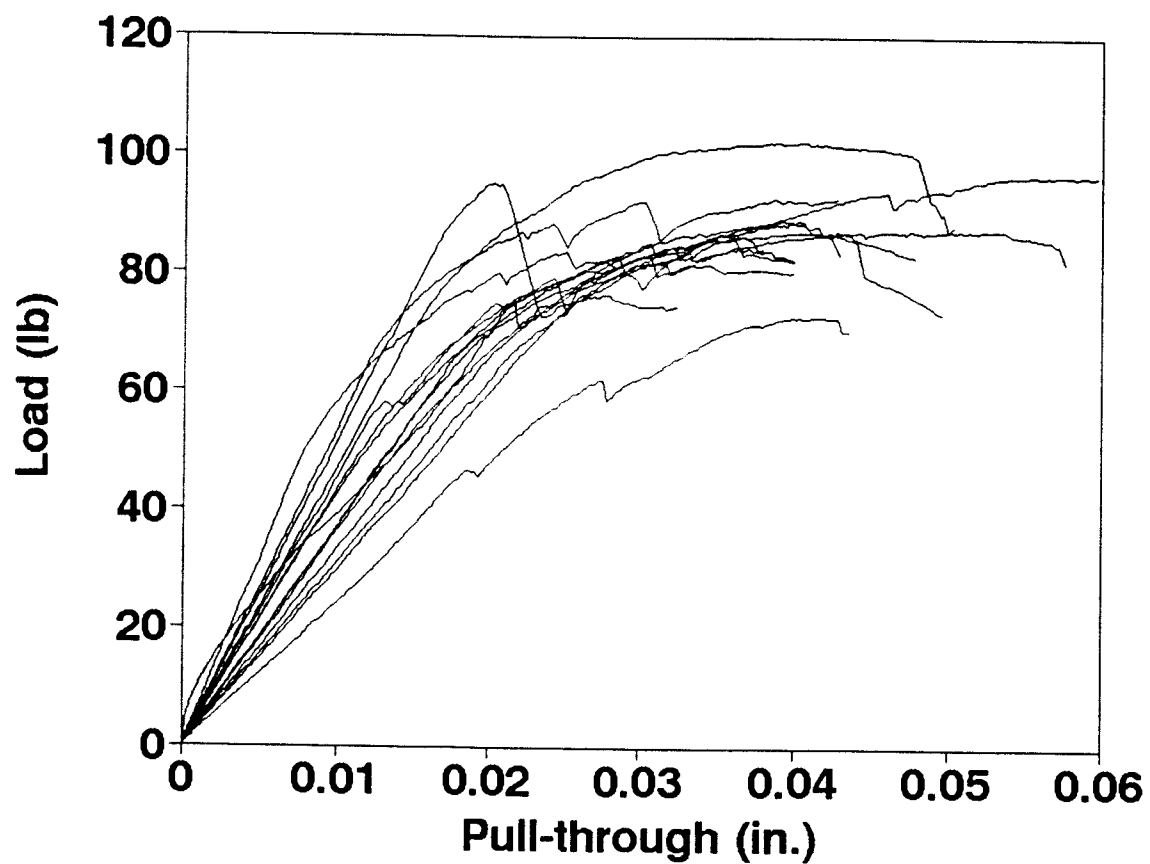
Figure A15. Combined results of the nail-head pull-through curves of a drywall nail passing through ½ in. of gypsum board.

APPENDIX B

Moment-Rotation Curves of Truss-To-Wall Connection
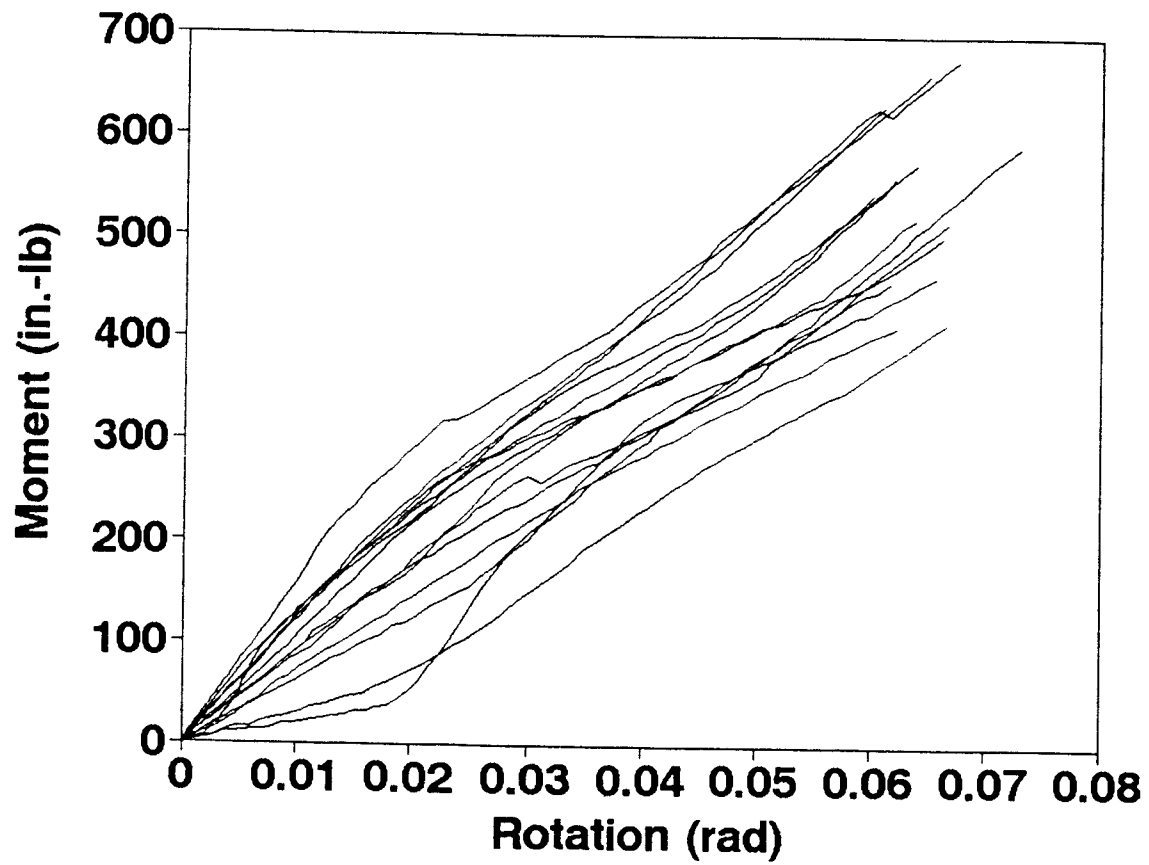
Figure B1. Combined moment-rotation curves of the experimental interior wall-to-roof truss connection rotating about the x-axis.
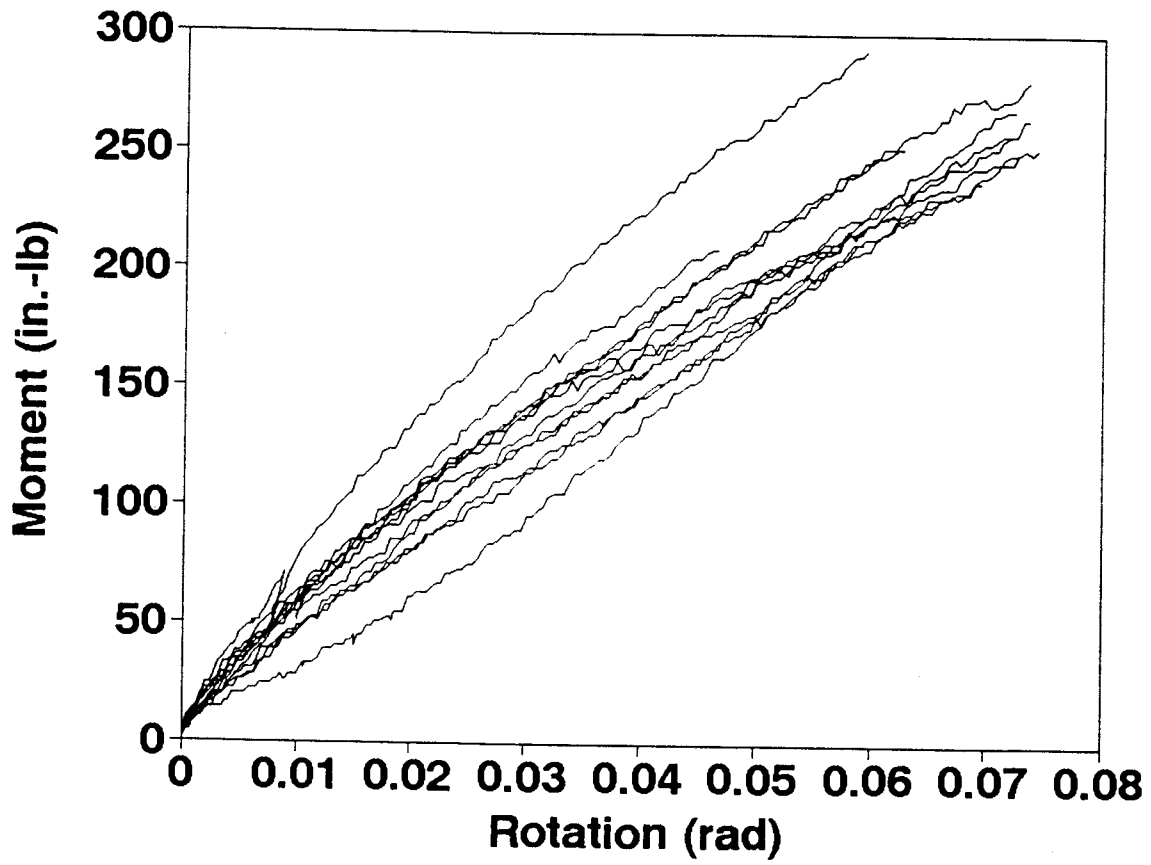
Figure B2. Combined moment-rotation curves of the experimental interior wall-to-roof truss connection rotating about the z-axis.

APPENDIX C

Load-Midspan Deflection Curves of the Sheathing Materials
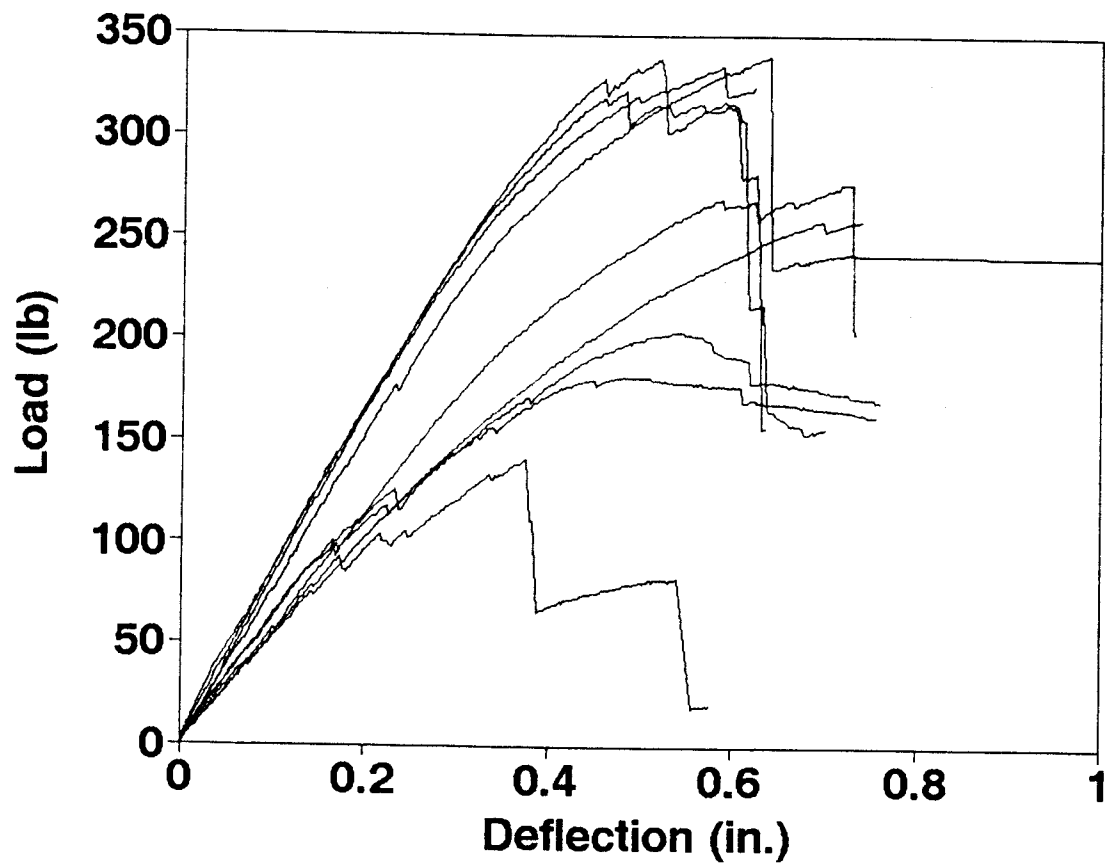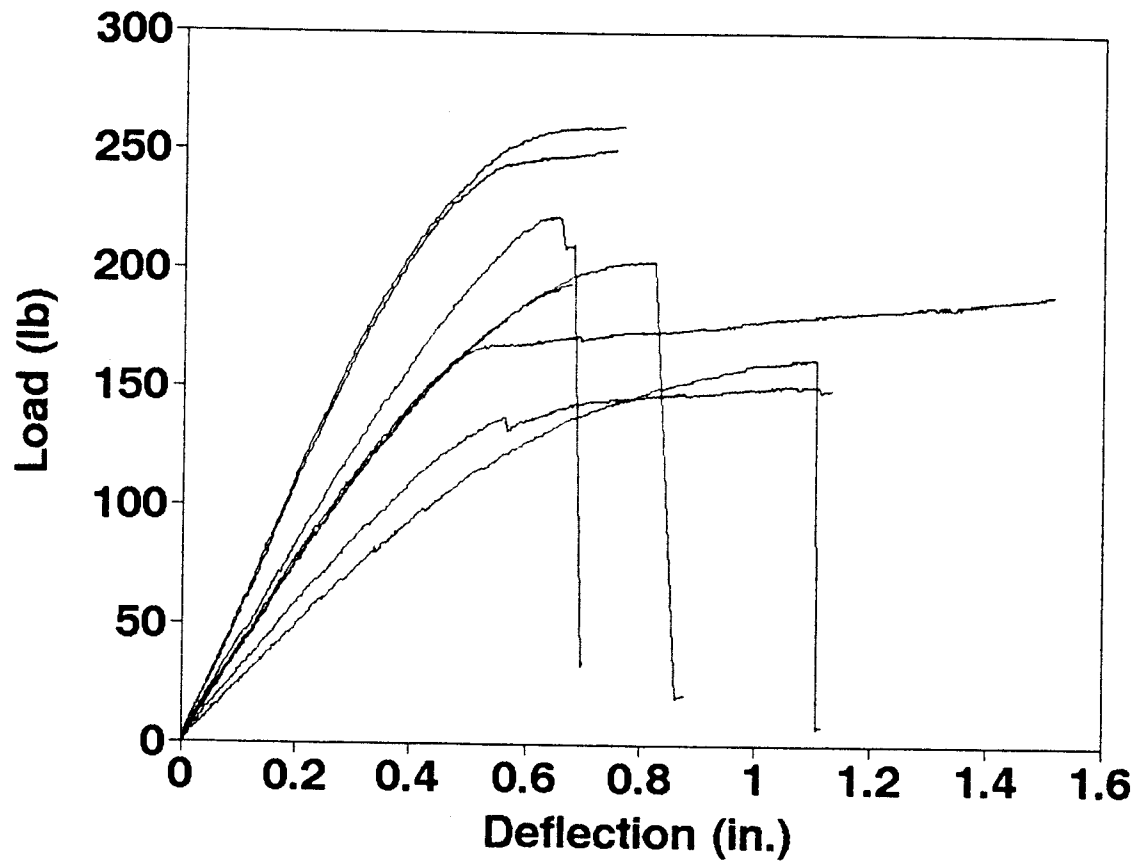used in the Exterior Wall-to-Exterior Wall Connection

Figure C1. Combined load-deflection curves of the exterior plywood used in the exterior wall-to-exterior wall connection tests. Bending is done with the fibers oriented parallel to the specimen length.

Figure C2. Combined load-deflection curves of the exterior plywood used in the exterior wall-to-exterior wall connection tests. Bending is done with the fibers oriented perpendicular to the specimen length.
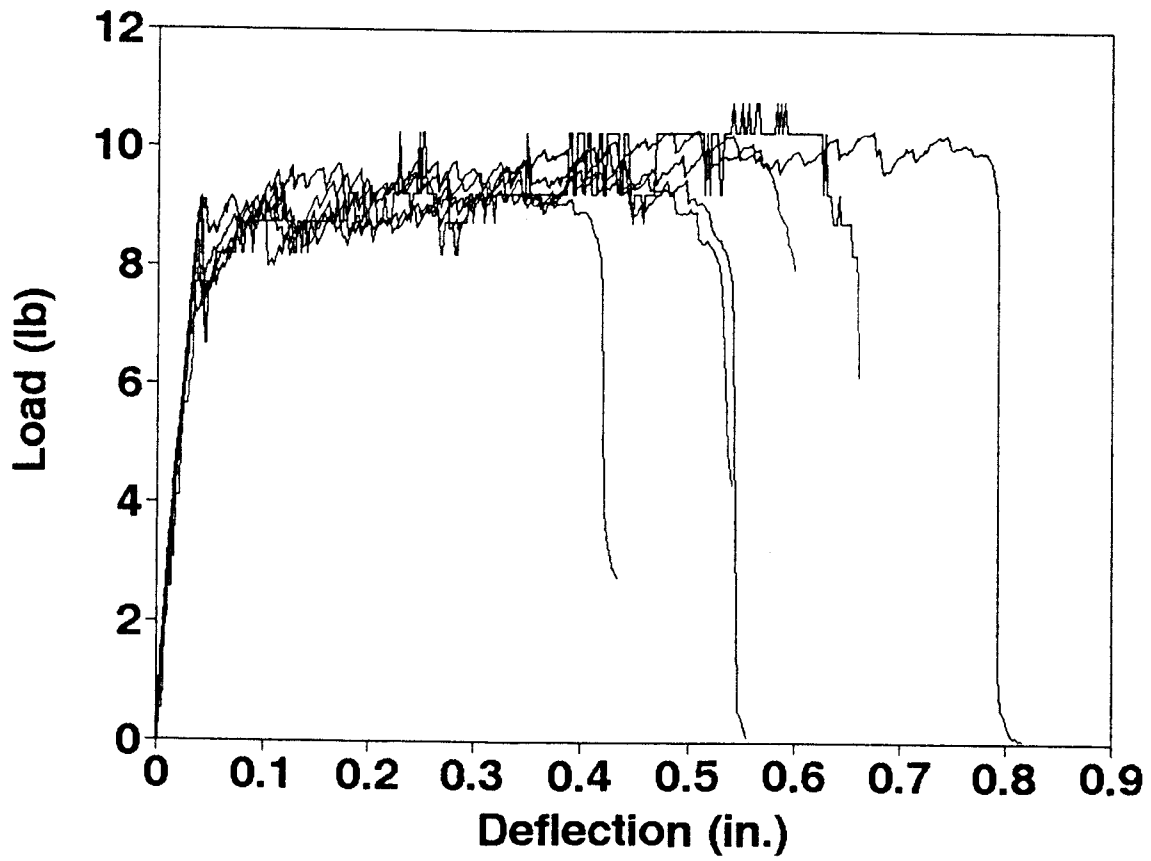
Figure C3. Combined load-deflection curves of the gypsum
board used in the exterior wall-to-exterior wall connection
tests. Bending is done with the paper fibers oriented
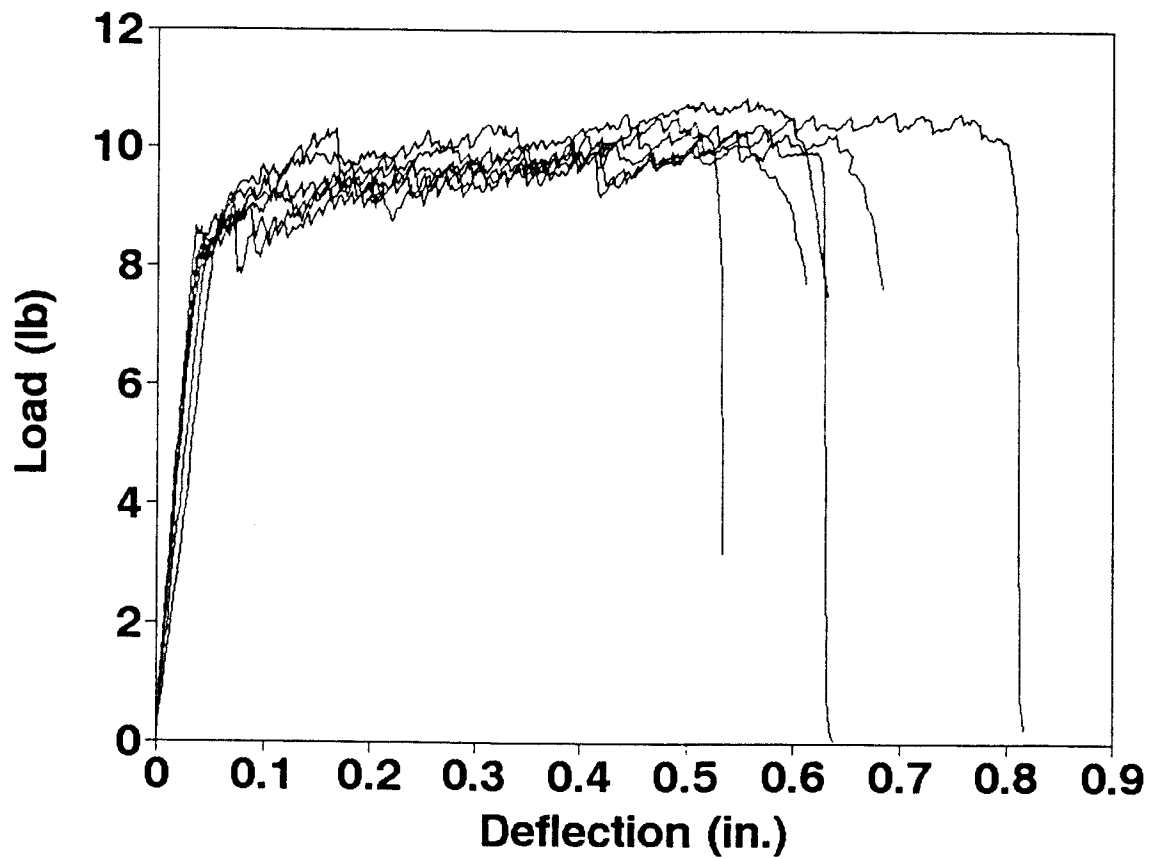parallel to the specimen length.

Figure C4. Combined load-deflection curves of the gypsum
board used in the exterior wall-to-exterior wall connection
tests. Bending is done with the paper fibers oriented
perpendicular to the specimen length.